Politechnika Lubelska

Sławomir Karaś

Mechanics of the Integrated Steel-Concrete Bridge Girder and Associated Issues

MONOGRAFIE

Lublin 2022

Mechanics of the Integrated Steel-Concrete Bridge Girder and Associated Issues

Monographs – Lublin University of Technology

Sławomir Karaś

Mechanics of the Integrated Steel-Concrete Bridge Girder and Associated Issues

POLITECHNIKA
LUBELSKA
LUBLIN UNIVERSITY
OF TECHNOLOGY

Lublin 2022

Reviewers:
Full Professor Wacław Szczesniak, Warsaw University of Technology
Assoc. Professor Sindy Seara-Paz, University of A Coruña

Cover photo courtesy of Eng Andrzej Leniak (2020)

English language proofreader: Kamila Rosińska-Balde

Edition financed by the ATEST – Lublin University of Technology consortium

Publication approved by the Rector of Lublin University of Technology

ISBN: 978-83-7947-539-5

Publisher: Wydawnictwo Politechniki Lubelskiej
www.wpl.pollub.pl
ul. Nadbystrzycka 36C, 20-618 Lublin
tel. (81) 538-46-59

Printed by: AKAPIT Sp. z o.o.
www.druksrniaakapit.pl

The digital version is available at the Digital Library of Lublin University of Technology: www.bc.pollub.pl

Circulation: 50 copies

Spis treści

Preface

The first composite bridge in which a grid of steel beams was supplemented with a concrete deck slab (54.60+55.075+55.075+54.60 m) was built in 1939 over the Sava River near Zagreb. Still, composite construction appeared at the beginnings of the use of reinforced concrete in which first wrought iron, and later steel, worked together with artificial stone, now known as concrete.

In this regard, the correct path to define the term "reinforced concrete" was presented by Melan, who described it as a rigid liner surrounded by concrete. In the history of reinforced concrete, one encounters concepts that are now referred to as 'filler beams'.

Early research on the slippage of reinforcement in concrete gave rise to solutions leading to the use of ribbed bars or shear transfer connectors. The development of the theory of reinforced concrete and composite girders continues uninterrupted and results in further improvements. The development of composite bridge technology has been described in detail, for example, in the papers (Pelke, Kurrer, 2015) and (Flaga, Furtak, 2014).

Nevertheless, this monograph does not deal with the history of the concept of composites structures – although, it does not mean that there are not numerous references to important theoretical and research achievements of the past. Essentially, the monograph aims to point out the relationship between mechanics and engineering in the field of composite bridges.

An interesting recurring process in the development of engineering concepts is that of heuristic solutions as primary solutions that can be ordered and developed through mechanics.

An example here is the period from the discovery of reinforced concrete by Gustav Lambot (1855) and Joseph Monier (1867) to the formulation of the theory, or, more precisely, the formulation of the equilibrium equations of internal forces, introduced by Mathias Koenen (1892).

Another example is the theory of the composite girder with head-stud connectors, which followed much experimental research by Newmark and his co-workers as well as by others. Nowadays, one can observe an analogous process concerning dowel shear connectors, which are now becoming an increasingly popular technology in bridge construction. As one of the creators of this technology, Wojciech Lorenc, said, the basis for application in technology is the applied solution repeatedly proven through laboratory testing and its compatibility with the results of relevant numerical modelling.

The above raises the following question: will numerical analysis replace classical mechanics? Possibly yes, as numerical modelling is a quantitative transfer of classical mechanics to complex structures. The criterion for correctness does not change – a sufficient condition is that the experimental results be consistent with the theory, numerical modelling. A consistent theory, understood in one way or another, leads to the formulation of design standards.

Of course, in near future, classical mechanics should still constitute the basic knowledge of every engineer. For this reason, basic topics such as, for example, the identification of deformations by comparing initial and actual configurations, the distinction between static states and dynamic processes, equilibrium states of internal forces, the distinction between Hooke's law and its generalisation, simplified models and their possible applications, as well as infinitesimal and operator calculus, should be taught accordingly, i.e. so that they form the basis of structural analysis.

The monograph considers the once widely used, simplified method for the analysis of bridge superstructures, the Jean Courbon method, not only because it is still applied in the case of simple bridge superstructures, but, above all, because it is both ingenious and borderline simple.

A short chapter on high strain rates discusses tests performed on a laboratory bench called the Hopkinson-Kolsky bar. The results obtained required corrections, which were next made by Janusz Klepaczko.

The issues listed are illustrative for the mechanical treatment of the composite girder problem. The basic issues are consistently examined under the assumption of the plane section principle formulated by Daniel Bernoulli and Claude-Louis Navier, (Timoshenko, 1953). This allowed for several generalisations and simplifications in the interpretation of, for example, deformations due to shrinkage. The treatment in question resulted in a reduced design scope.

To balance the design scope, a brief review of contemporary patents dealing with the important problem of the continuous composite girder and, more specifically, methods of transferring tensile stresses in a reinforced concrete slab in the zone of hogging moments is included.

Furthermore, the paper includes a concise chapter on fractional differential and integral operators, which, so far, constitute a kind of *carte blanche* – a theory looking for applications.

The chapter on viscoelasticity includes an example of the application of the residue theorem, given sufficient conditions, to determine the retransformation in a schematic and, therefore, simple manner. Viscoelasticity is a branch of mechanics that is not commonly used to describe variable material properties of structures. It has been pointed out that rheological models can be used to describe reversible and irreversible processes. In the derivation of the equations of rheological bodies, the *in extenso* method has been used to bring to attention the necessity of considering the loading history and its effects over time.

The last (but not (the) least) chapter is devoted to the aesthetics of bridges. In addition to discussing some commonly accepted canons of bridge aesthetics, a method is proposed, used by the author, which takes into account the simplest evaluation statistics in the bridge evaluation group. What makes it different is that it considers the impression made by the bridge object on each member of the evaluation group, so it is not a single person's assessment – even if they were a representative of an elite.

This monograph is atypical, but its layout is not accidental. It is an expression of the author's interests, but also the fruit of his spanning-over-a-decade professional practice of the development and teaching of the Fundamentals of Bridges course to Erasmus students. These student groups are characterised by multifaceted heterogeneity resulting from their social and cultural backgrounds and, above all, different levels of preparation to study the chosen subject matter. They are mostly students of architecture, industrial engineering, mechanics, and civil engineering. For this reason, the monograph addresses both elementary and advanced issues. The content of the monograph is dedicated to bridge engineers and, of course, students.

Author

1. Mechanical terms and principles

This chapter is devoted to the proposed system of nomenclature and designations. The listed definitions shall be used in further discussion of mechanics. The rationale is that different designations can be and are used in engineering papers. The terminology used below is one of many possible correct ones, used to varying degrees.

1.1. Internal force and stress vectors in a beam – Cartesian coordinate system

The reader can see the parallel double notation used in Fig. 1.1. In general, the right-hand coordinate system is depicted as x_m, where $m = 1, 2, 3$, however, in simple and obvious cases the traditional notation x, y, z is also admissible.

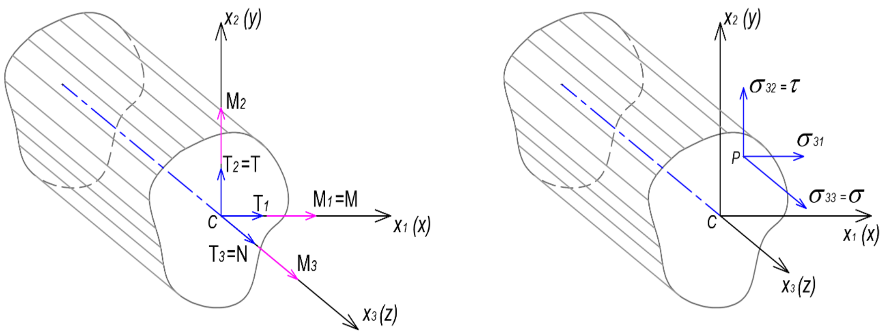

a) b)

Fig. 1.1. The assumed Cartesian coordinate system a) vectors of internal beam forces b) stress vectors at an arbitrarily chosen point P in the cross-section normal to the x_3 direction

Appropriately, the same notational system is used in the case of bending moments, shearing forces and stresses. Hence, in particular, $M_1 = M$, $T_2 = T$, $T_3 = N$, and $\sigma_{33} = \sigma$, $\sigma_{32} = \tau$.

Most often, mechanical problems are represented in a Cartesian orthonormal coordinate system, which in the case of a beam is shown in Fig. 1.1. By orthogonal coordinate system is understood that the basis vectors are mutually perpendicular to each other.

Orthonormality means that the basis vectors are unit vectors mutually perpendicular to each other.

We deal with an orthogonal system of reference when the basis vectors are mutually perpendicular to each other, but their moduli may not be unitary. Examples of such systems are the cylindrical or spherical system.

A very general understanding of coordinate systems is related to curvilinear coordinate systems. Both cylindrical and spherical systems are curvilinear and orthogonal (not orthonormal), but in other cases curvilinear systems can be non-orthogonal and non-orthonormal. Also, basis vectors can have their dualities. We speak of covariant and contravariant basis vectors.

A simple example of three linear coordinate systems explains the concepts introduced above, Fig. 1.2. Using a two-dimensional Cartesian coordinate system with a base vectors e_1, e_2 non-zero vector **u**, Fig. 1.2.a, can be decomposed obtaining its components u_1, u_2 by orthogonal projection into horizontal and vertical coordinates.

Keeping in mind the Cartesian origin of our considerations, let us modify the Cartesian coordinates by rotating the reference axis as shown in Fig. 1.2.b-c. We have obtained a reference coordinate system with unit basis vectors $\tilde{e}_1$, $\tilde{e}_2$ and e^1, e^2, however, these vectors are not perpendicular to each other. This type of coordinate reference is called an *oblique coordinate system*, which means a set of straight coordinate axes that are oblique.

At this point we face one of the key decisions. There are two options for finding the components of a vector. We can use orthogonal projection, Figure 1.2.b, or parallel projection, Figure 1.2.c. In the first case, we say that we have covariant components, while in the other case we get covariant components of the same vector **u**.

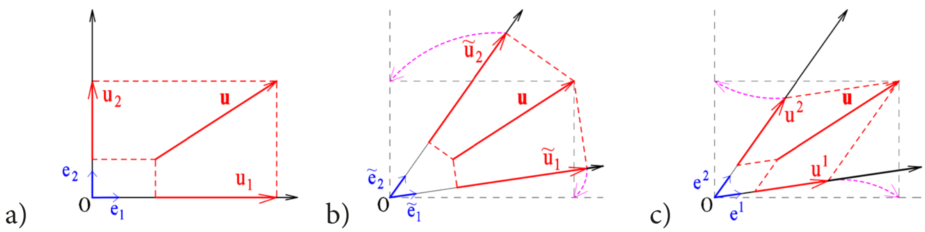

Fig. 1.2. Linear coordinate system a) Cartesian orthonormal Cartesian reference system b) oblique coordinate system with orthogonal projection c) oblique coordinate system with parallel projection

In each of the three cases considered, the component vectors u_i, u^i, $\tilde{u}^i$ [1] of the **u**-vector have different moduli i.e. $|u_i| \neq |u^i| \neq |\tilde{u}^i|$.

[1] Here the top index "i" is only a superscript, especially it is not a power exponent.

Concluding considerations, the component of the vectors u^i, $\tilde{u}^i$ (subscript – upper index) are the covariant components, and u_i (superscript – lower index) is the contravariant component, where i = 1, 2.

It is worth noting that this is not just a designation, as there are many further advantages associated with this notation, such as Einstein's well-known *summation convention*.

Finally, the reader is offered to guess what the magenta colour curves introduced in Fig. 1.2.b-c can be used for.

1.2. Initial and actual configuration

When one describes a deformation effect, it is necessary to compare the *initial and actual configuration* of the analysed structure or its element. In Fig. 1.3, two elementary cases characteristic for tasks concerning strength of materials tasks and beam bending are shown. The analysis of geometry in Fig. 1.3.a leads to the differential equation of the Bernoulli beam theory while Fig. 1.3.b illustrates the beam curvature in the function of normal stresses. Among others, this will be shown in the following chapters. The initial configuration is understood as a view or diagram of the initial/undeformed structure, while the actual configuration represents the deformed state of the same structure.

In addition, Fig. 1.3.b shows the deformation when the planar section in the initial configuration also occurs in the actual configuration.

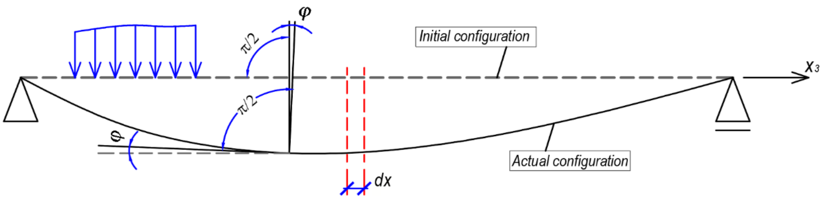

a)

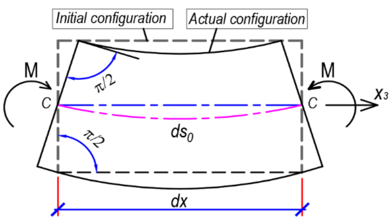

b)

Fig. 1.3. Initial and actual configuration a) simple beam bending case b) an infinitesimal element configuration

1.3. Assumption on flat cross-sections

The flat cross-sections perpendicular to the neutral axis in the initial configuration remain flat and perpendicular to the deformed neutral axis in the actual (deformed) configuration, see: Fig. 1.3.

In the beam theory, this assumption is named after Daniel Bernoulli and Claude-Louis Navier (B-N). In the classical plate theory, the equivalent of this assumption is known as Kirchhoff's assumption of three normal lines[2].

1.4. The principle of stiffness

The definition of the problem in question can be expressed by the following

the current configuration converges with the initial configuration.

There are different, also analytical, versions of the principle, however, the above statement is of greatest generality.

In terms of technique, the exemplification of this theorem is the limit state of serviceability (SLS). In the case of a composite carrying deck, the deflection caused by traffic loads is limited to

$$u_{\mathrm{lim}} \leq \frac{L_t\,[\mathrm{m}]}{400}, \tag{1.1.}$$

where L_t stands for the theoretical span (support span) expressed in metres. It is worth mentioning that the dynamic amplification factor (DAF) or dynamic enhancement factor (DIF) is included in the LM1 value[3], which means that it is treated as a static load.

1.5. Homogenous body

A homogeneous material (or discontinuous regular structure) is a continuum that has the same properties in any arbitrary direction at every point (sub-volume) in the body.

[2] Kirchhoff assumption: *straight lines normal to the mid-surface remain normal to the mid-surface after deformation.*

[3] Load Model 1 – LM1, EN 1991-2

1.6. Hooke's model

Hooke's model is a basic element when one depicts complex models in linear rheology.

In 1676, Robert Hooke formulated an anagram in Latin: *ceiiinosssttuv*, and, two years later, published (Hooke, 1678) the anagram solution as

Ut tensio, sic vis

this, in the case of a stretched spring, is understood as follows:

the extension is proportional to the force, as in the eqn (1.2).

Expressing this formula, one can write

$$F = k\,\Delta L\,, \tag{1.2}$$

where F is an acting force, k is a coefficient of proportionality, and ΔL is spring elongation. One should always bear in mind that this is the right relationship in the unidimensional isotropic problem where only one of the two material characteristics is in use. In this sense it is only a partial constitutive relation.

1.7. Constitutive relation

A constitutive relation, *stress* ~ *strain* or σ ~ ε, refers the definition of a material. Briefly, in the case of a simple beam, knowing the action and geometrical response, one can '*guess*' the material of the beam.

In detail, let us recall (1.2) an expression which is valid in a uniaxial tension/compression task, which, through an infinitesimal notation, becomes

$$\sigma = E\varepsilon \tag{1.3}$$

Here, E stands for Young's modulus which is known for different materials, hence, knowing the strain, one can calculate normal stress values.

The above relation is commonly known as Hooke's law.

1.8. Isotropy

Isotropy is the uniformity of a material in all orientations. Isotropic materials have the same elastic mechanical properties in every orientation or, in other words, are independent of the orientation of the coordinate axes.

An isotropic material has only two independent material characteristics, e.g. E, ν (Young's and Poisson's moduli, so-called technical characteristics) or μ, λ (Lamé characteristics). The infinitesimal *stress~strain* relation, in the tensor description, can be written as

$$\sigma_{mn} = 2\mu\, \varepsilon_{mn} + \lambda\, \varepsilon_{mk}\delta_m^k = \frac{E}{1+\nu}\varepsilon_{mn} + \frac{E\nu}{(1+\nu)(1-2\nu)}\varepsilon_{mk}\delta_m^k \tag{1.4}$$

where δ_m^k is Kronecker's delta or identity matrix or metric tensor in the Cartesian coordinate system, or a raising/lowering tensor; obviously $\mu = \frac{E}{2(1+\nu)}$ and $\lambda = \frac{E\nu}{(1+\nu)(1-2\nu)}$.

The $\varepsilon_{mk}\delta_m^k = \varepsilon_k^k = \mathrm{Tr}(\varepsilon_{mn}) = \varepsilon_{11} + \varepsilon_{22} + \varepsilon_{33}$ is known as a trace of strain tensor or a dilatation, or the first invariant of strain tensor.

In terms of technique, in simple uniaxial cases of stretching or compression, the constitutive relation – *generalised Hooke's law* – can be expressed as a function of two material constants E and ν.

$$\begin{cases} \sigma = E\varepsilon \\ \nu = \left| \dfrac{\varepsilon\_}{\varepsilon} \right| \end{cases}, \tag{1.5}$$

where ε _ is the strain component perpendicular to ε direction. Here, the (1.5) relation can be described as the *generalized Hooke's law*.

1.9. Orthotropy

An orthotropic material has material properties that differ within the range of orthogonal planes of the Cartesian axes $x_1 \times x_2$, $x_2 \times x_3$, $x_3 \times x_1$.

Wood is a commonly cited example.

Orthotropic materials have nine independent material characteristics.

It is worth mentioning an orthotropic bridge deck (Huber, 1929), which can be made of isotropic material (steel, RC – reinforced concrete), however, the whole structure has three mentioned above planes of different material properties. Thus, one can talk about martial orthotropy (wood) and structural orthotropy – bridge orthotropic steel plate.

1.10. Anisotropy

An anisotropic material is the most general case of material characteristics. Here, the material properties of any particle depend on a chosen direction, i.e. different characteristics occur in different directions. In the tensor notation, the stress~strain relation has the following form

$$\sigma_{mn} = E_{mn}^{kl}\,\varepsilon_{kl}\,, \tag{1.6}$$

where E_{mn}^{kl} is a fourth order stiffness tensor the components of which are a function of material characteristics.

By virtue of the following symmetries

$$\sigma_{mn} = \sigma_{nm}\,,\ \varepsilon_{kl} = \varepsilon_{lk} \text{ and } E_{mn}^{kl} = E_{kl}^{mn} \tag{1.7}$$

The number of 81 ($3^4 = 81$) components of E_{mn}^{kl} is reduced to 21 independent material characteristics.

Assuming the dimension of material volume in form of a cube edge a = 1 cm, one can expect that bridge concrete (heavy basalt aggregate) be an anisotropic material, but on the other hand, in the case of sand aggregate concrete the estimation be close to isotropy.

1.11. Saint-Venant's principle of normal stress distribution equivalence

"*If the forces acting on a small portion of the surface of an elastic body are replaced by another statically equivalent system of forces acting on the same portion of the surface, this redistribution of loading produces substantial changes in the stresses locally but has a negligible effect on the stresses at distances which are large in comparison with the linear dimensions of the surface on which the forces are changed.*", Fig. 1.4, (Saint-Venant, 1855).

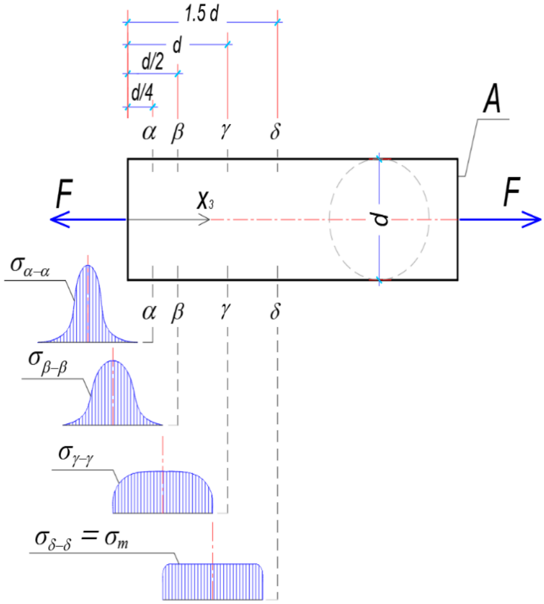

Fig. 1.4. Normal stress distribution as a function of the distance from the applied force

In Fig. 1.3, the concentrated force is applied at the rod end cross-section. This implies a material reaction in the form of Dirac's distribution at the rod ends. However, this local impact weakens gradually and at the distance 1.5d (d – the diameter of the rod cross-section) attains a uniform distribution amounting to $\sigma_{(m)}$, Fig. 1.4. One can write

$$F = F\int_A \delta(x_1)\,\delta(x_2)\,dA\Big|_{x_3=0} = \sigma_{(m)}A\Big|_{x_3\approx 1.5d}, \tag{1.8}$$

where F – concentrated force, A – area of the rod cross-section, $\delta(x_1)$, $\delta(x_2)$ Dirac's distributions, $\sigma_{(m)}$– normal stress mean value $\sigma_{(m)} = F/A$.

Nowadays, analogous tasks form a *shear-lag* problem. In the case of composite steel-concrete bridges, the most significant is the *effective width* of a concrete bridge plate combined with a precast steel beam, which, according to Eurocode 4 (EN 1994-2, p. 28-29, Fig. 5.1) is searched as shown in Fig. 1.5 (EN 1994-2), and Eurocode relations (*5.3-5*)

$$b_{ef} = b_0 + \sum b_{ei} \qquad \text{(in the span)}, \tag{5.3}$$

$$b_{ef} = b_0 + \sum \beta_i\, b_{ei} \qquad \text{(end of the span)}, \tag{5.4}$$

$$\beta_i = \left(0,55 + 0,025\frac{L_e}{b_{ei}}\right) \le 1 . \qquad (5.5)$$

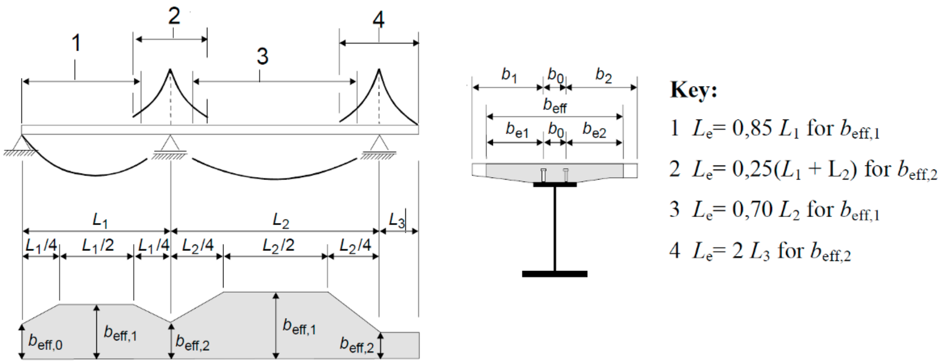

Fig. 1.5. Effective width of a concrete flange

L_e is an expression concerning simple beams freely supported and relates to the distance between the zero points of the bending moment value diagram – distances 1 and 2 in Fig. 1.5. Adequately, the same method is assumed in the case of both side cantilevers – 2 and 4 $b_{ei} = \frac{L_e}{8}$.

The calculated value of $b_{ei} \le b_i$, where $b_i = ½(b_{i-1} + b_{i+1})$. b_{i-1}, $b_i = 1$ are distances from the outer connectors on i-th beam to the outer connections of the neighbouring left and right beams or – in the case of an outer girder – to the free bridge edge.

Here, the effective width at beam bending signifies the width at which a uniform distribution of normal stresses is admissible.

An analytical examination of effective width was carried out by M. S. Troitsky (Troitsky, 1976).

1.12. Fibre concept of a bending beam

This is a very artificial concept with strong assumptions, i.e. elastic fibres are independent from each other – they do not press on each other and the friction between them amounts to zero, Fig. 1.6.

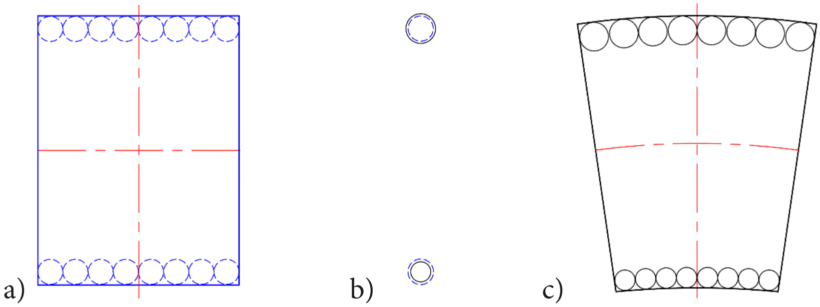

Fig. 1.6. Fibres in the beam cross-section a) upper and bottom layer of uniform fibres b) enlargement and narrowing of the upper and bottom fibre radii c) deformed configuration

They work in stretching or in compression without buckling. Without discussing the model's congruence with reality, it shows the cross-section formation in a deformed configuration of a beam subject to bending$_1$.

1.13. Geometric characteristics of a cross-section

Let us introduce the integral

$$I_{(\alpha,\beta)} = \int_A f_{(a,b)}(x_1, x_2)\,dA = \int_A (x_1)^\alpha (x_2)^\beta\,dA \tag{1.9}$$

which, in the following case, gives:

$\alpha = \beta = 0$: $\int_A dA = A$ – the area of a cross-section,

$\alpha = 1, \beta = 0$: $\int_A x_1 dA = S_2$ – static (first) moment of the area around x_2 axis,

$\alpha = 0, \beta = 1$: $\int_A x_2 dA = S_1$ – static (first) moment of the area around x_1 axis,

$\alpha = 2, \beta = 0$: $\int_A (x_1)^2 dA = J_2$ – inertial (second) moment of the area around x_2 axis,

$\alpha = 0, \beta = 2$: $\int_A (x_2)^2 dA = J_1$ – inertial (second) moment of the area around x_1 axis,

$\alpha = 1, \beta = 1$: $\int_A x_1 x_2 dA = J_{12} = D$ – moment of the area deviation.

1.14. Homogenization – transforming to steel

There are various analytical formulae for defining the homogenisation of a non-homogeneous material of various subareas to a respective homogenous cross-section. Now, let us define homogenisation by subarea changes, Fig. 1.7. The initial (real) cross-section consists of two sub-regions of the different areas A_1, A_2, characterized by different areal densities, respective to their materials C_1, C_2. The cross-section can be multiply-coherent or single-coherent. The transformed areas can overlap each other. The reference material is characterised by the material property C_0, which can be the same as or different from C_1, C_2.

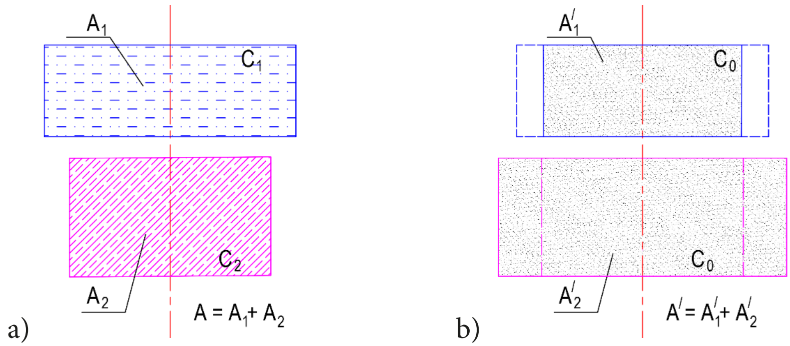

Fig. 1.7. Homogenization of non-homogeneous multiply coherent areas a) areas A_1, A_2 of the properties (material characteristics) C_1, C_2 , respectively b) areas $A_1{}^{/}$ and $A_2{}^{/}$ with reference material characteristic C_0.

Following the notation used in Eurocodes, homogenisation can be emphasised by any mechanical effect E = E{.}. Here, it is assumed as an effect of a geometrical characteristic of the cross-section

$$E = E\left\{ \int_A f_{(a,b)}(x_1, x_2)\, dA \right\} = E\left\{ \int_A f_{(a,b)}\, dA \right\}. \tag{1.10}$$

where $f_{(a,\,b)}\,(x_1,\,x_2)$ – function definition appropriate for the chosen geometric characteristic of a cross-section. Thus,

$$E\left\{ \int_A C_0 \left[\frac{\chi(A_1, A_2)\, f_{(a,b)}}{C_0}\, dA \right] \right\} = E\left\{ C_0 \left[\int_{A_1} \frac{C_1}{C_0} f_{(a,b)}\, dA + \int_{A_2} \frac{C_2}{C_0} f_{(a,b)}\, dA \right] \right\} =$$

$$= E\left\{ C_0 \left[\int_{A_1^{/}} f_{(a,b)}\, dA + \int_{A_2^{/}} f(x_1, x_2)\, dA \right] \right\} = E\left\{ C_0 \left[\int_{A^{/}} f_{(a,b)}\, dA \right] \right\} \tag{1.11}$$

where:

– C_1, C_2 – material characteristics which occur in the sub-regions A_1, A_2 respectively,

– C_0– material characteristic for a transformed homogenous cross-section,

– $\chi\left(A_1, A_2\right)=\begin{cases} C_1 & -\text{ for } A_1 \\ C_2 & -\text{for } A_2 \end{cases}$ – is an alternator depending on an affiliation to the cross-section area component,

– $A = A_1 + A_2$ – area of a real cross-section, $A^{/} = A_1^{/} + A_2^{/}$ – transformed area, $A \neq A^{/}$,

– $\dfrac{C_1}{C_0} = n_1$, $\dfrac{C_2}{C_0} = n_2$ – n_1, n_2 are the coefficients of the transformation, thus, $A_1^{/} = \dfrac{A_1}{n_1}$, $A_2^{/} = \dfrac{A_2}{n_2}$.

In the case of a steel and concrete composite girder, the term *transforming to steel* is used more often than *homogenisation* or, to put it briefly, *transformed cross-section*, see Fig. 1.8.

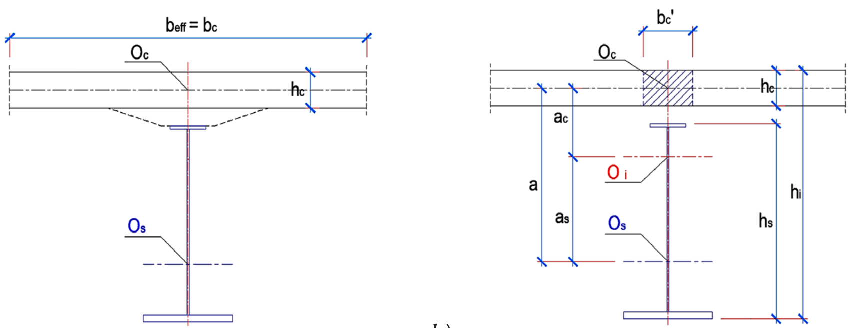

a) *b)*

Fig 1.8. Steel-concrete composite girder a) real girder composed of a concrete plate and a steel beam b) equivalent steel girder

According to the concrete slab transformation shown in Fig. 1.8, i.e. when only the concrete slab is transformed into steel, it can be written as follows

– $C_1 = E_{cm}$– secant modulus of the elasticity of concrete (EN 12390-13) which depends on the assumed concrete strength class (EN 206-1), characteristic compressive strength at 28 days $Cf_{ck,\,cyl} / f_{ck,\,cube}$,
– $C_2 = E_s$ – Young's modulus of steel,
– $C_0 = E_s$.

Thus, the coefficients of transformation are as follows

– $n = n_1 = \dfrac{C_1}{C_0} = \dfrac{E_s}{E_{cm}} \cong 7$,

– $n_2 = \dfrac{C_2}{C_0} = 1$ which means the characteristics of the steel beam after the transformation remain the same.

Finally, one arrives at

– $b_c^/ = \dfrac{b_c}{n}$, then $A_c^/ = b_c^/ h_c = \dfrac{A_c}{n}$.

The author found it difficult to determine the inventor of this method. It seems that it could be François Coignet or Mathias Koenen.

1.15. Pure bending

Pure bending is also an extremely artificial mechanical model – as artificial as the fibre concept of a bending beam, which constitutes the basic assumption concerning the task carried out here. Actually, it is not possible to put this theory to practice in laboratory conditions, if it is just an approximation. Pure bending means that only the bending moment is nonzero while other internal forces are null. For the plane $x_1 \times x_2$, this means

$$M = M_1 \neq 0 \text{ and } N = T_3 = 0,\ T = T_2 = 0 \tag{1.12}$$

see the graphs in Fig. 1.9.

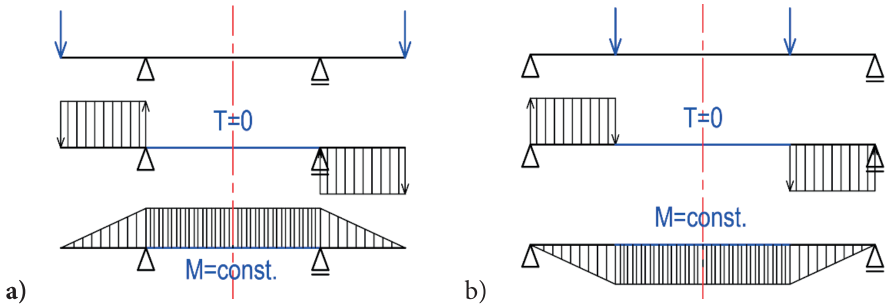

a) b)

Fig. 1.9. Pure bending static schemes for 4-point bending test a) cantilever beam b) simple beam

The sketch diagram in Fig. 1.9 serves the purpose of determining the bending stretch. Let us assume that the beam has a constant rectangular cross-section and that its material is elastic and homogenous. The beam is bent by a bending moment M causing deformation according to the principle of planar beam cross-sections (B-N principle). The deformation of the beam is shown in Fig. 1.10. The normal strains distribution follows from the B-N assumption. Consequently, the normal stresses have a linear course according to Hooke's law.

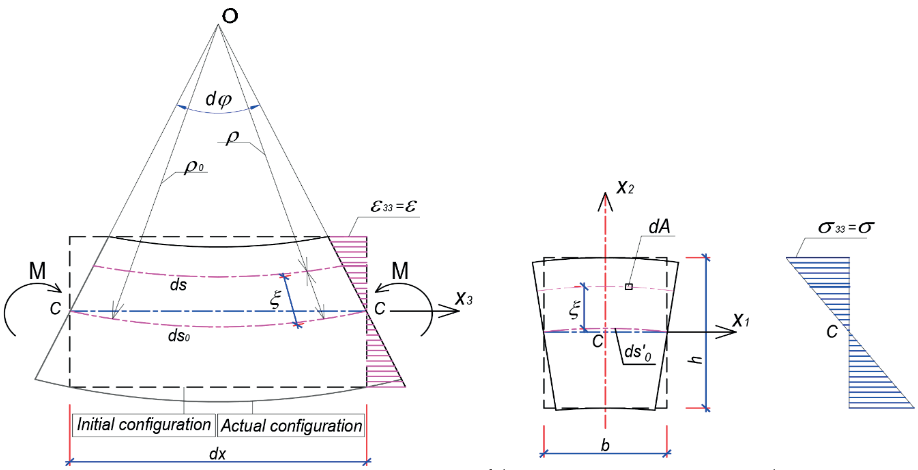

a) b) c)

Fig. 1.10. Pure bending a) side view of an infinitesimally short section of the bent beam b) section of the beam normal to x_3 c) linear normal stress distribution

Let us compare the initial and actual configuration, Fig. 8. The deformation is characterized by the strain ε which is a difference between the actual length of an arbitrary fibre denoted as *d*s and the fibre length in the initial configuration ds_0, hence, one obtains

$$\varepsilon = \varepsilon_{33} = \frac{dx - ds}{dx} = \frac{ds_0 - ds}{dx}, \tag{1.13}$$

where $dx = dx_3$ and it is assumed that $dx \approx ds_0$. Using the formula for the circle sector length, ds_0 as well as ds can be expressed as

$$ds_0 = \rho_0\, d\varphi, \quad \text{and } ds = \rho d\varphi = (\rho_0 - \xi)d\varphi, \tag{1.14}$$

where ρ_0, ρ stand for the curvature radii for ds_0, ds arcs, respectively, hence

$$\varepsilon = -\xi \frac{d\varphi}{dx} = -\xi \varphi', \tag{1.15}$$

where $$\frac{d\varphi}{dx} = \varphi' = \frac{1}{\rho} = \kappa \tag{1.16}$$

is a curvature in pure bending.

Using now the Hooke's low the normal stress can be calculated

$$\sigma = \sigma_{33} = E\varepsilon = -E\xi\varphi'. \tag{1.17}$$

Then, by integrating the static moment of stress about the x_1 axis, the bending moment M_1 is obtained

$$M_1 = \int_{A=bh} x_2 \sigma dA = -E\varphi' b \int_{-h/2}^{h/2} (x_2)^2 d\xi = -E\varphi' (b\frac{h^3}{12}) = -EJ_1\varphi' \tag{1.18}$$

where J_1 is the inertial moment of the beam cross-section area about the x_1 axis, which, for a rectangular, is $J_1 = bh^3/12$.. Thus,

$$\varphi' = -\frac{M_1}{EJ_1} \tag{1.19}$$

and, finally, one arrives at

$$\sigma = \sigma_{33} = \frac{M_1}{J_1} x_2. \tag{1.20}$$

Concluding this subchapter, it is worth stressing the validity of the formulae on curvature (1.16) and the normal stress in pure bending (1.20) for further derivations.

1.16. Pure bending with stretching/compression

This is a more general and advanced task, however, in the case of one plane bending with stretching, the result overlaps with pure bending. Let us start with an analysis of the initial as well as actual configuration shown in Fig. 1.11.

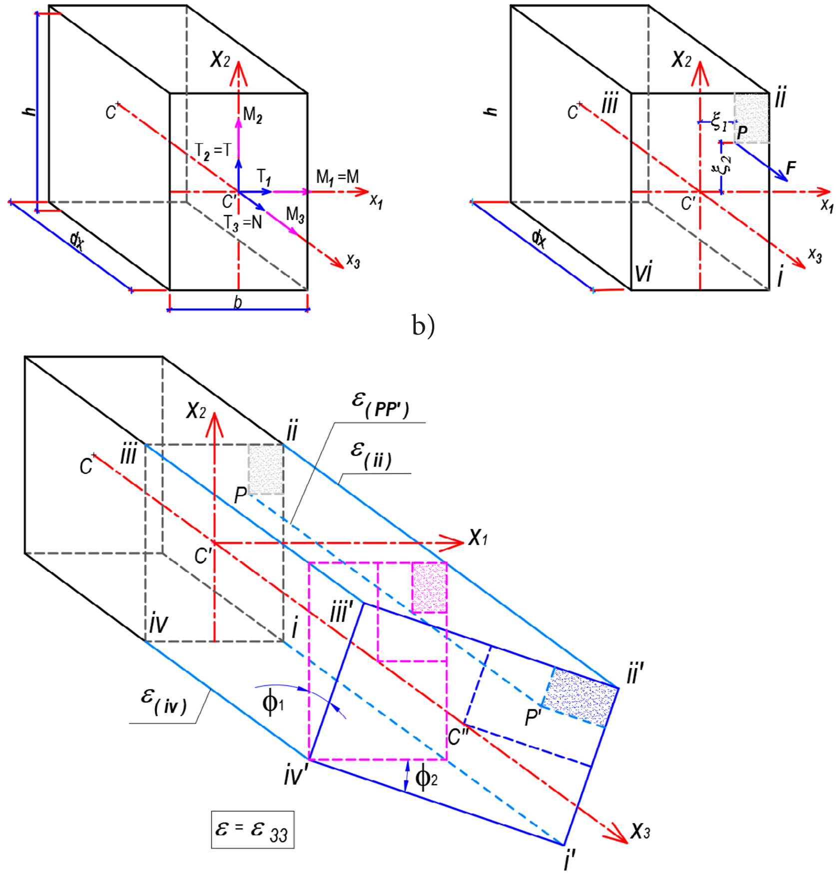

a) b)

c)

Fig. 1.11. Axonometry – initial and actual configuration in pure bending with stretching a) Cartesian coordinate system b) normal force F action c) an effect of the action is shown as a strain $\varepsilon_{(PP')}$, $\varepsilon_{(ii)}$, $\varepsilon_{(iv)}$

Initially, an infinitesimal beam sector of a length dx and of a rectangular cross-section with edges b, h, and with a face plane i – ii – iii – iv, Fig. 1.11.b, was stretched by a distance iii – iii', then twice rotated by the shown angles ϕ_2, and ϕ_1. The final rectangular plane face is marked as i' – ii' – iii' – iv', Fig. 1.11.c. This is a result of stretching caused by a normal stress at the point P located in the "*positive quarter*". Here, the assumption of flat cross-sections has being used.

Bearing in mind the equation of a flat plane in the Cartesian coordinate system

$$A_1 x_1 + A_2 x_2 + A_0 = 0. \tag{1.21}$$

One can define the strain as follows

$$\varepsilon_{33} = \varepsilon = A_1 x_1 + A_2 x_2 + A_0 \tag{1.22}$$

and, hence, by virtue of Hooke's law, one arrives at

$$\sigma_{33} = \sigma = E\varepsilon = E\left(A_1 x_1 + A_2 x_2 + A_0\right). \tag{1.23}$$

In the analysed case, the equilibrium equation set is limited to three of the six general conditions

$$\begin{cases} \sum x_3: & N = \int_A \sigma \, dA = E\left(A_1 S_2 + A_2 S_1 + A_0 A\right) \\ \sum M\_x_1: & M_1 = \int_A x_2 \sigma \, dA = E\left(A_1 J_{12} + A_2 J_1 + A_0 S_1\right) \\ \sum M\_x_2: & M_2 = -\int_A x_1 \sigma \, dA = E\left(A_1 J_2 + A_2 J_{12} + A_0 S_2\right) \end{cases}. \tag{1.24}$$

Let us recall:

– when the static moments $S_1 = 0$ and and $S_2 = 0$, it means that the origin of the x_1, x_2 axes is placed at the centre of a cross-section,
– when the deviation moment $J_{12} = D = 0$ then inertial moments have extreme values and are called principal inertial moments, while the axes to which the moments are related are known as the principal axes of inertia,
– for the cross-section with two axes of symmetry starting at the area centre, the symmetry axes are the principal axes of inertia.

The statements mentioned above apply in the case shown in the drawing Fig. 1.9. Thus, the solution of the equation set is as follows

$$A_0 = \frac{N}{A}, \qquad A_1 = -\frac{M_2}{J_2}, \qquad A_2 = \frac{M_1}{J_1}, \tag{1.25}$$

and, finally,

$$\sigma = \frac{N}{A} + \frac{M_1}{J_1} x_2 - \frac{M_2}{J_2} x_1 \tag{1.26}$$

or when the angle $\phi_1 = 0$, Fig. 1.11.b, the simplified equation is valid

$$\sigma = \frac{N}{A} + \frac{M_1}{J_1} x_2. \tag{1.26.1}$$

This approach, in the case of a steel-concrete composite girder, is more efficient than pure bending.

1.17. Delaminating force

The delaminating force Q can be obtained by performing an analysis of the elementary problem of material strength, known as the search for the distribution of shear stresses along the height of a beam section. It is worth noting that in this case these stresses include bending (M) and shear (T). Simplifying the problem, the cross section of the beam is rectangular. Fig. 1.12.a shows an infinitesimally small section of the beam of a length dx. When travelling by a distance dx, both the moment M and the shear force T change their values under a load q by infinitesimally small increments, taking the values M+dM and T+dT, Fig. 1.12.b.

The effect of the moment M and the force T can be replaced by the corresponding distributions of the normal stress σ and the shear stress τ, Fig. 1.12.c. By performing a horizontal section in the upper region of an infinitely small element, the resultant normal forces N can be related to the stress distributions σ and τ.

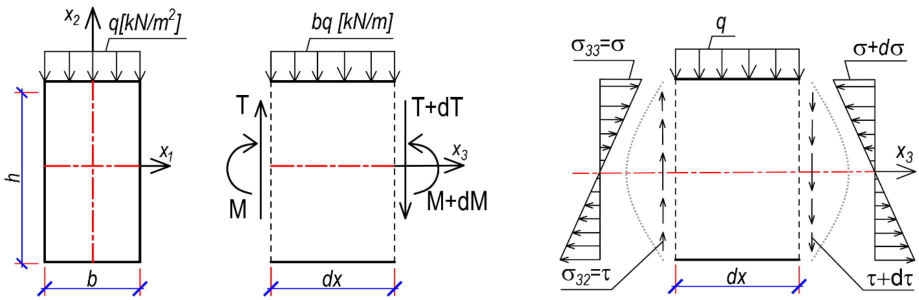

a) b) c)

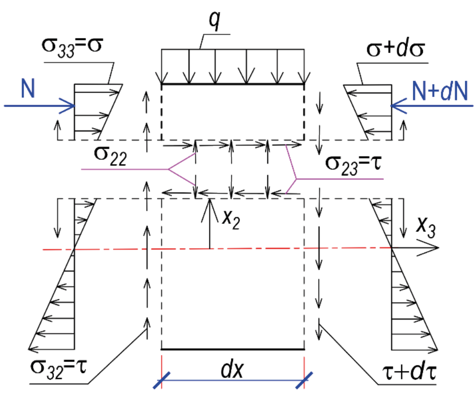

d)

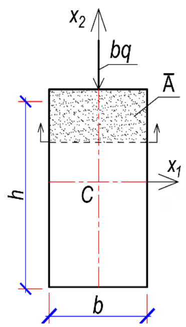

e)

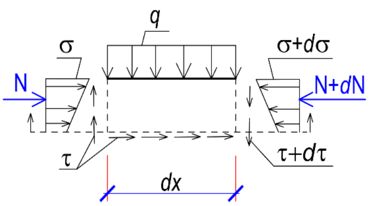

f)

Fig. 1.12. Bending with shearing a) rectangular beam cross-section b) loading and internal forces of an infinitesimal beam sector c) stress distributions in respect to internal forces d) horizontal upper section in the element dx e-f) a cut-off portion of the infinitely small beam sector in equilibrium

Writing down the equation of the projection of horizontal forces, one obtains the following corresponding differential relation

$$\Sigma\ x_1 \ \rightarrow \quad dN - \tau\, b\, dx = 0 \ \ \rightarrow \ \ \tau\, b = \frac{dN}{dx}, \tag{1.27.1}$$

where dN is the resultant force obtained by the integration dσ along the upper (cut-off) surface of the cross-section $\bar{A}$

$$dN = \int_{\bar{A}} d\sigma\, dA = \frac{dM}{J} \int_{\bar{A}} x_2\, dA = \frac{dM\, \bar{S}}{J}, \tag{1.27.2}$$

where $\bar{S}$ is the static moment of the cut-off area $\bar{A}$ (see Fig. 1.12.e-f) of the beam cross-section relative to the neutral axis in the beam cross-section, while T stands for a shearing force. Substituting (1.27.1) with (1.27.2) the following is obtained

$$\tau\, b = \frac{dM}{dx}\frac{\bar{S}}{J} = \frac{T\,\bar{S}}{J} \tag{1.28}$$

The *delaminating force* $Q_{[e]}$ is a result of the shear stress τ taken at the interface over the assumed length e. Therefore, one obtains in general and in the case where $e = 1\ m$ the following

$$Q_{[e]} = e\frac{T\,\bar{S}}{J} \ \ \rightarrow \ \ Q_{[1m]} = \frac{T\,\bar{S}}{J}, \tag{1.29}$$

where $Q_{[1m]}$ is in kN, for instance.

Comment:

It should be noted that the section *e* must include the area in the vicinity of the extreme value of the shear force T_{extr}.

In bridge engineering, the shear force envelope is analysed instead of shearing force.

The line of the influence of the support reaction can also be used to determine the maximum shear force, Fig. 1.13.

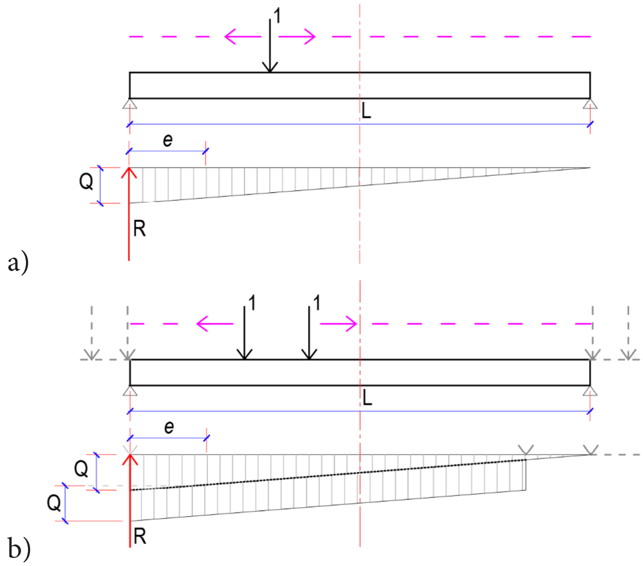

Fig. 1.13. Position of the section *e* a) influence line of the reaction R b) a case of two moving forces

Knowledge of the delaminating force distribution is essential for the correct design of connectors in a steel-concrete composite girder. It is also necessary for the design of structures reinforced by bonding FRP strips, (Oehlers, Saracino, 2004).

2. Traffic loads on bridges. Elements of EN 1991-2

Normative technical documents are written in a technically sophisticated, but concise manner. In general, these documents are accompanied by studies explaining their contents, which are generally much larger in volume than the standards themselves. Assuming that additional studies of EN 1991-2 and papers on relevant guidelines will be necessary, the following definitions of normative loads on bridges in an alternative way, facilitating their understanding, are presented below.

2.1. Road bridges

We are all aware of the diversity of bridge traffic. When designing a new bridge, different forms of traffic and values of vehicle weights must be taken into consideration.

The multiform nature of vehicular traffic on roadways and pedestrian traffic on pavements necessitates the use of load models for the purposes of highway bridges. Load Model 1 (LM1) is a basic model which, despite a very simple scheme and even artificial values of tandem concentrated forces, statistically corresponds to a real traffic action. Scaling of the LM1 model was performed on highway sections in several countries at the locations of maximum vehicle loading.

Other load models can also be used in bridge design, but the LM1 model plays a primary role. Moreover, other models should be incorporated into the design only when the LM1 model shows deficiencies in the adequacy of traffic loads. The models are discussed below.

When *tandem* is mentioned, it means a pair of vehicle axles (double axle).

2.1.1. LM1

In the basic version, the model consists of vehicle axle tandems depicted as concentrated forces on three lanes 1, 2, 3, while the remaining consecutive lanes are not loaded with tandems (concentrated forces) but have a *uniformly distributed load* (UDL), Tab. 2.1, Fig. 2.1. The last lane covers an area known as the residual area.

The LM1 model accounts for most of the effects associated with truck and car traffic and should be used to verify general and local bridge designs.

The standard lane width is 3.0 m, but narrower lane widths may also be specified. The graphic in Fig. 2.1 should be analysed simultaneously with Tab. 2.1. In addition to the basic version of LM1, some load modifications are allowed in general case design.

A vehicle axle consists of two vehicle wheels. The axle weight is α_{Qi} Q_{ik}, where α_{Qi} an adjustment factor of a value is $0.8 \leq \alpha_{Qi} \leq 1.0$. Q_{ik} is a characteristic value of wheel weight given in kN, and the index i stands for the number of lanes. Therefore, the characteristic weight of a vehicle is 0.5 (α_{Qi} $Q_{ik)}$ expressed in kN. Two parallel axles in one lane form a tandem.

Fig. 2.1.a-c shows vehicle wheel actions as concentrated forces. Fig. 2.1.a and Fig. 2.1.c present the basic version which should always be used. On the other hand, Fig. 2.1.b illustrates an acceptable modification if the bridge span $L_t \geq 10$ m and if the design is intended for general situations. In colloquial terms, the two-axle tandem model is transformed into a heavier single-axle vehicle model, with the weight of such a *double* axle amounting to, of course, 2 α_{Qi} Q_{ik}.

Figure 2.1.a-b also shows a UDL but the distribution of these loads is explained in more detail in Fig. 2.1.d, where Lane 1 was subjected to a load $\alpha_{q1}q_{m1} = \alpha_{qm}9\text{kN/m}^2$. Lanes 2 and 3 as well as other lanes and the remaining area were subjected to $\alpha_{qm}q_{mk} = \alpha_{qm}2{,}5\text{kN/m}^2$ vertical UDL, where m = 2,3,...,R.a.

Fig. 2.1.e shows another allowable modification of the tandem loading arrangement. This modification is only acceptable for general design. Instead of the standard tandem arrangement (Fig. 2.1.a, Fig. 2.1.c), the diagram shown in Fig. 2.1.e can be used. Again, using common language, tandems operating in Lane 3 can be relocated and added to the existing tandems in Lane 2. This transformation is very useful in design as it allows for a safety margin on a three-lane pavement.

The last item in Fig. 2.1 is an example of national annex. Two classes of bridge structures are designed in Poland. In both, the tandem arrangement coincides with LM1. The differences lie in the arrangement of UDLs. The layout of UDLs in the first load class is shown in Fig. 2.1.f. In the case of the second load class, the distribution of UDLs is as in LM1.

Tab. 2.1. Characteristic values of concentrated forces acting on vehicle axles and UDL actions

Lane	TS – tandem system	UDL
	Axle lads Q_{ik} [kN]	q_{ik} [kN/m^2]
Lane number 1	$Q_{1k} = 300$	$q_{1k} = 9.0$
Lane number 2	$Q_{2k} = 200$	$q_{2k} = 2.5$
Lane number 3	$Q_{3k} = 100$	$q_{3k} = 2.5$
Other lanes	0	$q_{4k} = 2.5$
Remaining area	0	$q_{rk} = 2.5$

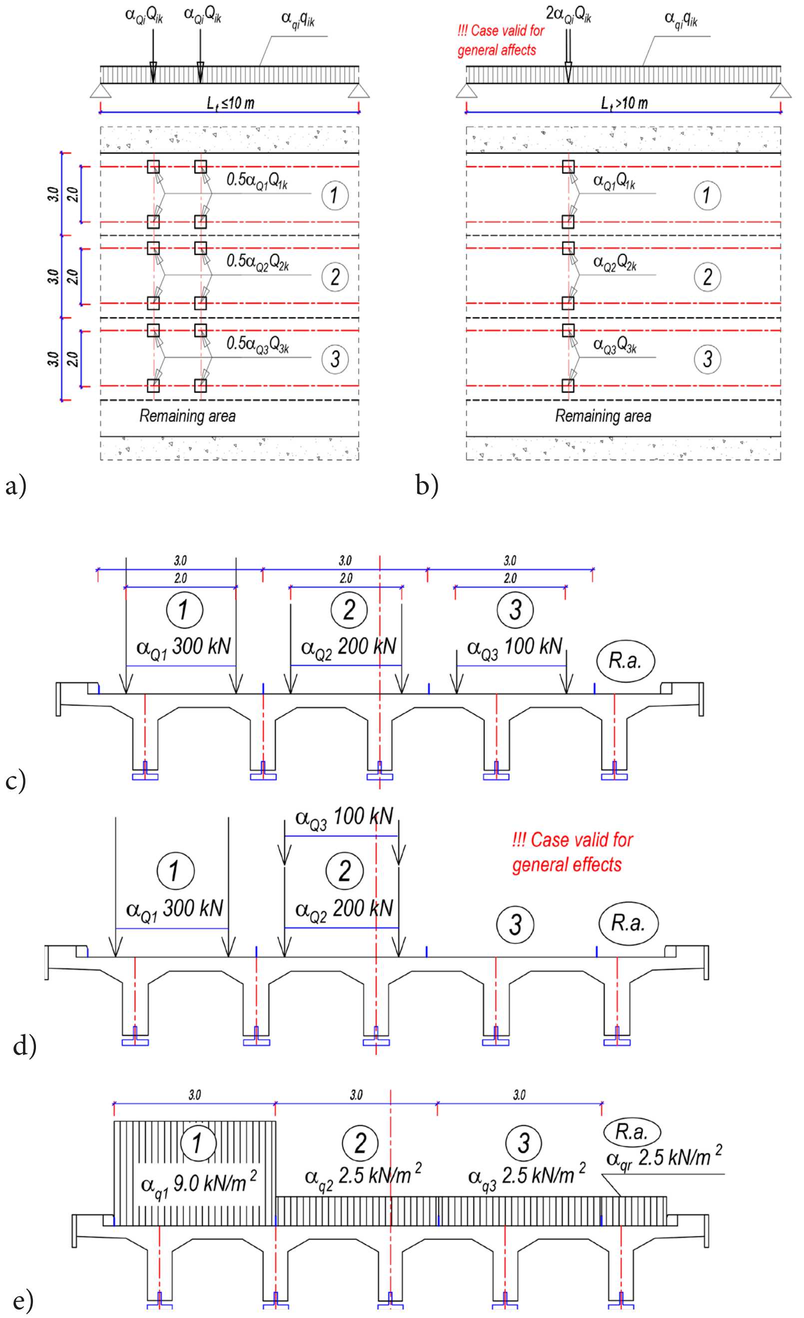

αQiQik
αQiQik
αqiqik
Lt≤10 m
0.5αQ1Q1k
0.5αQ2Q2k
0.5αQ3Q3k
1
2
3
3.0
2.0
Remaining area
a)
2αQiQik
!!! Case valid for
general affects
αqiqik
Lt>10 m
αQ1Q1k
αQ2Q2k
αQ3Q3k
Remaining area
b)
αQ1 300 kN
αQ2 200 kN
αQ3 100 kN
R.a.
c)
αQ3 100 kN
!!! Case valid for
general effects
αQ1 300 kN
αQ2 200 kN
R.a.
d)
αq1 9.0 kN/m2
αq2 2.5 kN/m2
αq3 2.5 kN/m2
R.a.
αqr 2.5 kN/m2
e)

f)

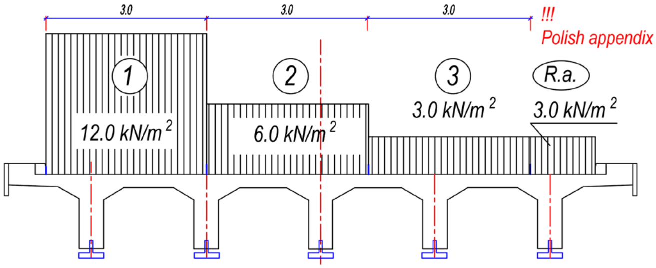

Fig. 2.1. Load configurations for LM1 a) the basic variant – a tandem system represented by concentrated forces (vehicle wheels) and, symbolically, UDL b) admissible modification of the basic variant c) tandems in the basic variant – viewed in cross-section d) UDL system for the basic variant e) admissible modification of the tandem system, two-lane loading, viewed in cross-section f) Polish Annex – 1st class in road bridge design

In 2019, new bridge load classes, linked to road classes (Regulation of the Minister… , 2019), were introduced in Poland. There are two classes based on the LM1 design model. Class 2 is a repetition of the LM1 model. In terms of tandems, Class 1 corresponds to the LM1 model with the adjustment factors listed in Table 2. As a result, the applied load factors on the first three lanes correspond to a decreasing geometrical sequence with the first number of 12 kN/m^2 and a multiplier of 0.5, Tab 2.2. Therefore, one obtains the UDL values of 12 kN/m^2, 6 kN/m^2 and 3 kN/m^2, respectively, see Fig. 2.1.f.

Tab. 2.2. Polish vehicle load classes – adjustment factors to LM1

Class of vehicle load	Values of adjustment coefficients					
	α_{Q1}	α_{Qi} $i > 1$	α_{q1}	α_{q2}	α_{q3} $i > 2$	α_{qr}
Class I	1.00	1.00	1.33	2.40	1.2	1.2
Class II	1.00	1.00	1.00	1.00	1.00	1.00

As mentioned earlier, the LM1 model can be used for local verification of a designed structure. However, this application proposes the layout shown in Fig. 2.2, where an additional description of the location of the tandem tyres and contact areas is introduced.

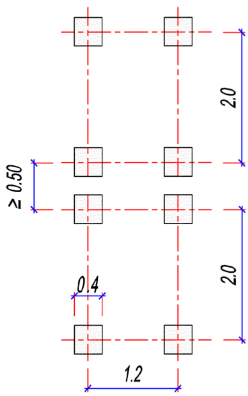

Fig. 2.2. LM1 for local verification

The impacts are expressed as characteristic quantities multiplied by appropriate adjustment factors.

2.1.2. LM2

It is a heavy twin-tyre axle, Fig. 2.3. LM2 can be positioned anywhere on the bridge roadway. The weight of the axle is $\beta_Q\ Q_{ak}$, where $\beta_{Q} = \alpha Q1$ is an adjustment factor and Q_{ak} = 400 kN is the characteristic value of the axle weight. If only one wheel is allowed in the design, then Q_{ak} = 200 kN. In general, LM2 includes dynamic amplification, but the dynamic (fatigue) factor $\Delta\varphi_{fat}$ concerning the vicinity of the expansion joint must be included. The model should be used for the purposes of short bridges or superstructure elements of the length between 3 m and 7 m. In LM2, the dynamic effects of vehicle traffic on the structure are taken into consideration.

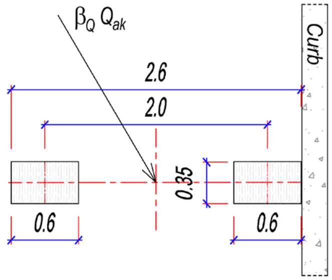

Fig. 2.3. Location of vehicle model and load value for LM2

Nowhere is it specified that the LM2 is to be used for local control of the designed structure, but it is obvious.

2.1.3. LM3

LM3 is used to design bridges taking into account the passage of special vehicles. A list of special vehicles with their axle arrangements is given in the standard EN 1991-2.

2.1.4. LM4

LM4 concerns crowd loading which should be UDL equal to 5 kN/m^2. It includes dynamic amplification. LM4 can be adjusted to a certain project.

2.2. Railway bridges

The part of the standard dealing with railway bridges differs methodologically from the part concerning road bridges. The design of railway bridges considers static methods supplemented by a correction – the *dynamic amplification factor* (DAF). At the same time, the determination of dynamic states – dynamic design – is simultaneously taken into account. There is a positive conservatism expressed in the fact that the results obtained in dynamic analyses should coincide with the results of the static design including the dynamic factor. Thus, given progress in the field of design, traditional proven methods are not discarded. While the section on road bridges deals with sophisticated traffic modelling, railways use computational models that reproduce real locomotives and trains well. Modern railway bridges are primarily concerned with high-speed trains.

A detailed discussion of EN 1991-2 has been deemed unnecessary. As in the case of road bridges, only basic design information will be referred to.

2.2.1. LM71

LM71 is the basic model for rail loading on railway bridges. It represents the static effect of a vertical load resulting from normal rail traffic. The model has been used in design for about 50 years. The characteristic concentrated forces Q_{vk} and UDL q_{vk} act on a single rail track. Q_{vk} refer to the action of the single axles of a locomotive, while q_{vk} represents wagon weight action.

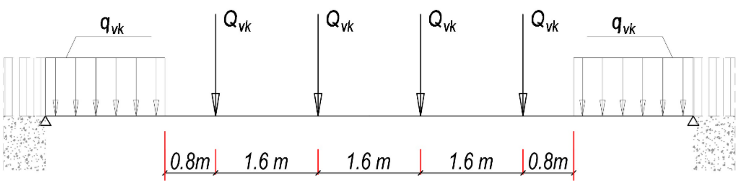

Fig. 2.4. Load distribution diagram for the LM71 model

There are several classes of loads. The characteristic loads Q_{vk} and q_{vk} must be multiplied by the classification factor α, which assigns a LM71 load to an appropriate class or, in other words, *classified vertical loads* are obtained. Explicitly, we have 8 classes defined in Tab. 2.3.

Tab 2.3. Classified vertical action on rail bridges

Formula 0.91^n, n=0,1,2,3.	α	Formula 1.1^m, m=1,2,3,4.	α
0.91^0	1.00	1.1^1	1.10
0.91^1	0.91	1.1^2	1.21
0.91^2	0.83	1.1^3	1.33
0.91^3	0.75	1.1^4	1.46

In Poland, the α = 1.21 class is used for trunk lines.

2.2.2. SW/0 and SW/2

The SW/0 is a vertical static action, representative of normal rail traffic on a continuous span bridge. SW/0 values should be multiplied by the α coefficient.

SW/2 is a static action, representative of heavy trains. Both load models are defined in Fig. 2.5 and Tab. 2.4.

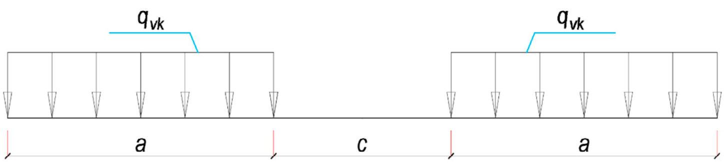

Fig. 2.5. The UDL load arrangement for SW/0 and SW/2

Tab. 2.4. Characteristic values of UDL for SW/0 and SW/2

Load Model	q_{vk} [kN/m^2]	a [m]	c [m]
SW/0	133	15.0	3.3
SW/2	150	25.0	7.0

2.2.3. Unloaded train

In this class, a vertical uniformly distributed load of the characteristic value of 10.0 kN/m is applied. This class of a moving load can be used to identify a dynamic response that is particularly important when the dynamic susceptibility of the bridge is significant.

2.2.4. HSLM

The High-Speed Load Model (HSLM) is used to model passenger trains travelling at speeds above 200 km/h. There are two types of HSLM in EN 1991-2, namely HSLM-A and HSLM-B. Both models generate dynamic effects specific to real passenger trains. Only HSLM-B is presented here.

Fig. 2.6 defining the HSLM-B model is not complicated. Two important parameters of the model are d = d(L) – the distance of vertical concentrated forces (axels) and N = N(L) – the number of axles. Both parameters are functions of the argument $L = L_t$, which stands for the span of the bridge, and are given in the next figure in the standard. The quantities d and L are expressed in metres.

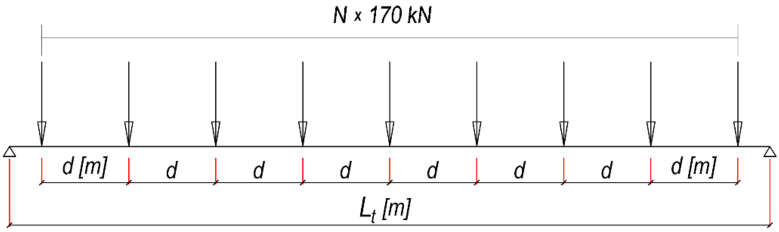

Fig. 2.6. HSLM-B – vertical impact on the railway track

2.2.5. Dynamic factors Φ_2, Φ_3

In the case of railway bridges, dynamic coefficients are used for the LM71, SW/0 and SW/2 models. The dynamic coefficients take into account a necessary correction of the static analysis results due to dynamic effects. In the dynamic factor the relevant dynamic characteristics of the structure are not considered, in particular, the resonance or other form of vibration of the whole structure or any of its components.

There are two dynamic coefficients which are applied taking into account the technical condition and maintenance of the tracks. The dynamical coefficient Φ_2 is used with regard to carefully maintained tracks while Φ_3 – in the case of standard maintenance. Mathematically, a non-linear relationship as a function of the *determinant length* L_Φ parameter is assumed.

$$\Phi\left(L_\Phi\right)=\begin{Bmatrix} \Phi_2=\dfrac{1.44}{\sqrt{L_\Phi}-0.2}+0.82, & 1.00\le\Phi_2\le1.67 \\ \Phi_3=\dfrac{2.16}{\sqrt{L_\Phi}-0.2}+0.73, & 1.0\le\Phi_3\le2.0 \end{Bmatrix}. \tag{2.1}$$

The description as well as the values of L_Φ can be found in expanded *Tab. 6.2 of EN 1991-2*. The dynamic factor Φ shall not be used with models of: *Real Train, Fatigue Train, HSLM* and the *unloaded train*.

3. Steel and concrete composite bridge girder

The concept of a steel and concrete composite girder is obvious. Concrete or reinforced concrete (RC) is placed in the compression zone, and steel – actually, the bottom flange of a steel double-T beam – works in the tension zone. As a rule, a steel beam is a prefabricated element, while a RC plate/slab is produced as a monolithic element in situ. The integration works due to connectors of different types, welded/ heat sealed to the upper surface of the upper beam flange. In recent years, the name "*steel and concrete composite girder*" has been increasingly replaced with "*steel and concrete integrated girder*".

In the case of beam bridges, a single composite girder can be analysed. Overload of the outer girder follows clearly from Courbon's method, for instance.

The default girder corresponds to the most heavily loaded girder of a composite bridge. In general, it is the outermost girder of the bridge deck.

3.1. Basic cases of integration

As far as beam integration is concerned, one talks about its

- lack of integration (separated),
- full integration, and
- partial integration.

In Fig. 3.1.a-c, all the above listed variants of integration are shown. For the sake of simplicity, two identical two-beam elements are used to present types of connection.

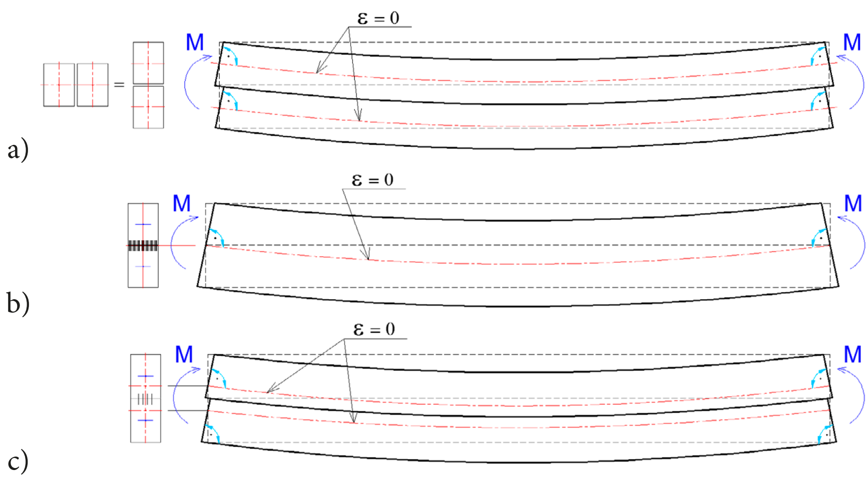

Fig. 3.1. Types of integration of two identical beam elements in pure bending a) no integration b) full integration c) partial integration

The *initial configuration* is marked with a dashed line, while the *actual configuration* is marked with a continuous line.

The contact surface between two connected beam/members shall be called *interface*.

In the cross-section, integration is represented symbolically by the different densities of vertical pin connectors (to the left from the integration variants).

The symbol ε stands for strain measured parallelly to the beam length; however, the expression $\varepsilon = 0$ should be understood as *strain null line*.

Separated beams, Fig. 3.1.a, where the first beam is located at the bottom and the other one lies upon it, correspond to the so-called *double beam*. The friction in the interface is omitted. The horizontal displacement, *slip*, of the beam ends in the interface is visible and obtains its maximum value. In this variant, there are, actually, two independent null strain lines which overlap with the symmetry axes of each beam.

Full integration, Fig. 3.1.b, means that two elements are connected totally and, as a result, the analysed beam is, in fact, a single beam of the height equal to the sum of the connected elements. The null strain axis overlaps with the interface line in the initial and deformed configuration.

The bending of the partially integrated beam elements falls somewhere in between the case of a fully integrated beam and the case of a non-integrated beam, Fig. 3.1.c. The slip is less than in the no-integration case. It is worth noting that the positions of the zero strain lines are also transient compared to the two limit cases, i.e., fully integrated and non-integrated ones.

From a bridge engineer's point of view, only the instance of full integration is admissible. Partial integration occurs when a composite structure weakens. The cause for partial integration is usually the wear of the connections between elements, (Seracino, Oehlers, Yeo MF, 2001). It may also be caused by an improper dimensioning of connectors resulting in an excessive flexibility of the connectors in the interface.

Non-integrated beams are not interesting at all.

As already mentioned, the partial integration case is not applicable to bridge construction. However, it is of great educational interest as it reveals the transient behaviour of composite girder members. For this purpose, the figures shown in Fig. 3.2 are used, which are, in a sense, extensions of the contents of Fig. 3.1.a and Fig. 3.1.c.

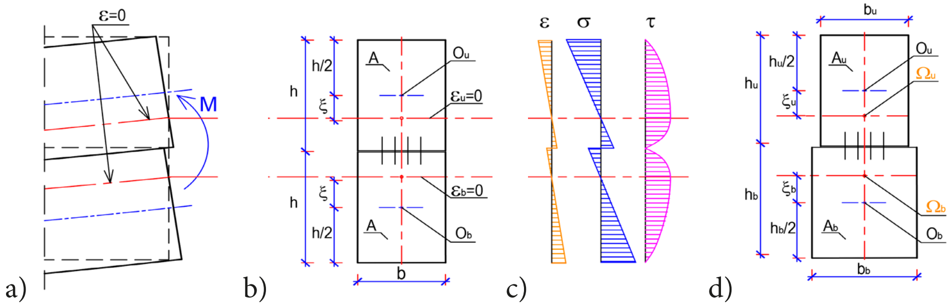

Fig. 3.2. Partial integration a) bending of a double beam b) cross-section, dimensions and markings c) distribution of strains ε, normal stresses σ and shearing stresses τ d) fitting of two cross-sections of two different component fields

The axes in red were formed after parallel displacements of the O_u and O_b axes to the positions where the neutral axes of the $\varepsilon_u = 0$ and $\varepsilon_b = 0$ strains in the partially integrated girder are.

Fig. 3.2 is a detailed supplement to Fig. 3.1.c. It shows the end parts of two geometrically identical beams, partially integrated and made of the same material.

The indices of the symbols $\varepsilon_u = 0$ and $\varepsilon_b = 0$denote the upper and bottom members and refer to the zero strain lines in the beam cross-sections. The centres of the gravity/mass axes O_u and O_b are marked in blue. The axes drawn in red were formed after the parallel shift of the O_u and $O_b$axes to the positions where the neutral axes of the strains $\varepsilon_u = 0$ and $\varepsilon_b = 0$ are located in the structural members of the partially integrated girder. Due to the bending of the members, the slip at the interface is visible.

Fig. 3.2.c shows three linear distributions of strain and normal stress and a parabolic distribution of shearing stress.

At the end of a beam, in the interface, a maximal slip is visible. As a consequence of the linear distribution, the steps of discontinuity in the strain and stress diagrams are located at the point corresponding to the interface.

In Fig. 3.2.d, the two members have different cross-sections. Therefore, the positions of the centroid lines and zero strain lines are also different. The symbols A_u, A_b, h_u, h_b, b_u, b_b, O_u, O_b and Ω_u, Ω_b have been introduced for clarity. The offsets of the zero strain lines (neutral lines) are also different and are denoted as ξ_u, ξ_b.

Using the applied notation and commonly known relations, one can calculate the basic characteristics of two partially integrated girder members by the following unnumbered steps.

- Partial integration:
  - area $\qquad A = A_u + A_b,$

– second moment of area $J = J_u + J_b$, $J_b = J_{b_0} + A_b\left(\xi_b\right)^2$,

hence $J = \left(J_{u_0} + J_{b_0}\right) + \left[A_u\left(\xi_u\right)^2 + A_b\left(\xi_b\right)^2\right]$.

- No integration:
  – second moment of area can be obtained by assuming

$$\xi_u = \xi_b = 0 \rightarrow J = 2J_0 \qquad \rightarrow J = \frac{bh^3}{6}.$$

- Full integration:
  –second moment of area has the following form

$$\xi_u = \xi_b = \frac{h}{2} \rightarrow J = 2J_0 + 2A\left(\frac{h}{2}\right)^2 \rightarrow J = \frac{2}{3}bh^3 .$$

In the case of the cross-section shown in Fig. 3.2.d, the Reader is asked to carry out the relevant calculations by themselves.

Calculation example

In the following example, the formulae are not numbered.

Consider a simple double beam in which the members are not integrated. The load is uniformly distributed along the beam, Fig. 3.3.a.

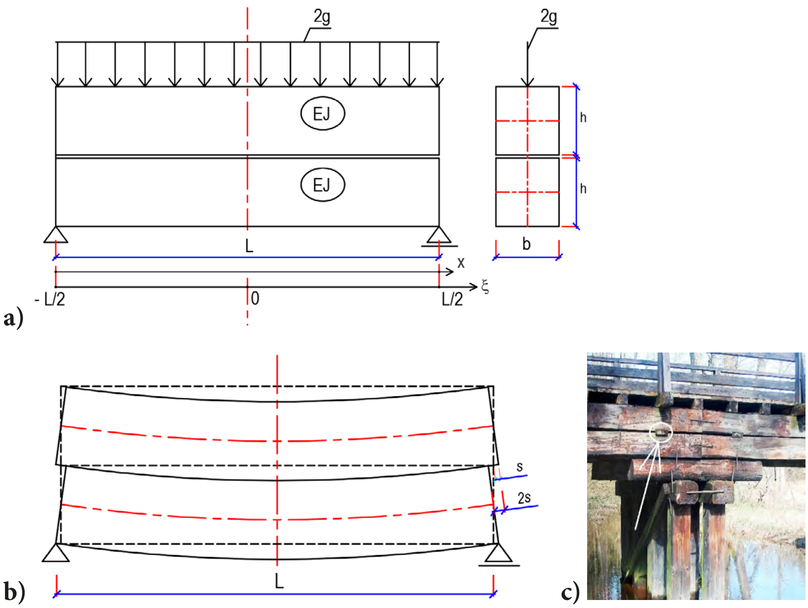

Fig. 3.3. Double beam a) initial configuration, UDL, dimensions b) actual configuration, slip measure c) timber bridge, double beam fully integrated by oak blocks

Assumptions

It is assumed that two oak logs of a simple wooden bridge are considered. The friction between the logs at the point of contact is neglected; the uplift is omitted as well. In this example, an artificial structure with a lack of integration between structural members is considered. In the case of a real timber bridge, there is almost always full integration resulting from the use of timber blocks as connectors, see: Fig. 2.3.c. The theory of linear elasticity is used. Technical parameter values can be understood as characteristic ones.

- Geometry: L = 6.0 m, b = 0.35 m, h = 0.35 m, $J = bh^3/12$.
- Material parameters: oak timber, density – 650 kg/m^3, Young's modulus E = 12 GPa = 12.E6 kP, bending limit stress value $f_{m,k}$ = 35 MPa.
- Maximum deflection u_{lim} = L/300.
- UDL value is assumed as 2g = 32 kN/m^2.

  The bending problem is examined with respect to the ξ abscissa, where

  – L/2 ≥ ξ ≤ L/2, Fig. 3.3.a.
- Due to the symmetry of the cross-section, the loading and the support of the beam, only one member of the double beam is to be analysed. The linear load density acting on a single beam is as follows:

  g = 8 kN/m. Then, one obtains

$$M(\xi)=\frac{1}{8}g\left[L^2-(2\xi)^2\right], \qquad M_{max}=M(\xi=0)=\frac{gL^2}{8}=72\,\mathrm{kNm}.$$

- The limit and maximum values of the beam deflection are given by

$$u_{lim}=\frac{L}{300}\approx 0.02\ \mathrm{m},$$

$$u_{max}=\frac{5}{48}\frac{M(\xi=0)L^2}{EJ}=0.018\ \mathrm{m}<u_{lim}.$$

– Extreme normal stresses are obtained as

$$\sigma(\xi)=\pm\frac{M(\xi)}{J}\frac{h}{2} \quad\rightarrow\quad \sigma_{max}=\sigma(\xi=0)\approx 10.08\,\mathrm{kMPa}<f_{m,k}$$

- Strains (*slip strain*)

Strain is understood here as the distribution of longitudinal strain at the interface. This distribution is also referred to as *slip strain*. Thus, one obtains

$$\varepsilon(\xi)=\frac{\sigma(\xi)}{E}=\frac{M(\xi)}{EJ}\frac{h}{2}.$$

Slip

Looking at Fig. 3.3.b, it can be seen that the maximum slip occurs at the interface at the end of the double beam. The slip consists of two components s_u (the bottom surface of the upper member) and s_b (the upper surface of the bottom member). Due to the symmetries involved, the equation $s = s_u - s_b$ occurs. The maximum slip is a sum, which in this case has the form $s_{max} = 2s$.

To find the value of s_{max}, the distribution of $\varepsilon(\xi)$ must be integrated along its domain,

$$s_{max} = 2s = 2\int_0^{L/2} \varepsilon(\zeta)d\zeta = \frac{1}{8}\frac{gh}{EJ}\left|\int_0^{L/2} \left[L^2 - (2\xi)^2\right] d\xi\right| = \frac{1}{24}\frac{ghL^3}{EJ} \approx 0.0034\,\mathrm{m}\,.$$

Conclusions from the example

- The slip is measurable.
- Analysing the values obtained, it can be concluded that in all the cases safe results were obtained with a reserve in relation to the limit values.

3.2. Classical analysis of composite girder – Newmark's concept of integration

The following chapter examines the classical approach to the theory of steel-concrete composite girders. It was first developed in the early 1920s and 1930s. At that time, the conclusions were summarized in the monograph (Ржаницын, 1948), as well as in Konrad Sattler's book (Sattler, 1953). Among recent publications the following are recommended: (Oehlers, Bradford, 1999), (Collings, 2005), and, in Polish, publications by Kazimierz Furtak (Furtak, 1999).

The assumptions for this problem are as follows:

- steel and concrete are elastic materials according to Hooke's law,
- the stiffening principle applies and, thus, the superposition method can be used,
- local stress concentrations are neglected; Saint-Venant's principle of the equality of stress fields is valid,
- (B-N) rule of flat cross-sections is basic for an initial, as well as actual configuration.

Above all, the works of Newmark et al. (Newmark, Siess, Penman, 1946), (Newmark, Siess, Viest, 1951), (Siess, Viest, Newmark, 1952) have facilitated the development of composite bridge structures. Based on the results of laboratory tests, the papers present a theory of stud connector design.

The following statement, Newmark's presupposition, is of utmost significance:

In a fully integrated beam, there is equality of curvature between the two members, the steel beam and the concrete slab.

Actually, it precisely means that there exists the equality of the curvatures of the member fibres crossing their centroids.

Fig. 3.5. shows two configurations of a steel-concrete composite beam in bending when no integration occurs. The initial configuration is marked with dashed lines – the grey one for the concrete slab, and the blue one for the steel beam. As a result of bending, both elements have been bent achieving the same curvature value of 1/ρ, marked by magenta dashed lines. The used magnification displays discontinuities occurring in two forms. The first one is a clearly pronounced *uplift*, while the other one is a *slip*.

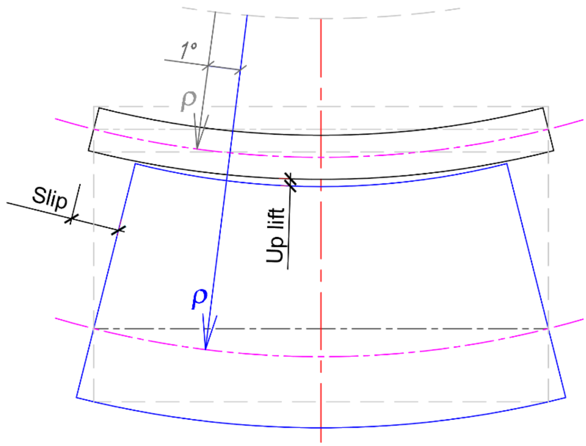

Fig. 3.5. View of a deformation of two unintegrated members where both have the same radii of curvature ρ, i.e. the curvatures of the slab and the beam are equal to each other and are 1/ρ.

In reality, in the case of full integration, the slip does not occur. Also, in the technical sense, the presupposition is admissible. By virtue of the stiffening rule and bearing in mind that the admissible flexure value of a bridge beam is L/400, where L is the span length in [m], one can measure the result of the introduced presupposition, which will be negligibly small. Therefore, assuming that Newmark's assumption is valid, it is expressed as follows

$$\left(\frac{1}{\rho_c} = \frac{M_c}{E_c J_c}\right) = \left(\frac{1}{\rho_s} = \frac{M_s}{E_s J_s}\right) . \tag{3.1}$$

Using the same method of problem analysis (Karas, 2010), Newmark's assumption can be generalised as follows

$$\left(\frac{1}{\rho_c}=\frac{M_c}{E_cJ_c}\right)=\left(\frac{1}{\rho_s}=\frac{M_s}{E_sJ_s}\right)=\left(\frac{1}{\rho_i}=\frac{M}{E_sJ_i}\right), \tag{3.2}$$

where:

- $1/\rho_c$, $1/\rho_s$, $1/\rho_i$ are, respectively, the curvature of the concrete element, the steel element, and the entire fully integrated composite girder,
- M_c, M_s(in pure bending) consist of bending moments acting on concrete and steel members and M is the total bending moment of the entire composite girder,
- E_cJ_c, E_sJ_s refer to the bending stiffness of the concrete and steel members, and E_sJ_i refers to the bending stiffness of the entire composite girder,
- J_i is the second moment of area of the integrated girder in which the concrete slab cross-section is replaced by the corresponding steel cross-section, in short, *second moment of transformed area,*
- E_s is the elastic modulus of steel (Young's modulus),
- E_c is the modulus of the elasticity of concrete and E_{cm} is the secant modulus of concrete in compression, Fig. 3.6, additionally, it is known that $E_c = 1.05\ E_{cm}$.

In the following applications E_c is understood in a general way as the modulus of the elasticity of concrete.

The secant modulus of the concrete E_{cm} concept is shown in Fig. 3.6.

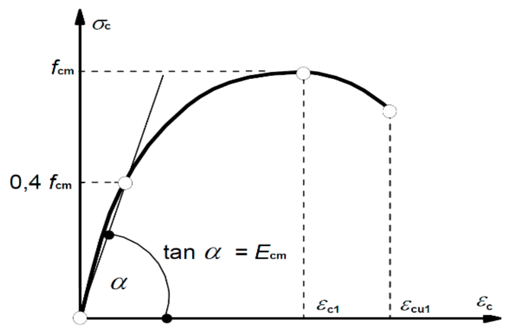

Fig. 3.6. The graph of the σ~ε model of concrete in compression (EC 1992-1-1).

Accordingly, the term *transformed composite girder* refers to a girder the cross-section of which consists of a steel beam cross-section and a concrete cross-section transformed into an adequate steel cross-section. In this sense, one can also speak of a *transformed cross-section* A_i and the *transformed second moment of area* J_i or, even more simply, the *second moment of area of a composite girder*.

In further considerations, images of the initial and current configurations are often simplified, as shown in Fig. 3.7.

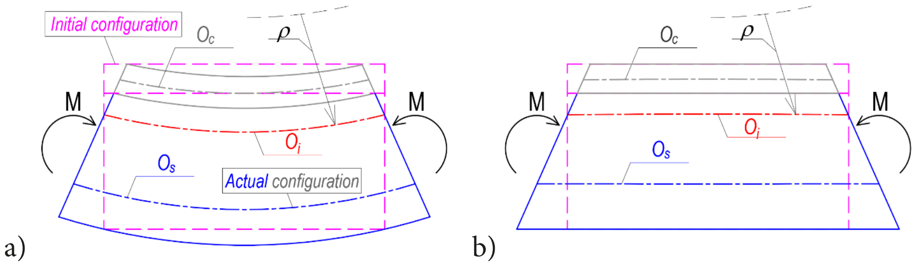

Fig. 3.7. Diagram of a poorly bent composite element a) curved lines in the actual configuration b) simplified model with straight lines

Strictly speaking, both terms are valid for pure bending but, on the other hand, the term is also used when bending with shearing occurs.

The transformation method used here has roots in early works on the reinforced concrete theory, so it is well proven and simple. It is based on the ratios of the mechanical characteristics of composite materials. In this case, the transformation is defined by the *transformation coefficient n* according to the following formula

$$n = \frac{E_s}{E_{cm}} \qquad \text{and then} \qquad b' = \frac{b_{eff}}{n}. \tag{3.3}$$

The transformation in question is shown in Fig. 3.8 where the cross-section of a concrete slab has been replaced by a corresponding steel section in light of the conditions (3.3).

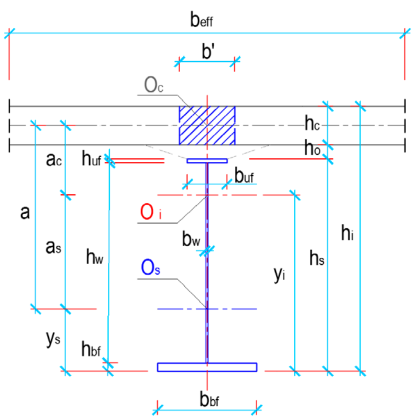

Fig. 3.8. The cross-section of a composite beam

In Fig. 3.8, the following symbols are used:

- h_c – the height of a concrete slab, which is constant in the case of the real width b_{eff} and transformed width b'; the offset area is omitted here,
- b_{eff} – the effective width, the sector of a concrete slab/plate which cooperates with the steel beam,
- b' – the width of a transformed concrete cross-section,
- h_o – the offset height,
- h_{uf} – the thickness of the upper flange of a steel plate beam,
- b_{uf} – the width of the upper flange,
- h_w – the height of a steel beam web,
- b_w – the width of a steel beam web,
- h_{bf} – the height of the bottom steel beam flange,
- b_{bf} – the width of the bottom flange,
- h_s – the total height of the steel beam,
- O_c, O_s – the centroid of concrete as well as the steel member cross-section, also the line of the member centroids when viewed from a side,
- O_i – as above, but in the case of a transformed composite girder,
- a – the distance between the centroids O_c and O_s,
- a_c – the distance between the centroids O_c and O_i,
- a_s – as above, but concerning the distance between the centroids O_i and O_s,
- y_s – the ordinate of the steel beam centroid,
- y_i – the ordinate of the transformed girder centroid.

Consequently, the following notation is used:

- A_c – area of a concrete cross-section,
- A_c' – area of a transformed concrete cross-section,
- A_s – area of a steel beam cross-section,
- A_i – transformed area of a composite girder,
- J_c – second moment of a concrete cross-section about the axis O_c,
- J_s – second moment of a steel beam cross-section about the axis O_s,
- J_i – second moment of a transformed girder about the axis O_i.

Here, the classical approach dealing with a two-dimensional problem shall be presented. Applying the (B-N) assumption of flat composite cross-sections to the initial and actual configuration involves a linear distribution of longitudinal strains, as well as of normal stresses.

In the case of shearing, a parabolic distribution of the shear stress, which follows from Bernoulli's beam theory, is assumed.

Regarding a two-dimensional problem, the set of equilibrium equations consists of three equations

$$\begin{cases} \sum | = 0 \\ \sum \_ = 0 \\ \sum M_0 = 0 \end{cases} \quad \text{or} \quad \begin{cases} \sum | = 0 \\ \sum M_0 = 0 \\ \sum M_{01} = 0 \end{cases} \quad \text{either} \quad \begin{cases} \sum M_0 = 0 \\ \sum M_{01} = 0 \\ \sum M_{02} = 0 \end{cases}, \tag{3.4}$$

where

$\sum |$ is understood as the sum of all force projections onto the vertical direction,

$\sum \_$ is the sum of all force projections onto the horizontal direction.

$\sum M_0$, $\sum M_{01}$, $\sum M_{02}$ are the sum of the vector products of all the forces in the plane in relation to any set of the points O, O_1, O_2 of the plane, however, points must not be collinear.

Let us adopt one more simplification. In the following derivations, the offset concrete area A_o is omitted, although its height h_o is taken into consideration. The offset area is insignificant compared to the rectangular concrete cross-section, while the height h_o has a share in the third power, when the second moment of area J_i is determined. Such an assumption results in a slightly decreased value of J_i and can be regarded as a *secure design*.

Following the characteristics introduced in Fig. 3.8, the geometrical parameters of a composite girder can be calculated in the following way

3.2.1. Step-by-step calculation of normal stresses due to pure bending by moment M

Using the above notation and the geometry shown, the following steps can be performed.

- Concrete and transformed concrete areas

$$A_c = b_{eff} h_c, \quad A'_c = \frac{b_{eff}}{n} h_c = \frac{A_c}{n}, \qquad A_i = A'_c + A_s. \tag{3.5}$$

- Second moment of concrete and transformed concrete cross-sections

$$J_c = \frac{b_{eff} \left(h_c\right)^3}{12}, \qquad J'_c = \frac{b_{eff}}{n} \frac{\left(h_c\right)^3}{12} = \frac{J_c}{n}. \tag{3.6}$$

It is assumed that the area A_s, the second moment of area J_s, and the ordinate value of the centroid y_s of steel can be easily calculated.

- Centroid of J_i

The key objective of the analysis is determining the second moment of a composite cross-section. The first step is to find the ordinate y_i of the centroid O_i. Assuming a horizontal line on the bottom level of the bottom steel flange as a reference, one can determine the first moment of area in relation to it:

$$S_{1-1} = A'_c \left(h_s + \frac{h_c}{2} \right) + A_s y_s \tag{3.7}$$

Hence, the centroid ordinate is

$$y_i = \frac{S_{1-1}}{A_i}. \tag{3.8}$$

- Second moment of a transformed girder cross-section

Then, by virtue of Huygens [4]– Steiner [5] theorem, also known as *the parallel axis theorem*, the second moment of area can be written as follows:

$$J_i = J'_c + J_s + A_s (a_s)^2 + A'_c (a_c)^2 = J'_c + J_s + a^2\lambda^2, \quad \lambda^2 = \frac{A'_c A_s}{A_i} \tag{3.9}$$

Let us discuss the components of the moment of inertia. The moment of inertia is the sum of three components, equation (3.4.1). The first two components give the moments of inertia for two unconnected elements (no integration). Therefore, the third component $a^2 \lambda^2$ can be thought of as the result of the integration of the elements or, in other words, as a *measure of integration*. In general, it is preferable to use relative measures rather than absolute measures because they provide a way to express the evaluation as a percentage. Let us suppose, therefore, that the relative measure will have the following ratio:

$$\mu_i = \frac{a^2\lambda^2}{J'_c + J_s}. \tag{3.10}$$

- Normal stresses and their distribution along the composite girder height

Given that this method deals with pure bending, normal stresses for a plain problem are very simple to obtain. It is sufficient to find the normal stresses at the extreme points of the sections, i.e., at the upper and bottom fibres of a transformed concrete and steel, i.e. σ'_{uc}, σ'_{bc}, and σ_{us}, σ_{bs}.

[4] Christiaan Huygens (1629–1695), Dutch mathematician and scientist, astronomer, physicist.
[5] Jakob Steiner (1796–1863), Swiss geometer.

$$\sigma'_{uc} = \frac{M}{J_i}\left(a_c + \frac{h_c}{2}\right), \qquad \sigma'_{bc} = \frac{M}{J_i}\left(a_c - \frac{h_c}{2}\right) \quad , \tag{3.11}$$
$$\sigma_{us} = \frac{M}{J_i}\left(h_s - y_i\right), \qquad \sigma_{bs} = \frac{M}{J_i} y_i$$

where M is a total bending moment acting on a composite girder.

Stresses in transformed concrete must be retransformed to real concrete which simply means that they must be divided by n as follows

$$\sigma_{uc} = \frac{\sigma'_{uc}}{n}, \qquad \sigma_{bc} = \frac{\sigma'_{bc}}{n} \tag{3.12}$$

Finally, the graph of a normal stress distribution in Fig. 3.9 shows a linear effect as a result of the assumptions adopted at the beginning of the analysis. The graph can also be used to verify the obtained results.

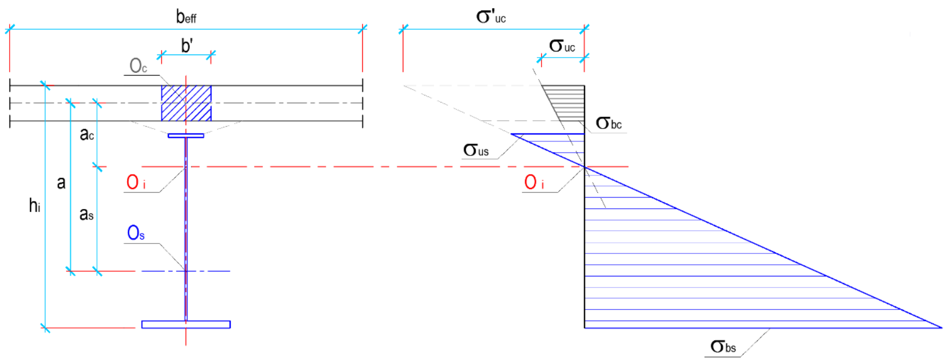

Fig. 3.9. Normal stress distribution in a composite girder section taking into account normal stresses in the concrete.

The stress distribution diagram has a *step* at the joint, contrary to the strain distribution, which, according to the B-N assumption, is a continuous line across the height of the girder cross-section.

- Shear stresses and delaminating force

In the case of a steel-concrete composite girder, the shear stresses at the interface between concrete and steel are the subject of analysis. It is at the interface that the connectors joining the steel beam to the concrete slab are installed. The appropriate surface to determine the delaminating force is the top flange of the steel beam. The value of the delaminating force is equal to $\tau b_{uf} e$, where

$$\tau = T\frac{\bar{S}_i}{J_i b_{uf}} = T\frac{A'_c a_c}{J_i b_{uf}}, \tag{3.13}$$

and T is the internal shear force in the cross-section, $\bar{S}_i$ is the first moment of area of the transformed concrete cross-section with respect to the horizontal axis intersecting the centroid O_i and has the following form

$$\bar{S}_i = A'_c a_c . \tag{3.14}$$

Finding the delaminating force Q is essential for joint design. Integrating the shearing stress τ of the upper steel flange surface one obtains

$$Q = \int_{A_{\text{upper flange}}} \tau\, dA = b_{uf}\int_{x_0}^{x_1} \tau\, dx \rightarrow Q = |\tau|_{max}(x_1 - x_0) b_{uf} = (x_1 - x_0)\frac{|T|_{max}}{J_i}\bar{S}_i \,, \tag{3.15}$$

where b_{uf} = const., $(x_1 - x_0) = e$ is a chosen representative length at which the internal shear force T attains its extreme value; the length is usually assumed to be $e = 1$ m.

3.3. Distribution of bending moment M on the members of a composite girder

This is another approach to composite girder analysis. It is more general and, consequently, can be applied to more complicated cases of action effects.

The same assumptions as before are valid, however, now, the primary role is played by the (B-N) assumption of flat cross-sections in the initial and actual configurations. Fig. 3.1 shows the mechanism of the problem. Still, an infinitesimal section of the girder of the length *d*x is analysed here. The curvature of a composite girder is symbolised by φ which is defined as

$$\varphi' = \frac{d\varphi}{dx} \approx \frac{d^2 w}{dx^2} = \frac{1}{\rho_i} = \frac{M}{E_s J_i}, \tag{3.16}$$

where w is a deflection at the analysed point of a girder.

Now, the expression (3.2) can be rewritten in the following form

$$\varphi'_c = \varphi'_s = \varphi'_i \;\rightarrow\; \varphi' = \varphi'_i . \tag{3.17}$$

Comment

It is worth mentioning that in a variant of finite analysis i.e. when the length of the girder section is 1m, for instance, one obtains φ instead of φ', but, at this moment, one loses the possibility to use the simple uniaxial strain concept.

Fig. 3.10 shows the effect of the B-N assumption on the strain distribution in a real composite girder, where a real concrete slab and a steel beam are bent. On the left side of the infinitely small excerpt, the bending moment M acts and on the right side the linear strain distribution causing partial shifts and rotations of the real elements. These shifts and rotations result from the action of the respective normal forces N_C, N_S and torques, in this case, the bending moment M_C, M_S. The common curvature φ' is clearly visible.

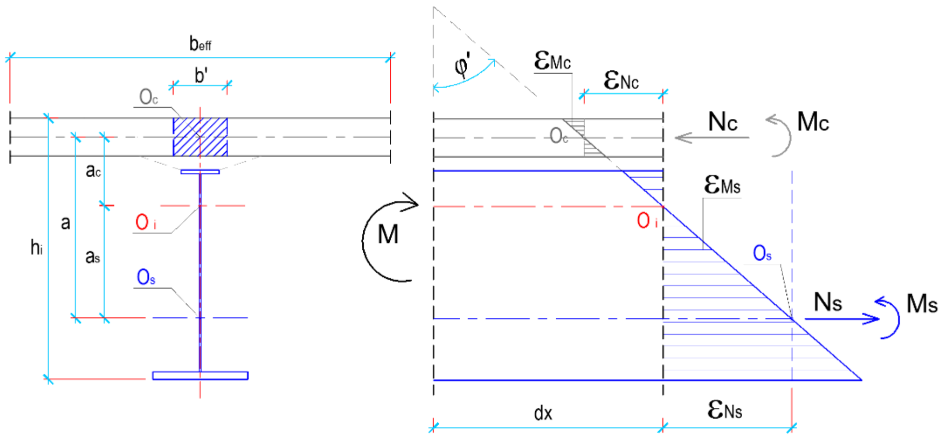

Fig 3.10. The bending moment distribution in composite girder elements

Comment to Fig. 3.10.

From the analysis of an infinitesimally small section of a deformed composite beam it follows that the curvature φ' is constant for each horizontal fibre, i.e. not only in the cases of $\varphi'_C = \varphi'_S = \varphi'_i$. Therefore, Newmark's assumption is the only possible option.

The derivation can be conceived schematically as a sequence of the following steps:

- the interaction of a set of the internal forces N_C, M_C, N_S, M_S, leads to the same result as for a fully integrated composite girder,
- the internal forces N_C, M_C act on real concrete – *here, transformed concrete is not dealt with,*
- in other words, the result coincides with the bending moment action when connectors are present at the interface.

The mechanism bases on the superposition of shifts caused by the normal forces N_c, N_s and rotations effects due to the M_c, M_s actions. In both cases the faces of concrete and steel sections were shifted and rotated.

Therefore, the force N_c causes a horizontal shift of the concrete face by a length ε_{Nc}. Next, the moment M_c rotates the concrete face by φ'. The geometrical effect of this rotation is given by the strain ε_{Mc} distribution shown in Fig. 3.10. Consequently, the same mechanism exists in the case of a steel element.

Having the values of internal forces, one can use the equation set of equilibrium which now has the following form

$$\begin{cases} \sum | = 0: & \text{is not applied} \\ \sum \_ = 0: & N_c = N_s = N \\ \sum M_{Os} = 0: & M = M_c + M_s + Na \end{cases} . \tag{3.18}$$

Further analysis can be performed in various manners. Let us assume the simplest one. Based on the constitutive relation – in this case it is sufficient to assume Hooke's law – one can write

$$\varepsilon_{Nc} = \frac{\sigma_c}{E_c} = \frac{N_c}{E_c A_c} = a_c \varphi_c^{/}, \tag{3.19.1}$$

and

$$\varepsilon_{Ns} = \frac{\sigma_s}{E_s} = \frac{N_s}{E_s A_s} = a_s \varphi_s^{/}, \tag{3.19.2}$$

One arrives at

$$\varepsilon_{Nc} + \varepsilon_{Ns} = a\varphi^{/} = N\left(\frac{1}{E_c A_c} + \frac{1}{E_s A_s}\right) = \frac{1}{\lambda^2}\frac{N}{E_s}, \tag{3.19.3}$$

And, hence, the moment Na is defined as

$$Na = \varphi^{/} E_s \left(a\lambda\right)^2, \tag{3.20}$$

And by virtue of (3.16), finally the following is obtained

$$Na = M\frac{\left(a\lambda\right)^2}{J_i}. \tag{3.21.1}$$

The values of the bending moments M_c and M_s are easy to find by means of Newmark assumption (3.2), as follows

$$M_c = M\frac{J'_c}{J_i}, \qquad M_s = M\frac{J_s}{J_i}. \tag{3.21.2-3}$$

Approaching the conclusion, let us recall the formulae (3.9), (3.18.3) and (3.21.1-3) in explicit form as follows

$$J_i = J'_c + J_s + (a\lambda)^2$$

$$M = M_c + M_s + Na$$

$$M_c = M\frac{J'_c}{J_i} \qquad M_s = M\frac{J_s}{J_i} \qquad Na = M\frac{(a\lambda)^2}{J_i}$$

Now, the conclusion is clearly obvious and can be expressed as follows:

The distribution of the bending moment M over the internal moments M_s, M_c and Na acting on the members of the composite girder is determined by the ratio of each component of the sum of Ji (J'_c, J_s and $(a\lambda)^2$) to the sum of Ji multiplied by the value of M.

Normal stresses are to be calculated using the sum of bending action and tension/compression action as follows

$$\sigma = \pm\frac{N}{A} \pm \frac{M}{J}y \tag{1.26.1}$$

Hence, according to Fig. 3.10, for concrete one has

$$\sigma_{uc} = -\frac{N}{A_c} - \frac{M_c}{J_c}\frac{h_c}{2}, \qquad \sigma_{bc} = -\frac{N}{A_c} + \frac{M_c}{J_c}\frac{h_c}{2}, \tag{3.22.1-2}$$

And for steel, respectively

$$\sigma_{us} = \frac{N}{A_s} - \frac{M_s}{J_s}(h_s - y_i), \qquad \sigma_{bs} = \frac{N}{A_s} + \frac{M_s}{J_s}y_i, \tag{3.22.3-4}$$

where minus " – " denotes compression.

Let us note that the stress results obtained from (3.11) relations and (3.22.3-4) conform fully. Bearing in mind Hooke's law, strains can be calculated immediately.

In summary, solving the bending problem of a composite girder involves the following sequence of steps:

- determination of the transformation factor n which enables the replacement of the concrete cross-section with an adequate steel section – $n = \frac{E_s}{E_{cm}}$,
- knowledge of the bending moment M,
- determination of the composite cross-section characteristics – A_S, A_C, A'_C, J_i,
- establishing values of internal moments and the force acting on the members of a composite girder – M_S, M_C, N,
- determination of normal stresses at vital points of the composite girder cross-section using formulae (3.22.1-4) and strain distribution shown in Fig. 3.10 – σ_{uc}, σ_{bc}, σ_{us}, σ_{bs},
- deflection of the composite girder due to the moment M – $u_M = \frac{5}{48} \frac{M(L_t)^2}{E_{cm} J_i}$.

The +/- signs in the equations (3.11) result from the strain distribution shown in the cross-section of the composite girder under the assumption of a flat cross-section (B-N), Fig. 3.10.

3.4. Normal force distribution in composite girder elements

When a composite girder is subjected to tension, the distribution of the normal force N in the composite girder members results from the equality of the member strain values. Fig. 3.11 shows the mechanism of this distribution.

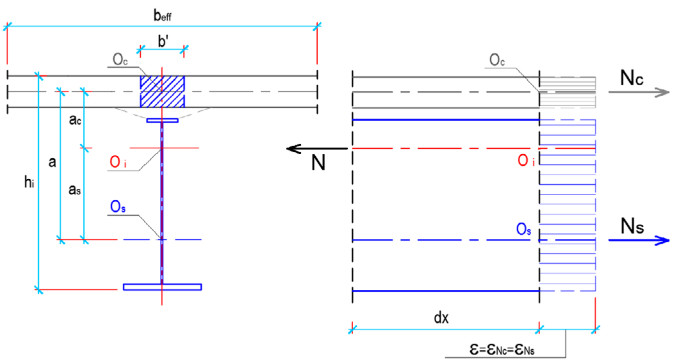

Fig. 3.11. Distribution of the axial force N in composite girder members

This is a relatively simple task, therefore, the result is given without derivation, although the reader is advised to carry out the relevant analysis by themselves using the drawing in Fig. 3.11. Finally, one obtains

$$N_s = N\frac{A_s}{A_i}, \quad N_c = N\frac{A'_c}{A_i}. \tag{3.23}$$

Basing on (3.5.3), i.e. $A_i = A'_c + A_s$ the following conclusion seems natural:

The distribution of the axial force N onto the internal normal forces N_c and N_s which act on composite girder members, is determined by the ratio of the area value of each member (A_c and A_s) to the value of A_i, which is multiplied by N, according to (3.23).

Comment regarding further derivation

In the subsequent calculation phases of the composite girder, the method of the effective modulus of the elasticity of concrete is used.

The most obvious case has already been used above, i.e. the secant modulus of concrete denoted as E_{cm} (or variant E_c), from which the transformation factor n (often denoted as n_0) is derived.

In the case of the concrete shrinkage of a slab element, there is an effective modulus denoted E_{c_sh} and $n_{\_sh}$, respectively.

Similarly, the effective modulus E_{c_creep}, associated with the transformation factor $n_{\_creep}$, will be used to account for the creep effects of the concrete slab.

3.5. Composite girder – shrinkage of the concrete slab

The shrinkage of concrete is a complicated and interdisciplinary problem, (Bažant, 1975), (Bažant, Wittmann, 1982), (Heath, Roesler, 1999), (Holt, 2001).

In short, the concrete mix (cement concrete before setting) has a larger volume than the concrete formed after setting.

Concrete is formed by the binding of cement particles to the mixing water. This involves the autogenous shrinkage of concrete, which can vary depending on the water to cement ratio (w/c). Autogenous shrinkage is significant when w/c < 0.4, resulting in shrinkage cracks in the concrete. The evaporation of unbound water from concrete causes drying shrinkage. Drying shrinkage is caused by the exchange of moisture between the concrete and the environment. Simply put, if the concrete is tightly sealed, drying shrinkage does not occur.

Thus, it is assumed that there are two sources of shrinkage: the hydration process of cement and the evaporation of unbound water in the hydration process.

There are phases to shrinkage – it is very intensive during the concrete mortar setting and hardening, although it continues over the next 3 years. Shrinkage causes micro cracks, which, due to a service load action, can develop to cracks that cause degradation of concrete. The process is not beneficial to concrete structures. The shrinkage process is not uniform – it occurs apparently in the external areas of solid concrete. Here, the problem is treated as a medium case, i.e. the whole concrete volume shrinks uniformly.

As far as the Eurocodes are concerned, there are two reference documents, namely (EN 1992- Part 1-1) and (EN 1994-2 Part 2).

In EN 1992-1-1 (3.8), the total shrinkage ε_{cs} is given by the formula

$$\varepsilon_{cs}(=\varepsilon_{sh})=\varepsilon_{ca}+\varepsilon_{cd} \quad ^{6}, \tag{3.24}$$

where ε_{ca} is autogenous shrinkage, ε_{cd} is drying shrinkage. Formulas and references for determining ε_{cs} can be found in section 3.1.4.

References to EN 1992 can be found in the bridge standard EN 1994-2.

Effect of concrete slab shrinkage

In the classical approach, the effective modulus of concrete is calculated according to the following formula

$$E_c \to E_{c,sh}=\frac{E_{cm}}{1+\psi\left(\infty,t_0\right)}, \tag{3.25}$$

where, generally in an open area, $\psi = 1.5$(see: Johnson, Buckby (1979), ACI (2005)).

3.5.1. Initial and actual configuration appropriate for shrinkage

The crucial element of this derivation is to understand the idea of initial configuration. To start with, it is assumed that the composite girder elements, i.e., the concrete slab and the steel beam, are not integrated. In this situation, shrinkage only affects the concrete slab as an unconfined process. The effect of shrinkage along the height of the concrete slab is neglected. The result can be seen in Fig. 3.12.a, where the strain ε_{sh} has occurred at a distance dx. The steel beam remains unchanged. *This is the initial configuration.*

Still, in reality, the connection at the interface exists and constitutes a case of full integration. Assuming planar cross sections (B-N), no other form of deformation than the one shown in Fig. 3.12.b is possible, which corresponds to the *actual configuration* in the process under study.

[6] In this study, total shrinkage is denoted by the symbol ε_{sh}.

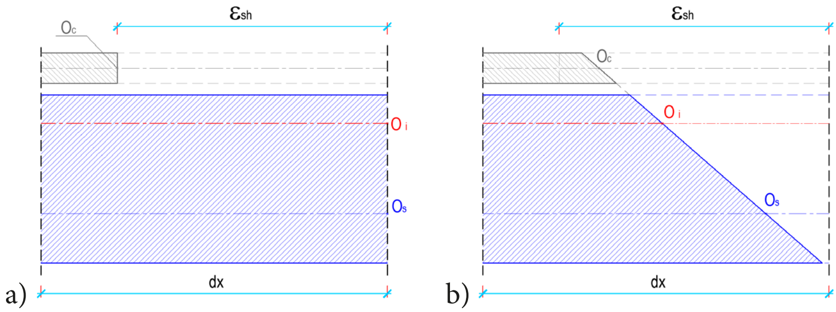

Fig. 3.12. Model of shrinkage a) initial configuration b) actual configuration

3.5.2. Strain distribution as a result of the flat cross-section assumption. Solution to the problem

Now, it is necessary to apply the internal forces N_C, M_C, N_S and M_S to the concrete and steel sections in the initial configuration to obtain the actual configuration. This is shown in Fig. 3.13.

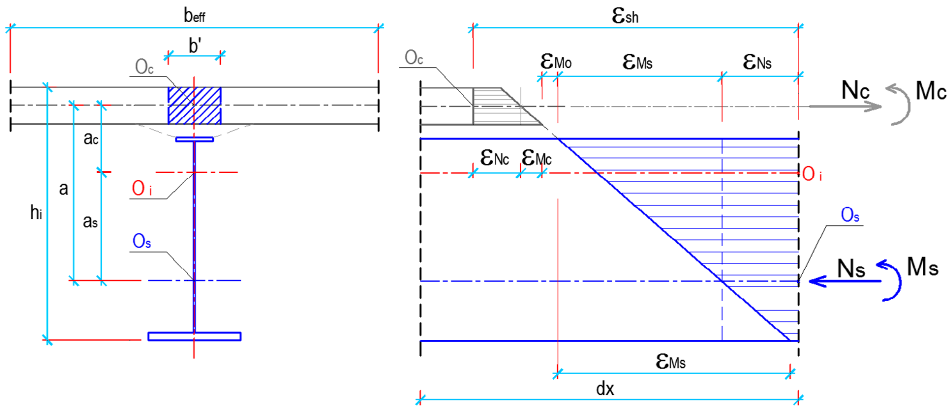

Fig. 3.13. Strain distribution and internal forces in the shrinkage process

Again, a force implies a shift while a rotational moment results in the inclination of a section, faces of concrete, and steel, independently. It is worth noticing that *shrinkage causes stretching in concrete* and compression of the bottom fibres of steel beam.

Having established the forces, one can write the equilibrium equations appropriate for the plain problem

$$\begin{cases} \sum | = 0: & \text{is not applied} \\ \sum\_ = 0: & N_s = N_c = N \\ \sum M_{Os} = 0: & 0 = M_s + M_c - Na \end{cases} \quad . \tag{3.26}$$

Newmark's presupposition is useless because it leads to a trivial solution. In this case, the problem is statically indeterminate. It is necessary to formulate an additional condition which in terms of elasticity is known as compatibility relation. Basing on Fig. 3.13, in the interface there are as follows

$$\begin{aligned} &\varepsilon_{sh} = \varepsilon_{Nc} + \varepsilon_{Mc} + \varepsilon_{Mo} + \varepsilon_{Ms} + \varepsilon_{Ns} = \\ &= (\varepsilon_{Nc} + \varepsilon_{Ns}) + (\varepsilon_{Mc} + \varepsilon_{Mo} + \varepsilon_{Ms}) = \varepsilon_N + \varepsilon_M \end{aligned} \quad . \tag{3.27}$$

By virtue of Hooke's law, one arrives at

$$\varepsilon_N = N\left(\frac{1}{E_c A_c} + \frac{1}{E_s A_s}\right) = \frac{N\lambda^2}{E_s} . \tag{3.28}$$

While in the case of ε_M, based on deformed configuration geometry, the following is obtained

$$\varepsilon_M = \varphi' a. \tag{3.29}$$

Now, using the (3.26.3) $M_s + M_c = Na$ and Newmark's assumption in the form of a modified relation (3.17)

$$M_s = \varphi' E_s J_s \quad \text{and} \quad M_c = \varphi' E_c J_c, \tag{3.30}$$

The curvature is as follows

$$\phi' = \frac{1}{E_s} \frac{Na}{J'_c + J_s} . \tag{3.31}$$

Using (3.27), (3.28) and (3.31) one has

$$\varepsilon_{sh} = \frac{N}{E_s} \frac{1}{\lambda^2} \frac{J_i}{J'_c + J_s} \tag{3.32}$$

And, hence,

$$M_s = \varepsilon_{sh} E_s \lambda^2 a \frac{J_s}{J_i}, \qquad M_c = \varepsilon_{sh} E_s \lambda^2 a \frac{J'_c}{J_i}, \qquad Na = M_s + M_s = \varepsilon_{sh} E_s \lambda^2 a \frac{J'_c + J_s}{J_i}$$

(3.33.1-3)

Therefore, of course

$$N = \varepsilon_{sh} E_s \lambda^2 \frac{J'_c + J_s}{J_i} . \qquad (3.33.4)$$

The set of the formulae (3.33.1-4) concludes the derivation of the shrinkage problem solution.

All in all, the expected conclusion is not simple, although possible. The actual configuration, shown in Fig. 3.13.b, overlaps with the actual configuration in the case of poor bending shown in Fig. 3.10.

Comment

Planar geometry is of great virtue. If geometrical effects are analogous, then actions must also be analogous. So, there is a bending moment M_{sh} analogous to the bending moment M, Fig. 3.10.

This allows the expression $\varepsilon_{sh}E_s\lambda^2 a$ *to be treated as an appropriate, but fictional, bending moment.*

Hence, based on the above comment, one can write

$$M_{sh} = \varepsilon_{sh} E_s \lambda^2 a , \qquad (3.34)$$

If so, it yields the following

$$M_{s\_sh} = M_{sh} \frac{J_s}{J_i} , \qquad M_{c\_sh} = M_{sh} \frac{J'_c}{J_i} , \qquad N_{-\,sh} a = M_{sh} \frac{J'_c + J_s}{J_i} , \qquad (3.35.1\text{-}3)$$

Since this is the case, the formulas (3.21.1-2) are analogous to the formulas (3.35.1-2), while the relations (3.21.3) and (3.35.3) are not analogous due to the different form of the equilibrium equations (3.18.3) and (3.26.3).

3.5.3. Normal stresses distribution

The value of ε_{sh} is the key to use in the design practice. This value can be taken from *shrinkage versus time* graphs which are commonly found in technical literature regarding concrete, e.g. (Bazant, 2001). In a simplified procedure, the following estimation of the value ε_{sh} can be used:

- 2E-4 – after 14 days of concrete hardening,
- 4E-4 – after 28 days,
- 5E-4 – as a limit value.

Fig. 3.13 and the relations (3.35) can be used to determine normal stresses at relevant points in the cross-section of the girder.

For the upper and bottom fibres of the concrete slab there are

$$\sigma_{uc} = +\frac{N_{\_sh}}{A_c} - \frac{M_{c\_sh}}{J_c}\frac{h_c}{2}, \qquad \sigma_{bc} = +\frac{N_{\_sh}}{A_c} + \frac{M_{c\_sh}}{J_c}\frac{h_c}{2} \qquad (3.36.1\text{-}2)$$

And for the upper fibres of the top flange and the lower fibres of the bottom flange of the steel beam the result is as follows:

$$\sigma_{us} = -\frac{N_{\_sh}}{A_s} - \frac{M_{s\_sh}}{J_s}\left(h_s - y_i\right), \qquad \sigma_{bs} = -\frac{N}{A_s} + \frac{M_s}{J_s} y_i \,. \qquad (3.36.3\text{-}4)$$

The signs in front of the components in the formulae for normal stresses follow directly from the returns of force and moment in Fig. 3.13.

When carefully reading the graph of the deformed body, Fig. 3.13, one can see the strain and stress distribution along the girder height. To complete the analysis, a graph of the variation of normal stresses in the cross-section of the composite girder is added below, Fig. 3.14.

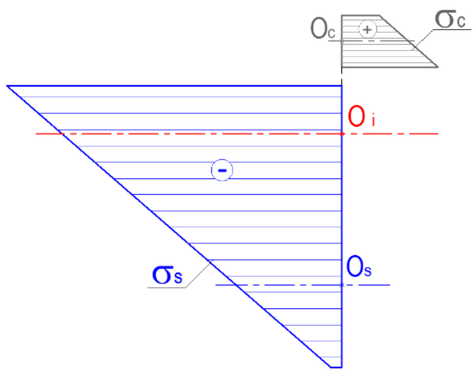

Fig. 3.14. Normal stresses distribution due to shrinkage, " + " for tension

Comment:

Commenting on the diagram in Fig. 3.14, it should be emphasised that the concrete is in tension and the steel in compression in the vicinity of the interface. The characteristic element of the graph is a *step* in the stress distribution in the interface. The step also signifies the reversal of the stress sign.

The search for normal stress values shall be performed as follows:

- coefficient of transformation $n_{sh} = \frac{E_s}{E_{c\_sh}}$,
- bending moment caused by shrinkage of a concrete member – $M = M_{sh}$,
- geometrical characteristics of the composite girder cross-section – A_S, A_C, A'_C, J_i,
- internal forces acing on composite girder members – M_{S_sh}, M_{C_sh}, $N_{_sh}$a,

- normal stresses based on the formulae (3.27), the deflection due to the moment M_{sh}

$$u_{sh} = \frac{5}{48} \frac{M_{sh} (L_t)^2}{E_{c\_sh} J_i}. \tag{3.37}$$

The same mechanism occurs in the case of expansive types of concrete (expansive cements) and in the task of uniform cooling of a concrete slab.

3.6. Another approach to the shrinkage problem (force method)

The initial configuration shown in Fig. 3.12 can also be drawn for finite dimensions (not infinitely small) see (Sattler, 1953). Here, however, the focus is on the work of H.W. Birkeland (Birkeland 1960) who listed three stages, which are discussed in detail. The drawings in Fig. 3.15 are copied from Birkeland's work.

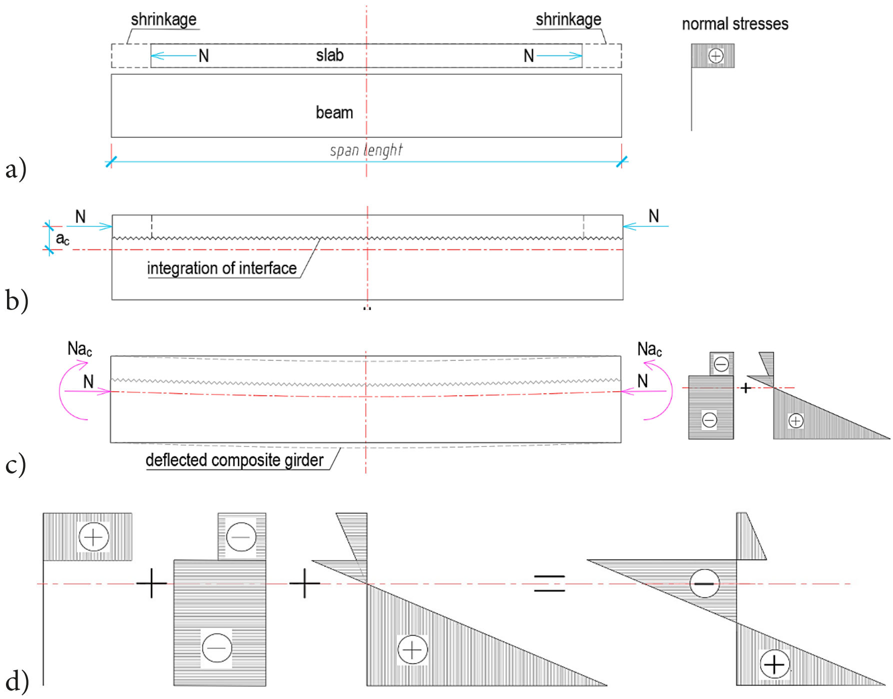

Fig. 3.15. Birkeland's stages of the cancellation of the effect of shrinkage a) initial stage – unconfined slab shrinkage which is reduced by tensile forces applied to the concrete slab centroids b) final stage after the member integration c) alternative final stage supplemented by adding the view of composite girder deflection d) summation of normal stresses

Let us discuss Birkeland's concept. Subsequent patterns that occur are not numbered. The value of the normal force N can be easily calculated when the shrinkage strain is known. The following can be then obtained

$$N = \varepsilon_{sh} E_c A_c$$

Due to *unconfined (free) shrinkage*, the length of the concrete slab is shortened. At this point the key element of the theory is introduced – the external tensile force N is applied in such a manner that the length of the previously shrunken slab becomes equal to the length of the steel beam.

In this state of the forced elongation of the slab, the concrete slab is integrated with the steel beam to form a composite girder.

The introduced tension state of the concrete slab now acts on the composite girder, and at the same time there is a change in the direction of the force N applied further through the centroid of the concrete slab – now, the force N compresses and bends the entire composite girder.

The displacement of the force N towards the centre of the composite girder involves the bending moment $M = N a_c$. This allows the problem to be treated as the sum of pure bending and compression.

Comment:

Fig. 3.15.c shows the deflection of a composite girder that is caused by shrinkage of the concrete slab. Considering that shrinkage is part of chemical (cement hydration) and physical (moisture changes in concrete pores) processes, it ultimately leads to flexure as a permanent action. In other words, it causes concrete creep.

This method is also used for shrinkage when the slab is cast in sections, (Johnson, Buckby 1979).

3.7. Cooling the concrete slab

Let us assume that the concrete slab has been cooled uniformly. The vertical cooling depletion of the concrete height can be omitted. The longitudinal strain can be calculated from the following data

- $\alpha_T = 9.8E-6\ \frac{1}{K} \approx 1.0E-5\ \frac{1}{K}$ – the coefficient of concrete thermal expansion,
- $\Delta T = \left[10-(-20)\right] = 30\ K$ – seasonal temperature amplitude,
- $\varepsilon_{temp} = \alpha_T\, \Delta T = 1.0E-5 \cdot 30 = 3.0E-4$.

Now, by means of the formulae (4.1.33), (4.1.34.1-3) regarding shrinkage, one can determine the normal stresses during thermal shortening of the reinforced concrete slab caused by the ε_{temp} strain. One should only replace the ε_{sh} in the ε_{temp} and use the following relations

$$M_{temp} = \varepsilon_{temp} E_s \lambda^2 a \quad , \tag{2.25.1}$$

$$M_s = M_{temp} \frac{J_s}{J_i}, \quad M_c = M_{temp} \frac{J'_c}{J_i}, \quad Na = M_{temp} \frac{J'_c + J_s}{J_i}. \tag{2.25.2-4}$$

In this case, the value of the modulus $E_c = E_{cm}$ remains unchanged and the normal stress values can be found using the equations (2.25.1-4). The cooling of the concrete slab is a transient process and does not cause any creep of the slab.

3.8. Creep effect of the concrete slab

Creep and *relaxation* are rheological processes described by visco-elasticity or visco-plasticity theories. Both processes are elements of rheology where the term rheology[7] is after Greek philosopher Heraclitus's *πάντα ῥεῖ – 'everything flows'. πάντα ῥει was used as the motto of the Rheological Society founded in 1929.*

Relaxation process is a time dependent process of stresses weakening in the body subjected to forced permanent deformation**.**

The best example is a prestressing cable that is stretched and then attached at its ends to a concrete beam. The loss of stresses in cable wires is a classical relaxation problem.

Creep is the process of creating deformation/displacement over a long period of time as a result of a constant load.

In engineering technology and design, the work of the 1960s has made significant contributions. At the same time, the rheology of concrete has been the subject of continuous research with the use of contemporary testing methods, (Nowacki, 1963), (Blaszkowiak, 1958), (Zerna, Trost, 1967), (Trost, 1968), (Bazant, Wittmann, 1982), (Partov, Kantchev, 2007).

The reader can find information on rheology, rheological models and applications of the Laplace Transform in Chapter 13.

All materials used in building engineering are subjected to creep, especially concrete, (Roussel, 2012).

[7] The word *rheology* is composed of the Greek words *rhéos* – 'something flowing' and ñology – 'study'.

In the case of a composite girder, the concrete slab is under constant compression due to dead weights. Therefore, creep constitutes an important element of design. Although, in the classical approach, the action is not extensive and the problem boils down to taking account of creep by introducing the effective modulus E_{c_creep} as a function of time and humidity. In the Eurocodes (EN 1992-1-1) the characterization of shrinkage is quite extensive – it is presented in the closing section of this chapter. Also basing on the information contained there, one can relate creep to the type of loading, shrinkage and prestressing of concrete by means of the following expression

$$n = n_0\left(1+\psi_L\varphi_t\right), \tag{3.29}$$

where $\varphi_t = \varphi(t, t_0)$ is a creep factor, $\psi_L$refers to different situations and takes the following values: 1.1 for permanent loads, 0.55 for primary and secondary effects of shrinkage, 1.5 for prestressing.

From a mechanistic point of view, such a formulation is not clear enough. For this reason, the classical formulation proposed by Heinrich Trost can be adopted for creep

$$E_{c\_eff} = \frac{E_{cm}}{1+\varphi(t,t_0)} \xrightarrow{\lim} \frac{E_{cm}}{1+\varphi(\infty,t_0)}, \tag{3.30}$$

where φ (t, t_0) the creep coefficient relevant to the load application at a t_0 moment and time interval (t, t_0), t is a current time value.

It is worth mentioning that in the case of bridges exposed to environmental impacts, the following relation is applied

$$E_{c,creep} = \frac{E_{cm}}{1+\varphi}, \text{ where } \varphi = 2. \tag{3.31}$$

On the other hand, the search for $\varphi(t, t_0)$ is included in Annex B of (EN 1992-1-1) as follows but without numbering

$$\varphi(t,t_0) = \varphi_0\ \beta_c(t,t_0),$$

where

$$\varphi_0 = \varphi_{RH}\,\beta_c(f_{cm})\,\beta(t_0), \qquad \phi_{RH} = \left[1+\frac{1-RH/100}{0.1\left(h_0\right)^{1/3}}\alpha_1\right]\alpha_2,$$

$$\beta(f_{cm}) = \frac{16.8}{\sqrt{f_{cm}}}, \qquad \beta(t_0) = \frac{1}{0.1+(t_0)^{1/5}}$$

$$h_0 = \frac{2A_c}{u}, \qquad \beta_c(t,t_0) = \left(\frac{t - t_0}{\beta_H + (t - t_0)} \right)^{0.3},$$

$$\beta_H = 1.5\left[1 + (0.012RH)^{18}\right] h_0 + 250\alpha_3 \le 1500\alpha_3, \qquad \alpha_3 = \sqrt{\frac{35}{f_{cm}}}.$$

The two creep estimates are convergent.

The following sequence of calculations needs to be performed when searching for normal stress values:

- coefficient of transformation $n_{creep} = \frac{E_s}{E_{c\_creep}}$,
- bending moment caused by dead loads acting on a composite girder $M = M_{d.l.}$
- geometrical characteristics of the composite girder cross-section – A_S, A_C, A'_C, J_i,
- internal forces acing on composite girder members – M_S, M_C, N, (Na),
- normal stresses based on the formulae (3.21),
- the deflection due to the moment M and $E_{c,eff}$ or E_{c_creep} can be calculated as follows

$$u_{creep} = \frac{5}{48} \frac{M_{d.l.} (L_t)^2}{E_{c,creep} J_i}. \tag{3.32}$$

Finally, the reader's attention is recommended to a paper (Machelski, 2022) that deals with the deformation analysis of composite bridges by measuring and modelling the girder curvature under the influence of concrete deck slab creep.

4. Shear connectors

Wooden bridges with multi-span girders use different types of connectors, e.g. wooden dowels, blocks, steel rods and skilfully shaped steel plates; concrete or reinforced concrete has also been used to form connectors. Wood technology expertise has been applied to steel-concrete composite bridges, while connectors have changed significantly. Nowadays, considerable financial resources are devoted solely to the study of composite bridge connectors – there is, in fact, a scientific sub-discipline devoted to such connectors, which continues to undergo dynamic development.

4.1. Rigid connectors

Rigid connectors have been replaced by flexible connectors, mainly for technological reasons.

An overview of rigid connectors will be given by citing an excellent research paper (Siess, Viest, Newmark, 1952). Fig. 4.1 shows black and white replica images of various rigid connectors sourced from the paper (Siess, Viest, Newmark, 1952).

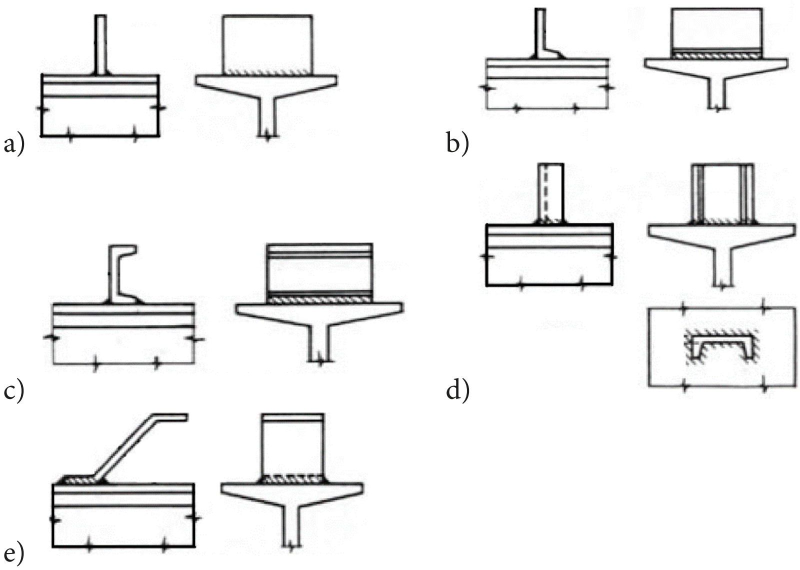

Fig. 4.1. Rigid connectors a) vertical steel flat bar b) steel angle bar c) hot rolled steel C channel d) hot rolled steel channel, vertically oriented e) inclined Z section

Fig. 4.2 shows several other examples of rigid connectors in axonometric drawings, Fig. 4.2.a-c. In Fig. 4.2.d, loop pins are shown as connectors. It is worth noting that these fasteners have a higher shear capacity than steel headed bars by about 40%.

The surface of a rigid connector acts on the concrete of the slab, and, in response, the concrete acts inversely on the connector. The same is true for the prone connectors. For this reason, the connection is dimensioned in two ways: for steel and for concrete. In both cases, part of the delaminating force Q/k, Fig. 4.2.e, is due to the interaction between the steel fastener and the surrounding concrete; in this case, k is the number of fasteners per metre.

The verification calculations for steel mainly consider the shear and bending resistance of the welds connecting the abutment to the flange of the girder. The connection structure itself is also checked for bending. As for the concrete, the pressure of the connector face on the concrete and the shear of the concrete along the perimeter of the connector face or along the conventional shear line are checked.

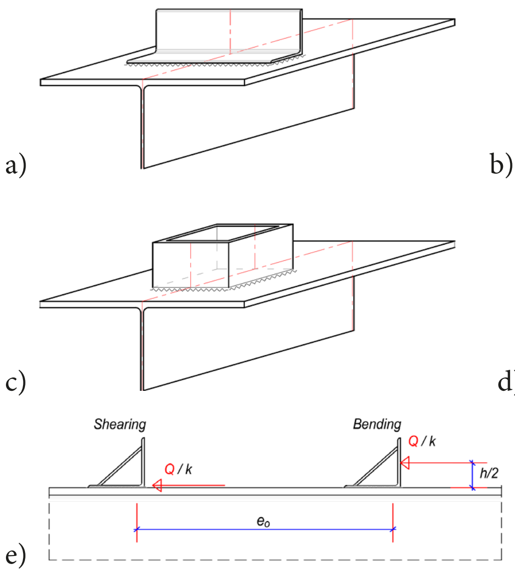

Fig. 4.2. Rigid connectors a) isosceles steel angle b) isosceles steel angle with a spacer c) box d) pin connector with a loop e) delamination force Q/k inducing shearing and bending in the perimeter weld

Fig. 4.3 shows photographs of worn steel beams of composite bridges with remnants of rigid and flaccid connectors. To avoid adverse stress concentrations in the concrete, flaccid anchor connectors have been used – smooth bars of min. 30d – with the final anchor hook placed in the concrete, Fig. 4.3.a-b. Most anchors were d =12 mm in diameter. The anchors were inclined from the girder axis by an angle smaller than or equal to $\pi/4$ and were aligned to the trajectory of the principal tensile stresses.

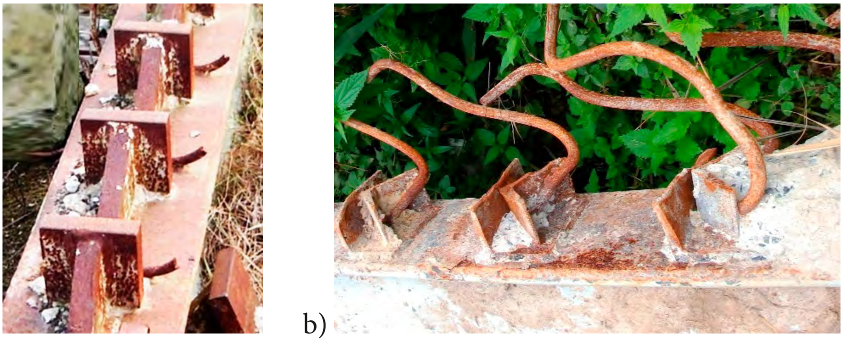

a) b)

Fig. 4.3. Degraded composite beams a-b) rigid connectors and remnants of flaccid anchors

Rigid connectors, such as those shown above, are not currently in use, but who knows what the future holds.

4.2. Headed stud connectors

At present, the predominant form of connection at the interface between a steel beam and a concrete slab are headed connectors, Fig. 4.4. This results from the ease of designing the connectors, the ease of installation and the ease of checking the quality of their connections – welds. The connector head prevents uplift. The connector pull-out force from concrete is estimated at 10% of the delaminating force.

a) b) c)

Fig. 4.4. Headed stud connectors a) view of the connectors in a commercial version b) prefabricated steel beam of a frame rafter with headed stud connectors c) checking the correctness of the connector weld by means of a hammer test

In the Eurocode (EN 1994-2), the scope of joint design at the interface has been limited to the design of headed stud connectors. The resistance of a single connector is expressed by two formulas for steel and concrete, respectively. Out of the two determined resistances, the smaller resistance is taken as decisive. Thus, one has

$$P_{Rd} = \min \left\{ \begin{array}{l} \dfrac{0.8 f_u \pi d^2}{4\,\gamma_v} \\ \text{or} \\ \dfrac{0.29 \alpha d^2 \sqrt{f_{ck} E_{cm}}}{\gamma_v} \end{array} \right\}, \tag{4.1}$$

where: $f_u \leq 500$ MPa – ultimate strength of steel, d – stud (shank) diameter; 16 mm $\leq d \leq$ 25 mm, γ_v (= 1.25) – material partial safety factor, f_{ck} - characteristic cylinder compressive strength of concrete, E_{cm} – value of the secant modulus of concrete, h_{sc} – overall nominal height of the stud,

$$\alpha = \left\{ \begin{array}{l} 0.2\left(\dfrac{h_{sc}}{d}+1\right) \quad \text{if} \quad 3 \leq \dfrac{h_{sc}}{d} \leq 4 \\ \text{or} \\ \alpha = 1 \quad \text{for} \quad \dfrac{h_{sc}}{d} > 4 \end{array} \right\}. \tag{4.1.1}$$

The Eurocode EN 1994-2 provides useful guidance on detailed design. Some figures from the quoted Eurocode are given below. Fig. 4.5 shows two basic cases of the placement of connectors inside a concrete slab.

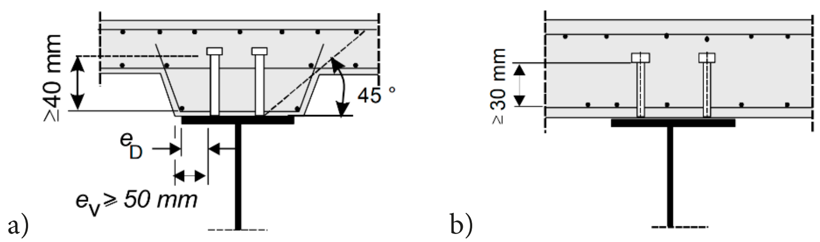

Fig. 4.5. Forming the concrete zone of the slab over the steel beam a) haunch (offset) of concrete slab b) flat slab case (*EN 1994-2, Fig. 6.14*)

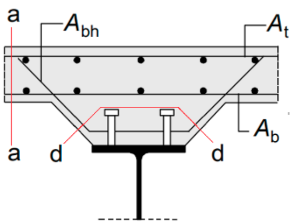

a)

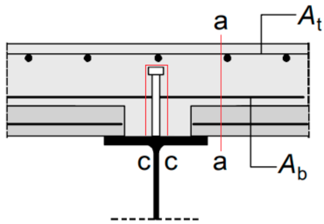

b)

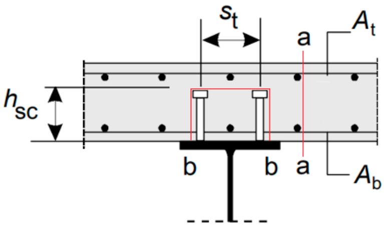

c)

d)

Transverse shear reinforcement	
type	A_{sf}/s_f
a-a	$A_b + A_t$
b-b	$2\ A_b$
c-c	$2\ A_b$
d-d	$2\ A_{bh}$

Fig. 4.6. Conventional concrete shearing surfaces (here, visualised by lines of symmetry) a) haunch (offset) case b) instance of prefabricated permanent shuttering d) A_{sf} / s_f – the effective transverse reinforcement per unit length, A_b, A_t and A_{bh} – areas of reinforcement per unit length of a beam anchored in accordance with (EN 1992-1-1) for longitudinal reinforcement, (*EN 1994-2, Fig. 6.15*).

In this chapter, the method of general description is followed, without giving detailed information about the design, analytical methods or discussing the details of test results. However, the citations provided facilitate a full cognitive understanding of contemporary solutions used in bridge engineering. At the same time, only a few papers are cited here, but their content and authors are at the *forefront* (whatever that may mean).

4.2.1. Ultimate state of a headed stud connector

The Reader can find various damage models concerning headed stud connectors. Nevertheless, only one drawing, Fig. 4.7, from (Oehlers, Bradford, 1999) is quoted below.

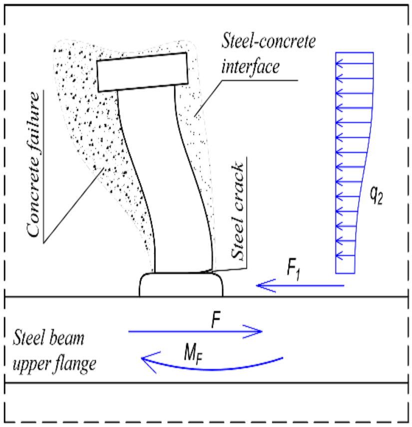

Fig. 4.7. Forces and failure zones for a headed stud shear connector

By simplifying the failure mechanism of the headed stud connector shown in Fig. 4.7, the concrete failure process can be analysed according to the theory of fracture mechanics of concrete as a brittle body. In the case of steel failure, fracture mechanics including plastic deformation must be applied.

4.3. VFT ®

The concept of VFT [8] girders is evolving and this is an ongoing process. Nevertheless, it is not yet a prevailing technology (Seidl, Petzek, Băncilă, 2013), (Kołakowski, Lorenc, 2015).

In short, VFT is a prefabricated composite girder consisting of composite elements – a steel beam and a concrete slab; the height of the steel beam or the concrete element can be reduced accordingly, as shown in Fig. 4.8 as an example.

The load-bearing capacity of the prefabricated element takes into account the loads occurring in the transition state, in which the concrete slab is over-concreted to its full height; there are also loads resulting from the installation of other elements of the superstructure. A full load-bearing capacity is achieved when the concrete of the precast slab is integrated into cast-in-place concrete. The connectors are located both in the precast elements and at the interface between the precast slab and the cast-in-place concrete. Fig. 4.8 shows selected forms of VFT girders.

[8] VFT® *German:* VerbundFertigteilTräger – prfabricated composite girder

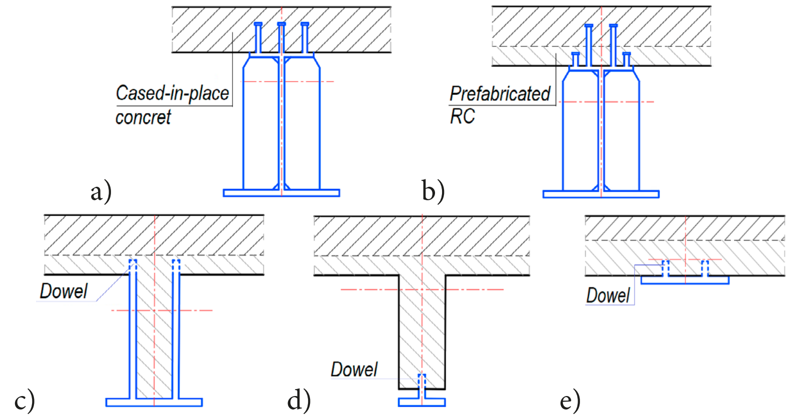

Fig. 4.8. Evolution of VFT technology a) classic composite girder b) basic VFT concept c) inverted double-T shaped VFT steel beam integrated by dowel connectors d) low height inverted T-beam with dowel connectors – external reinforcement e) VFT plate with external reinforcement

4.4. Perfobond rib shear connectors

The concept of ribbed perfobond shear connector was published in 1987 by Fritz Leonhardt et al., (Leonhardt, Andrä, 1987).

A composite girder structure consists of a steel beam modified by a fillet welded longitudinal vertical steel plate (strip), which is perforated in a regular manner. The perforations may run in a single axis, Fig. 4.9.a, or in a sequence of two axes located at two different levels, Fig. 4.9.b. The perforations have a correspondingly larger diameter than the transverse reinforcing bars.

This forms a composite that carries shear and compression/tension. A joint is formed in which internal forces are transferred by both steel and concrete. Enforced by the stiffness of the horizontal concrete slab, this arrangement corresponds to an approximately plane state of strain. This causes the concrete to *be confined* in the plane of the concrete slab.

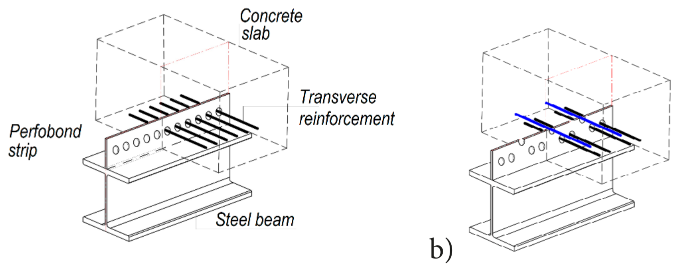

Fig. 4.9. Perforated shear connector concept a) one perforation line b) two perforation lines

The authors of the cited paper emphasise the high fatigue resistance of the tested joints to both concrete and steel dowels.

Further research on the load-bearing capacity of different variants of perforated connectors was carried out by Fritz Leonhardt's colleague, Hans-Peter Andra. Thanks to the digitisation of old resources, his old article is now available demonstrating the development of technical knowledge in this field. To this day, perfobond shear connectors have been undergoing numerous laboratory tests combined with FM analyses, e.g. (Andrä, 1990).

The case shown in Fig. 4.9.b leads directly to today's modern dowel connectors. Perfobond ribbed shear connectors are widely used in bridge engineering. Expressions for their shear capacity can be found in (EN 1994-1-1), (Su et al., 2016) and (Hai et al., 2020).

4.5. Dowel connectors

The constant drive to decrease the cost of bridge structures finds its technical expression in the search for a technology that would reduce the amount of steel in composite girders. The aim is not only to reduce costs, but also to increase the load-bearing capacity and durability of bridges. As always, prefabrication is a tried and tested method in such cases, as it allows a high degree of precision, e.g. in the construction of bridge girders. Referring to the basic design principle of a composite girder, i.e. that concrete works in compression and steel in tension, a new type of connector has appeared – the *dowel connector (longitudinal strip/slat with "teeth")*, Fig. 4.10, (Preco-Beam, 2013).

With a high degree of generality, one can say that a dowel joint is a rigid connector – but a longitudinal one. In fact, the dowel consists of two elements: a concrete dowel and a steel dowel, which are interconnected. Certainly, this is a great simplification, as the resultant resistance of the dowel is determined by various other elements involved. Although dowel connectors have been only in use for about two decades, the literature on the subject is extensive. At the same time, there still takes place an intensive examination process of the mechanism of this connection.

Dowels are usually extracted by cutting the I-beam along its neutral axis. The cutting is performed by means of oxy-fuel cutting, Fig. 4.10.a-b. There are many variants of the dowel shape, Fig. 4.10.c-e. A variant of the modified clothoid shape (MCL) is considered to be optimal, Fig. 4.10.f. This variant is the result of previous experiences with puzzle, clothoid and fin shapes.

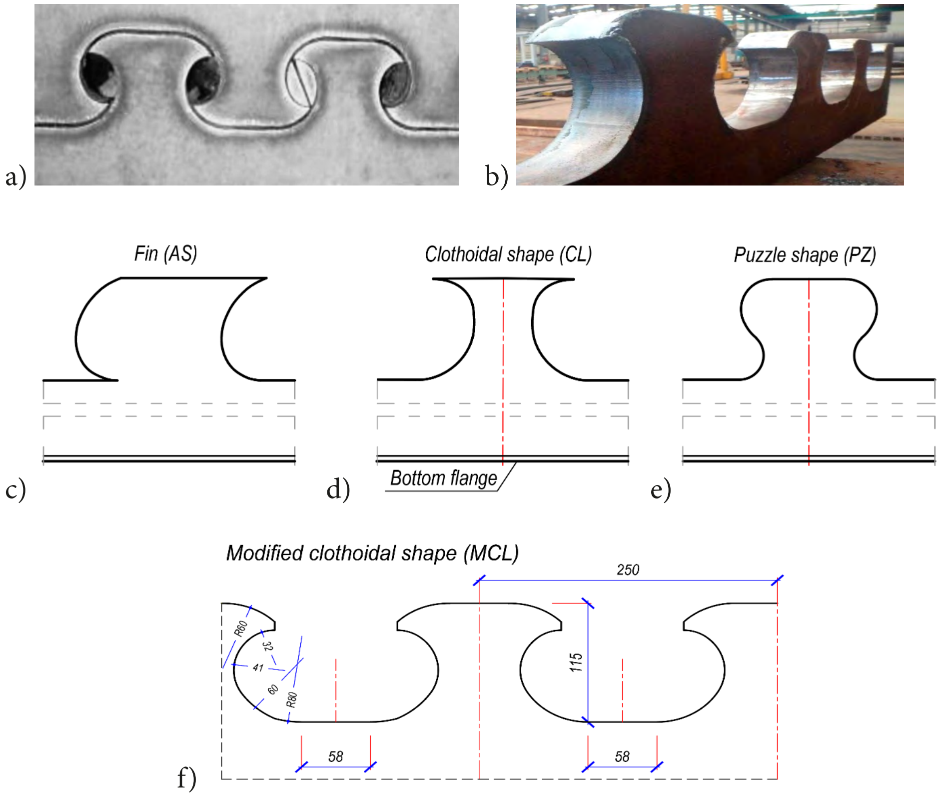

Fig. 4.10. Dowel connectors a-b) cut line in the web of a steel I-beam c) shark fin shape d) clothoidal shape e) puzzle shape of dowel f) example of geometry for MCL dowel

When classifying MCL geometries, the characteristic length/height/thickness dimensions of a web are considered. Thus, in Fig. 4.10.f, 250/115/27, (Lorenc, 2020) expressed in millimetres is shown.

A composite dowel shear connector caries the shearing which concerns both steel and concrete, Fig. 30.a. The basic challenge is to recognise and design the toughness against fatigue in a steel element of a composite dowel, which should have an appropriate shape. The main role of the surrounding concrete and reinforcement is to form a confining zone for a concrete dowel.

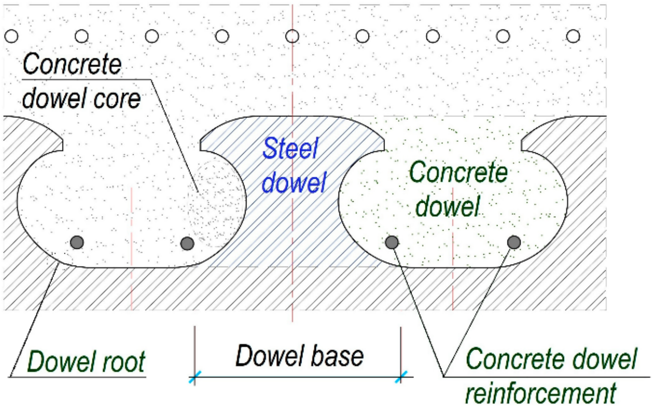

Fig. 4.11. Elements of composite dowel elements

This type of composite girders is also known as PreCoBeam – Prefabricated Composite Beam. The monograph (Preco-Beam, 2013) is especially recommended to the Reader, simply because one can find there information on everything that has happened in the discipline in recent years. It is a guide containing design principles for composite dowels in girders subjected to bending loads according to the Eurocode. It presents a brief history of the development of composite dowels, as well as suggestions for shaping the geometry and constructing the reinforcement. On the one hand, the results for many static and cyclic loadings used in numerous laboratory tests are described, and, on the other hand, a wide range of numerical models is presented. Finally, fire design is included. In short, the monograph is a very accessible description facilitating the subject studies for both students and engineers.

Figure Fig. 4.12.a shows a clothoid dowel (CL). Strain gauges are mounted near the root of the steel dowel. The location of the root was determined in a numerical analysis, the result of which can be seen in Fig. 4.12.b. The map shows the result when the assumption that only each odd composite dowel is subjected to cyclic loading is used. Even dowels perform similarly to the perfobond shear connector. The graphs in Fig. 4.12.c-d show the measured results of the vertical displacement (f) in the beam axis and the slip (s) at the interface (more precisely, the mutual displacement of steel and concrete) at the end of the tested beam.

The term *delta* denotes the difference between the maximum and minimum values inherent in a sinusoidal pulsed loading action.

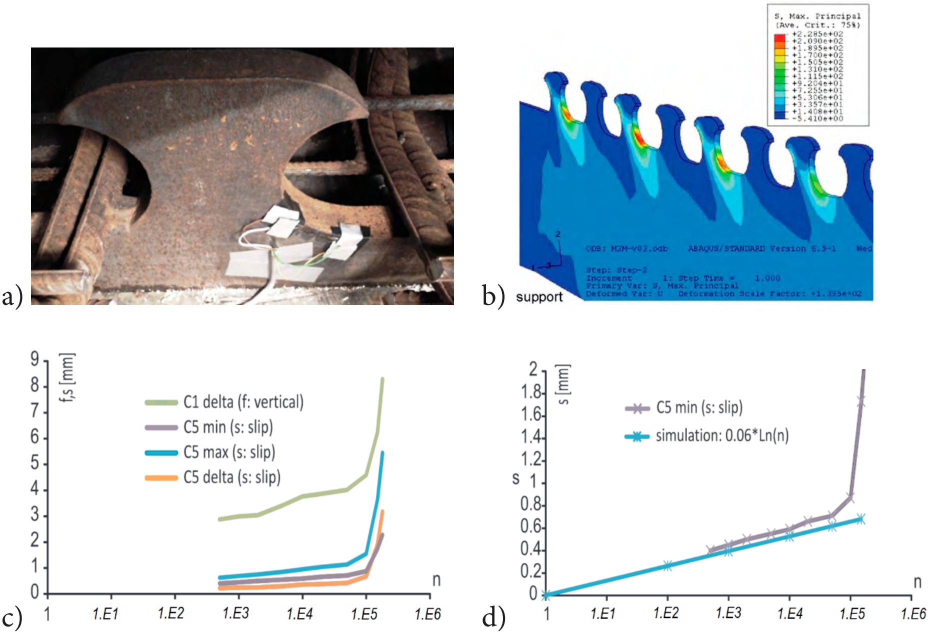

Fig. 4.12.[9] Experimental studies for the construction of a bridge over the Wierna River a) steel dowel (CL) with strain gauges b) principal stress map for a steel (dowel) c) vertical displacement (f) *delta*, slip (s) values and its *delta* d) slip (s) graph and its simulation as a logarithmic function of the number of cycles s = 0.6 Ln (n)

Of similar educational importance is the paper (Feldmann, Kopp, Pak, 2016) that provides a design concept for composite dowels approved in Germany. It gives static and fatigue load formulas, construction details, and precast fabrication guidelines, supplemented by relevant background information.

4.5.1. Concluding comment

As with stud connectors, the problem of the load-bearing capacity of dowel connectors has been fully recognised thanks to basic and specialized laboratory tests carried out. At the same time, each study and design has been supported by numerical analyses of various elements of the components under study and the structure as a whole. There is an opinion among researchers of this problem that no other engineering problem has been studied in such detail. The research was initiated in 2000s and has been continued in Germany, Poland, Austria, and Romania, as well as in other countries. A number of bridges have been built and have passed acceptance trials without comment. Of course, one still needs to wait about 20 years to say with certainty that shear transfer with dowel connectors is

[9] The images in Fig. 4.12 are presented courtesy of Wojciech Lorenc.

effective and failure-free without any doubt. In any case, the heuristic concept has been proven in laboratory tests and through the operation of new bridges. The relevant European standards will soon be developed.

It is highly likely that the dowel connector will be further optimised, but it is already possible to build composite bridges with dowel connectors today.

5. Methods and phases of composite bridge construction

Composite bridges of steel and concrete can be built in many ways. For the purposes of the discussion, two of these methods have been selected:

- **Method 1**: a method using a full temporary support on scaffolding of the structure under construction over the entire construction period. Once the scaffolding is removed, the composite bridge carries permanent and temporary material and traffic loads – symbolically denoted as LM1,
- **Method 2**: a two-phase method:
  - **PH** [10] **1**: in which the steel beams are set on an additional temporary single support, a bridge pillar, which carries the dead weight of the steel structure, the concrete slab formwork and the weight of the reinforcement along with the weight of the poured wet concrete mix,
  - **PH 2**: once concrete has hardened and set, the temporary support is removed, the composite girder is unloaded by removal of the slab framework and loaded with the bridge utility equipment and, finally, with LM1 vehicle loads.

Let us apply the following simplifying suppositions and notation:

- materials are linearly elastic,
- instead of stresses, strain distributions shall be drawn because in bridge engineering, even if the material has non-linear properties, the strain diagrams are invariant,
- a single composite girder shall be discussed instead of a composite bearing deck,
- the rheological effects (creep and shrinkage) will be omitted,
- the volumetric weight of the composite bridge elements is to be understood as follows
  - weight of concrete $\gamma_c = 24\ \mathrm{kN/m^3}$,
  - weight of RC $\gamma_{RC} = \gamma_c + 1\ \mathrm{kN/m^3} + 2\ \mathrm{kN/m^3} = 27\ \mathrm{kN/m^3}$ where the weight of the reinforcement is $1\ \mathrm{kN/m^3}$ and the weight of basalt gravel is $2\ \mathrm{kN/m^3}$,
  - weight of fresh concrete with reinforcement $\gamma_{yRC} = \gamma_{RC} + 1\ \mathrm{kN/m^3} = 28\ \mathrm{kN/m^3}$, where $1\ \mathrm{kN/m^3}$ is the weight of the batch water,
  - weight of structural steel $\gamma_s = 78.5\ \mathrm{kN/m^3}$,
  - weight of bridge equipment γ_{eq}, where it contains hydro-isolation, asphalt layers, curbs, barriers, and balustrades, checking gates, streetlamps, etc.,
  - weight of a slab formwork (transient loading) – $\gamma_{formwork}$.

[10] PH is the abbreviation for *phase*

When analysing a composite girder, it is possible to operate using a linear load density, i.e. a linear load(s) which, e.g., enables obtaining the linear load for a steel beam $g_s = \gamma_s A_s$ and for RC slab $g_{RC} = \gamma_{RC} A_c$, etc.

Now, let us define the group of loads:

PH 1:
- dead loads of the constructional elements of a carrying deck: $g_s + g_{\gamma RC}$,
- slab formwork (transient load) $g_{formwork}$.

PH 2:
- unloading of formwork $g_{formwork}$,
- unloading of batch water g_{HOH},

loadings:
- non constructional dead weights g_{eq},
- road traffic g_{LM1}.

5.1. Carrying deck deflection(s)

Actually, the most significant element of SLS is the final deflection the elements of which need to be known and understood. In Fig. 5.1 (a slightly modified drawing sourced from EN 1990) the total deflection u_{tot} is explained.

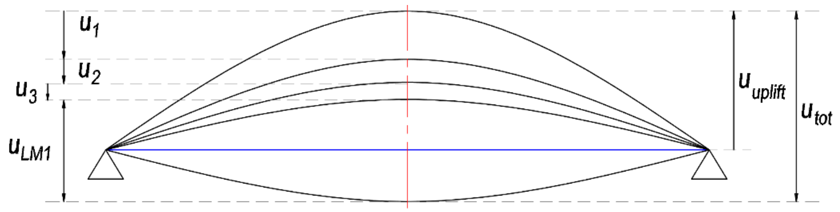

Fig. 5.1. Diagram of bridge carrying deck deflection and its elements

Note that the grade line on the bridge should have a minimum longitudinal slope of 0.5%. The longitudinal slope line is directed towards the lower of the abutments (to the lower support). In Fig. 5.1, this detail is omitted.

It is crucial that the aesthetics of a side view of the bridge is not disrupted by a sagging bottom line of the support deck. To avoid such an unfavourable image, a preliminary executive uplift is applied – u_{uplift}. The uplift line is the one from which the deflection components are identified as follows

- $u_1$stands for the deflection due to the loading effect of permanent structural weights – $g_s + g_{\gamma RC}$,
- u_2 is the deflection due to the permanent weights of non-structural elements – g_{eq},

– u_3 includes bending effects of creep and shrinkage – $u_3 = u_{rheo} = u_{creep} + u_{sh}$,
– u_{LM1} is the effect of moving loads on the bridge, and LM1/LM71 are currently the most significant traffic models in Europe.

It is worth mentioning that u_{LM1} is a reversible deflection, while the other listed elements are not. It follows that, at the very least, irreversible deflections should be compensated for by an inverse pre-deflection (uplift).

$$u_{uplift}^{(min)} = \sum_{n=1}^{n=3} u_n \tag{5.1}$$

However, in many sources – and bearing in mind the aforementioned aesthetic considerations – other reasonable pre-deflection values are used. One of these is the following formula

$$u_{uplift} = u_{uplift}^{(min)} + 0.5\,u_{LM1} \tag{5.2}$$

as shown in Fig. 5.1.

5.2. Composite bridge construction methods

Assumptions and designations are discussed in the introduction. The considerations are qualitative and do not concern structural design.

The structure under consideration is a simple single-span composite bridge (a steel beam bonded to a RC slab), Fig. 5.2.

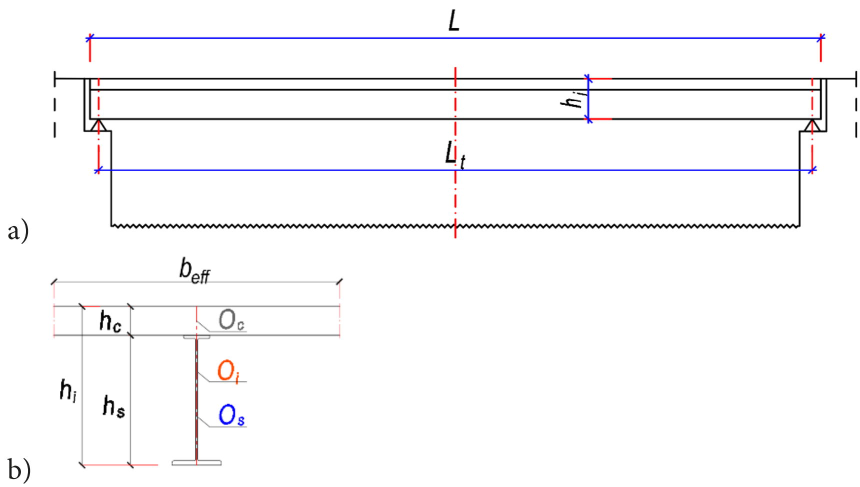

Fig. 5.2. Composite steel-concrete bridge a) side view b) cross-section

5.2.1. Method 1

The bridge carrying deck is supported on a set of pillars or, alternatively, continuously on temporary scaffolding, Fig. 5.3.

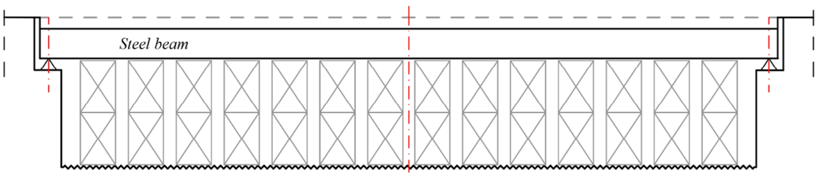

Fig. 5.3. Continuous scaffolding

As mentioned earlier, scaffolding can be removed when the load-bearing platform is ready to carry traffic loads. Therefore, in this case, it can be said that one deals with only one phase of the forming of the structure. Still, this will not be a great change if, somewhat artificially, successive phases of the bridge formation are introduced.

PH 1

- The scaffold takes the weight of – a steel beam g_s, formwork $g_{formwork}$, and fresh reinforced concrete of a slab $g_{\gamma RC}$.
  Once the concrete has set, it is permissible to start the second phase.

PH 2

Now, on the scaffold lies a composite steel-concrete carrying structure. The following steps are admissible:

- dismantling of the scaffold – unloading of $g_{formwork}$,
- the volume of concrete due to evaporation has a weight g_{RC}; the lack of batch water $g_{HOH}$is taken into account,

The composite steel/concrete currying structure, the slab/girder, now lies on the scaffold. Therefore, the following operations are permitted:

- dismantling of the scaffold – removal of the load $g_{formwork}$,
- change in the weight of the reinforced concrete slab due to evaporation of the batch water, the current weight is g_{RC},
- putting non-structural elements – g_{eq} on the carrying deck,
- finally, allowing vehicle traffic on the bridge, i.e. loading with g_{LM1}.

To complete the erecting process, a sequence of drawings is presented in Fig. 5.4.

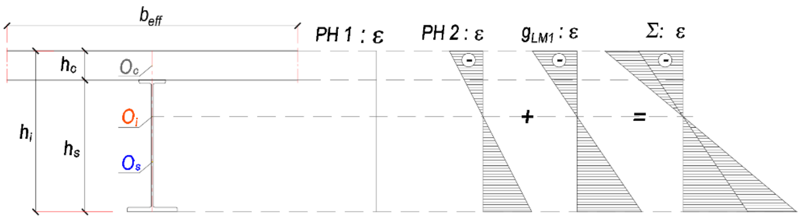

Fig. 5.4. Strains distribution in the two phases and for the traffic load

Summarising Method 1, again, there are some options to mount a continuous scaffold and as it is shown in Fig. 5.4 Phase 1 can be omitted.

5.2.2. Method 2

In this method, PH 1 brings about significant changes in the redistribution of strains and consequently leads to a reduction in normal stresses from permanent loads. Designers proceed in different ways, but in this case the design should take into account the initial executive uplift in the steel beam.

PH 1

In PH 1, deformations, strains and, of course, stresses only occur in the steel beam. Deformation is caused by structural dead weights g_S and $g_{\gamma RC}$, formwork $g_{formwork}$ supported or suspended on the steel beams resting on three supports.

A temporary single support corresponding to an additional bridge pillar is used, Fig. 5.5.a. The single temporary column takes interactions resulting in the vertical reaction R. There is a change in the static scheme from a simply supported beam to a continuous one with two shorter spans. The distribution of bending moments in a two-span continuous beam leads to a hogging bending moment zone, Fig. 5.5.b, which induces tensile stresses in the upper part of the steel beam.

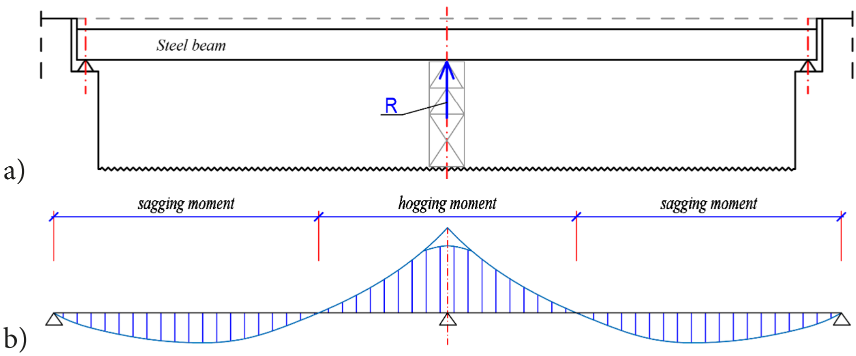

Fig. 5.5. Simple steel beam with an additional temporary column a) static scheme of the beam in question b) bending moment distribution

PH 2

Phase 2 occurs after the concrete has set and hardened. This is the time point at which the temporary support can be removed. In Phase 2, one already has a composite girder subjected to unloading and loading, respectively.

Unloading:

- concentrated force R with a vector in line with the gravitational return, which is the static effect of the removal of the temporary support, Fig. 5.6,
- dismantling of the concrete slab formwork, unloading of $g_{formwork}$,
- taking into account the evaporation of unbound water from the batch, unloading of g_{HOH}.

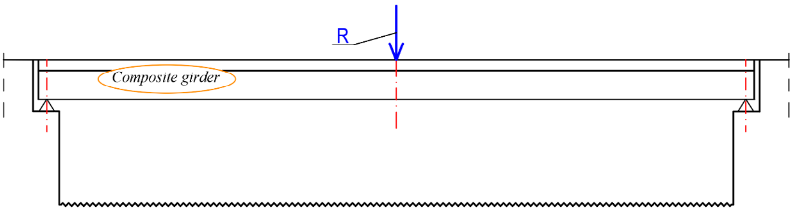

Fig. 5.6. Composite beam, static effect of the temporary column removal

Loading:

- the weights of carrying deck non-structural elements – g_{eq},
- finally, vehicle traffic on the bridge g_{LM1}.

When restricting the consideration to the vertical section at the centre of the bridge span, the strains distribution is as shown in Fig. 36.

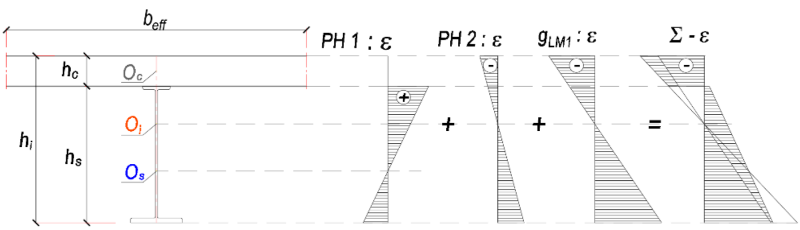

Fig. 5.7. Strains distribution in the case of Method 2

Method 2 can be used in different variants, differing in the number of temporary supports, such as two or more support columns, Fig. 5.8.

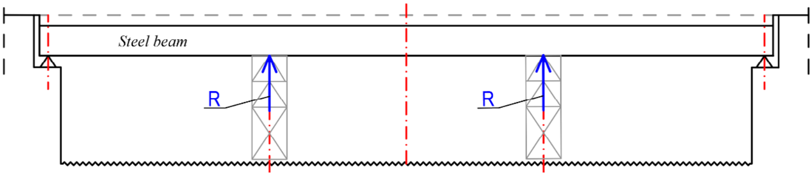

Fig. 5.8. Static diagram of steel beam on abutment bearings and two temporary columns in the span

***

The two methods detail discussed are only selected examples among many applied. A comparison between Method 1 and Method 2 shows the potential benefits of using more or less advanced technologies. In practice, each designer or contractor prefers their own tested methods for the construction of load-bearing structures. There are many criteria for evaluating the optimisation used, but the construction period appears to be the key indicator for the technology selection.

6. Zone above the pillar of the continuous carrying deck of a steel-concrete composite bridge

In addition to bridges with simply supported spans, composite bridges with continuous multi-span structures supported by articulation are commonly built.

In the case of continuous structures, the tensile moments (negative moments or hogging moments) occur in the zones above the pillars in the upper fibres of composite girders, i.e. in the concrete slab. The concrete deck slab is in tension, while the bottom flange and the lower web section of the steel beam are in compression.

If so, then it is the case of a complete inversion of the composite girder concept, which is not beneficial.

As a solution to the problem, the height of the steel beam in the zone above the pillar can be increased, which will help reduce the values of negative moments and enable the use of an appropriate number of reinforcing bars in the concrete slab according to the rules applied to reinforced concrete.

Another often-used method consists in keeping the height of the steel beam constant while increasing the number of reinforcing bars in the concrete slab. The criterion of the permissible limit crack opening in a concrete slab must then be met.

Moreover, controlled imposed vertical displacements on additional temporary bearings above the pillars can be used.

It should be noted that the imposed vertical displacements in the elastic range reduce the bending moments over the pillar, while increasing the bending moments in the span. In the case of the bridge shown below, the controlled imposed vertical displacements of the girders over the pillars (before concreting the deck slab) are about 50 cm.

In the first decade of the 21st century, forced uplift was introduced through the use of so-called sand bearings.

Selected examples of continuous composite bridges are given below, Fig. 41-49.

In 2008, the bridge in the village of Neple over the River Bug was rebuilt by reconstructing the shape of the previous reinforced concrete beam structure with main girders of variable height, using a steel-concrete composite deck in the design. The abutments were rebuilt, and the pillars were renewed Fig. 6.1.a-b.

a)

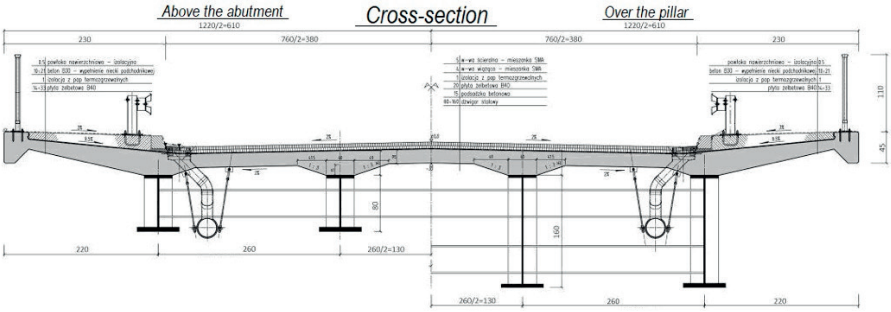

b)

Fig. 6.1. Continuous composite bridge in Neple over the Bug River a) general side-view from the river inflow b) design drawing – cross-section

The load capacity of the bridge corresponds to the load class A according to the Polish standard (PN-85/S-10030), which allows the movement of vehicles with a total weight of 500 kN. The total length of the superstructure is L = 86 m with the spans Lt = 24.0 + 31.0 + 24.0 m (0.77 : 1.0 : 0.77). Four steel girders of variable structural heights ranging from 80 cm in the middle span sections to 160 cm above the pillars were used. On the outer faces of the outermost girders, smooth web surfaces were retained for aesthetic reasons, using only full-height ribs in the support axes above the pillars and abutments. The internal bracing was made of HEB beams with single bracing in the spans and double bracing in the variable height section.

The aesthetics of bridges are always important, especially with regard to bridges that are distinctive architectural elements located simultaneously in the riverside and lowland landscape. Thoughtful design situations result in a calm and harmonious bridge image, Fig. 6.1.a and Fig. 6.2.a. In contrast, the bridge in Fig. 6.2.b, while satisfying the aesthetic principles regarding bridges, e.g. (Wasiutyński, 1971), particularly the rhythmicity of the elements, may trigger a slight uncertainty about the visual impact of the series of ribs used to stiffen the webs.

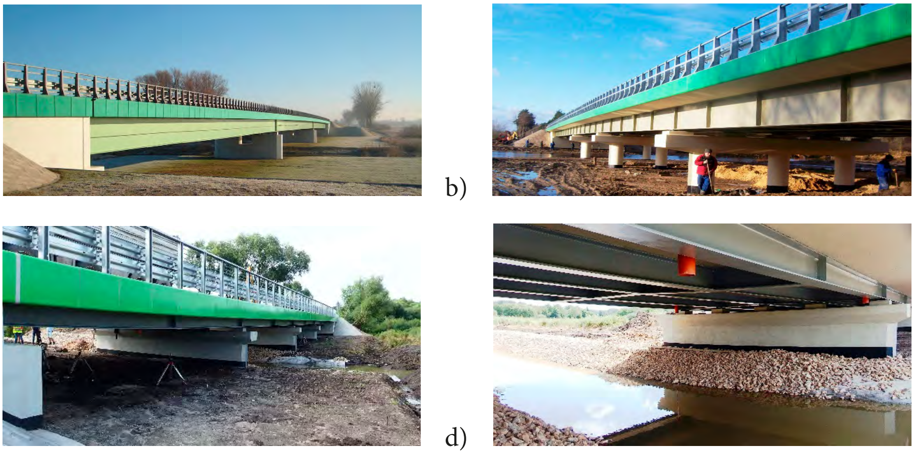

a) b) c) d)

Fig. 6.2. Composite bridges with continuous steel beams a) Dorohucza bridge (2006) b) Osuchy bridge (2008) c) Wirkowice bridge load test (2019) d) Wirkowice – composite steel grid with RC slab

Let us return to the problem at hand. How to make a continuous steel beam using two steel beams? The answer is obvious – through connecting their adjacent ends by a butt weld or by overlaps, which can be welded with a fillet weld or riveted. However, the same question regarding a composite beam is problematic.

Steel is a homogeneous material with uniform tensile and compressive limits, and, consequently, the tensile and compressive stiffness. More generally speaking, the flexural stiffness is also the same, if one ignores for a moment the possibility of the buckling of a compression member. Reinforced concrete is a different material as it is a composite of two components: steel bars that carry tensile stresses and concrete that forms the matrix for this composite. In the case of a reinforced concrete beam, in terms of the compression zone, the matrix enlarged by the transferred steel area carries the compression. Unfortunately, the slab in the composite beam is a thin element (~30 cm) in relation to the height of the composite beam. Therefore, in the zone above the pillar, in the hogging moment zone, the slab is fully in tension. The tensile stiffness of a reinforced concrete slab is significantly lower than that of a compressed slab. In the composite beam, its stiffness above the pillar is also lower than that of the composite beam in the middle of span. This is a feature that is always present during a test loading of continuous composite bridges. For this reason, numerical modelling of the continuous composite beam, which is an obligatory part of the load test design, requires the use of ordinary concrete in the sagging moment zone and a different concrete model in the hogging moment zone. Numerical modelling of tensile reinforced concrete is a complex problem; suffice it to say that the weakening of the concrete matrix due to cracking must be taken into account.

An alternative way of achieving the full continuity of simply supported spans is to construct a massive reinforced concrete junction of the composite girders above the pillar (concrete cross-beam). This is a highly efficient solution that is commonly used to ensure the continuity of prestressed girder technology Fig. 6.3.a. Furthermore, massive concrete cross-beams are always used in the construction of bridge structures using VFT girders, Fig. 6.3.b, as well as when the full continuity of rolled beam spans is required.

a) 

b) 

Fig. 6.3. Examples of girder continuity with a rigid monolithic cross-beam a) continuity of T-type prestressed beams, S12 ring road of Lublin (2021) b) construction of an integrated bridge with VFT-type girders, Piaski near Lublin (2009)

6.1. Espacenet

Full compression of a composite girder is not always sought. Intermediate solutions are also useful, as long as there is continuity of the pavement on a bridge and, more importantly, properly functioning waterproofing.

An incomplete continuity or service continuity is understood to be a type of expansion joint filling that only covers the height of the concrete slab or, alternatively, a mechanism that only partially transmits bending in the zone above the pillar.

Several contemporary solutions for the incomplete continuity of multi-span composite bridges are presented below.

The Espacenet web browser, developed by the European Patent Office together with the member countries of the European Patent Organisation, has been used to view patent documents. The browser provides access to more than 90 million published patent applications. After typing in the subject matter contained in the title, 537 results appeared in various versions, which always have several links to similar patents. A few subjectively selected patents corresponding to the topic analysed are presented below.

A patent document shall be drafted according to the following model: patent applicant, inventor, patent classification codes, priorities, patent application, designation and date of publication, title, abstract, drawings. In the following, a simplified but sufficient model will be used: patent designation, date of publication, summary description of the patent and some drawings. The way patents are described varies. Some are very detailed and indicate the application of the patent to the bridge structures under construction. There are also descriptions that are much more modest, where a detailed study of the drawings is necessary. Nevertheless, drawing is an excellent language for engineers.

The language of patents is very condensed to the extent that some details are only clear when studied with the use of relevant drawings. Except for a small group of specialists, patents are not studied on a daily basis. It is, therefore, an opportunity to become even vaguely familiar with the language and abbreviations used in patenting.

CN211772737U 2020-10-27 Assembly type composite beam bridge

The patent concerns a prefabricated composite bridge with an original static scheme for the assembly of a continuous hinged beam, which is converted into a single continuous structure.

Prefabricated beam elements used are edge 4, the beam above the column 3 and intermediate beam 5. The steel beam has a corrugated plate web with a small linear variation in the height of the beam above the column support – corresponding to the variation in the negative moment. In the tension zone of the concrete slab above the pillars, prestressing cables are used, and the bottom chord has a U-shape (more precisely, a stacked channel) filled with concrete bonded to the bottom chord, Fig. 6.4. c.

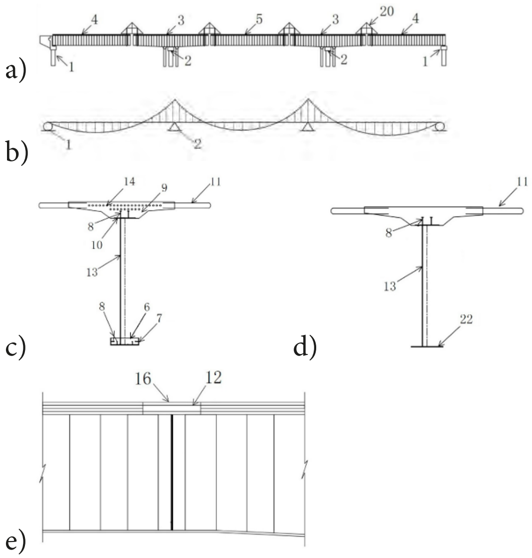

Fig. 6.4. Prefabricated composite bridge, assembly states a) locking diagram of 20 beam elements b) diagram of bending moments from permanent loads in the service phase c) cross-section of the prefabricated beam above the pillar; visible prestressing in the concrete of the upper flange and the extended lower flange of the steel beam d) cross-section of the prefabricated end (4) and the intermediate span beam (5) e) locking of the beam elements in the junction, wet-formed concrete slab continuity

CN210458905U 2020-05-05 Variable-height steel-concrete composite beam bridge with support

The utility model relates to a steel-concrete composite girder of variable height above the support. The solution consists in creating cantilevers over the pillar. The outreach of an individual cantilever along the bridge axis amounts to approximately 0.15 to 0.25 of the length of the adjacent bridge span. The traditional variable-height steel beam in the zone above the pillar has been replaced with a solution consisting in combining a fixed-height steel beam located at the top with a variable-height prestressed concrete cantilever located at the bottom. The figures show the stages of the pushing (*the pushing process*) of a steel beam onto the prepared pillars with prestressed supports, Fig. 6.5. In Fig. 6.5, the following numbered designations are used: 1 – bridge pillar, 2 – prestressed concrete cantilever, 3 – steel beam, 4 – grooves/troughs where the cantilever and the steel beam are joined, 5 – groups of pin connectors, 6 – assembly deck, 7 – guide beam (launching nose), 8 – jacking equipment.

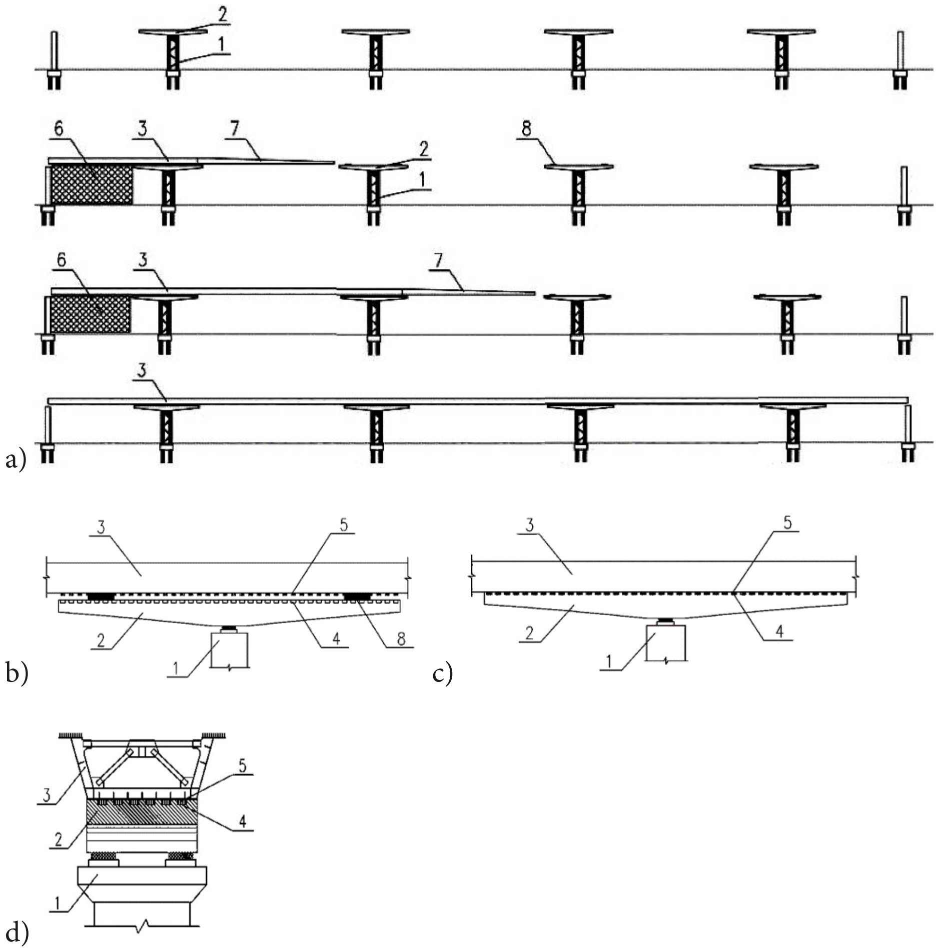

Fig. 6.5. Continuous steel-concrete composite bridge of variable beam height above the cantilever support a) technology used in the design of the steel beam slip-on progress pattern b) slip-on beam to cantilever support c) steel beam after its integration with the cantilever support d) bridge cross-section

During slip-on, the lifting devices of the slip-on beam with groups of pin connectors welded into its lower flange/surface, which slide over the prepared grooves on the upper surface of the support, are operated, Fig. 45.a. Once the sliding is complete, the grooves are filled with a concrete mix and the lifting devices are removed. A steel-concrete composite beam of variable height in the pillar zone is formed, Fig. 45.c. During the assembly, the pillar is connected monolithically to the prestressed support in the longitudinal direction.

CN212103670U 2020-12-08 Bridge deck semi-rigid continuous structure applied to simply supported reinforced concrete composite beam bridge

The patent in question regards the introduction of a tensile element stretched over the pillar and the sections of the girder ends joined to the concrete, Fig. 6.6.b. The tensile element placed in a previously prepared trough consists of a slab of ultra-high-performance concrete (UHPC) (3) and a bituminous layer (4).

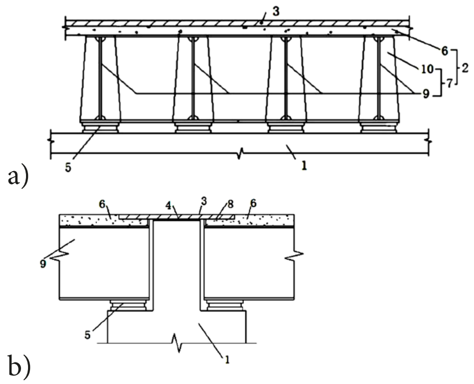

Fig. 6.6. Incomplete continuity of simply supported steel beams on a pillar with a so-called "soul" a) bridge cross-section b) partial/ incomplete continuity of spans

The continuity applies to structures the pillars of which have a reduced width at the height of the simply supported beams, Fig. 6.6.b, the aforementioned section of the pillar is sometimes referred to as 'the soul' and runs between the ends of simply supported beams.

CN211200026U 2020-08-07 Simply supported steel-concrete composite beam bridge deck continuous structure

The utility model concerns the ensuring of the partial continuity of adjacent composite structures over the pillar. The continuity of the wet-applied concrete slab is ensured by pin connectors, Fig. 6.7.

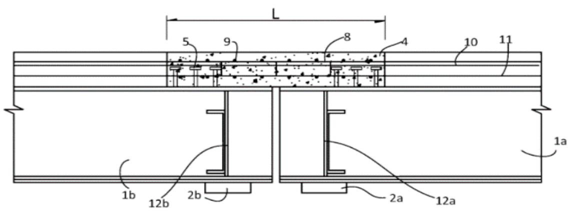

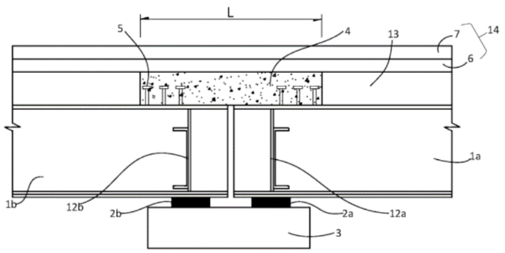

Fig. 6.7. Continuity of adjacent beams simply supported in the zone over the pillar

The continuity zone (L) is assumed to be of a length of 100 mm < L < 180 mm. Negative moments are transmitted partly within a range corresponding to the flexural stiffness of the continuity plate.

Relevant numerical designations: 8, 11 – longitudinal steel bar reinforcement, transverse reinforcement. Indication 10 is not described.

CN211772849U 2020-10-27 Steel-concrete composite beam bridge deck continuous structure adopting annular joints

The patent addresses the partial continuity of adjacent simply supported structures through the introduction of a continuous section of the concrete slab over the expansion joint using a solution that is a feature of the patent proposal. What is characteristic about the patent is that concrete is reinforced with loops/rings of steel bars (2), Fig. 6.8.a, and longitudinal bars of reinforcement (1), released from the ends of the concrete slabs above the intermediate support. The joint plate (5) is made of UHPC high performance concrete. In plan view, the steel continuity plate (3) has trapezoidal cut-outs and is attached to the upper flanges of the steel beam, Fig. 6.8.b.

a) 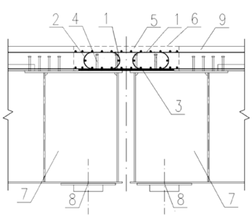

b) 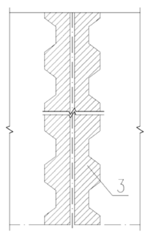

Fig. 6.8. Channelling of adjacent simply supported steel-concrete composite bearing structures: a) continuity elements in the longitudinal section; b) shape of the steel continuity plate in plan view

CN104727218A 2015-06-24 Anti-cracking structure for hogging moment region of steel beam-concrete slab combined continuous beam bridge

The patent concerns a continuous composite beam. It is distinctive in that the purpose of the patent solution is to limit cracks in the concrete slab from the action of negative moments. A telescopic (expansion) device is used above the intermediate support is used. The device has a dual role: it implements a visco-elastic continuity mechanism and deforms accordingly, reducing cracks in the concrete slab, Fig. 6.9.

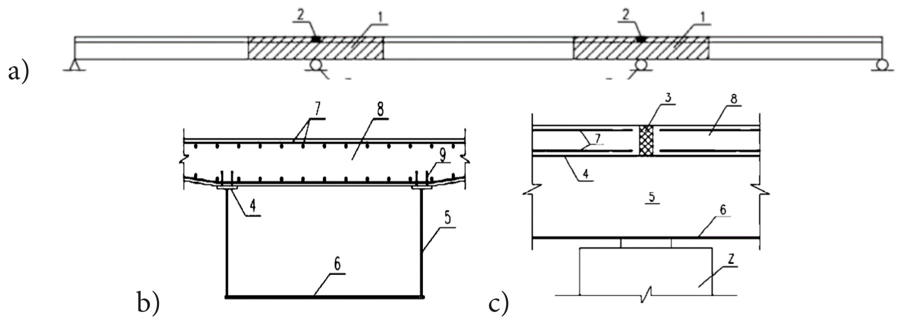

Fig. 6.9. A composite bridge in which a telescopic expansion joint device is used a) negative moment influence zone (1), expansion joint device (2), b) box steel girder (4, 5) with a bottom plate (6), composite (9) with a concrete slab (8) reinforced transversely and longitudinally 7 c) longitudinal cross-section of a concrete slab and a bridge with a schematic layout of longitudinal reinforcement bars and an expansion joint device (3)

CN106480818A 2017-03-08 Composite connecting plate structure for simply supported beam bridge and method for constructing composite connecting plate structure

The invention concerns a simply supported composite beam bridge with the utilitarian continuity achieved through an appropriate arrangement of the continuity reinforcement. There is no mention of negative moments. The patent solution is characterised by the reinforcement of the continuity zone with steel bar nets and the reinforcement mesh condensed in the zone adjacent to the support, Fig. 6.10. It is also significant that the layer (13) marked in the figure is a slip layer.

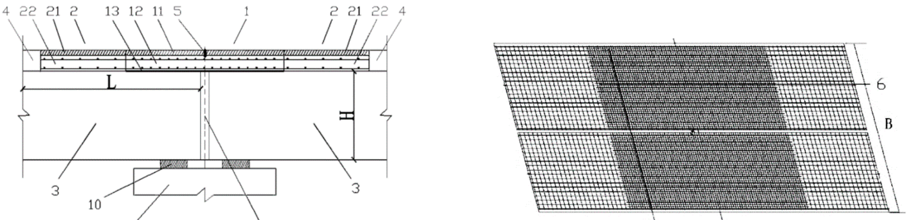

a) b)

Fig. 6.10. Bridge continuity a) longitudinal cross-section b) continuity reinforcement mesh in top view

The following designations are used in the figure: 1 – section of continuity not associated with the steel beam 3, 11 – asphalt concrete layer, 12 – reinforced concrete layer, 13 – slip layer, 2 – composite zone of continuity, 21 – asphalt concrete, 22 – reinforced concrete, 4 – deck slab, 5 – transverse joint, 6-7 – rebar.

CN112502017A 2021-03-16 Durable web butt joint type prefabricated combined beam bridge and construction method

The essence of the patent is the use of prefabricated composite girders with a reinforced concrete flange, which, at the same time, constitutes the deck formwork that actively cooperates in the transfer of permanent and live loads, Fig. 6.11. Prefabricated girders are placed side by side on pre-prepared supports and joined together for assembly. The deck slab and support cross-beams are then wet-fabricated on the top of these. This creates a monolithic span. In the patent application, the precast reinforced concrete shelf is called the lower deck and the part of the deck slab made in situ is called the upper deck.

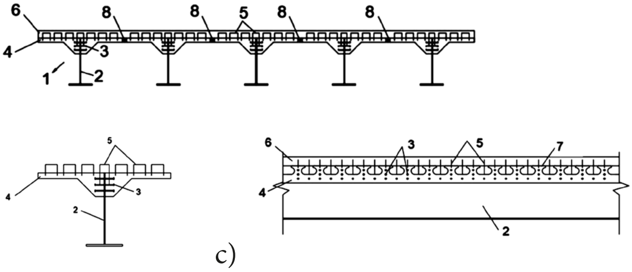

a)

b) c)

Fig. 6.11. Prefabricated steel girder bridge with reinforced concrete flange a) cross-section of a composite bridge structure b) prefabricated composite girder c) longitudinal cross-section – connector strip with openings for passing transverse bars

Significant numerical designations: 2- steel beam, 3 – transverse reinforcement (nails) anchor reinforcement/pinch, 4 – lower deck, 6 -upper deck, 7 – dowel joint/strip, 8 – lock.

CN110847007A 2020-02-28 Profile steel-concrete composite beam hogging moment area structure based on high-performance material

The patent document describes a technology for joining two simply supported composite beams to produce a continuous composite beam over intermediate supports. The technology is characterised by the connection of the steel beams with a composite steel casing/filled with HPC (High Performance Concrete). The composite concrete slab over the support is made in situ with HPC (designation 3 in Fig. 6.12). High-quality HPC concrete is placed along the length a of the negative moment zone.

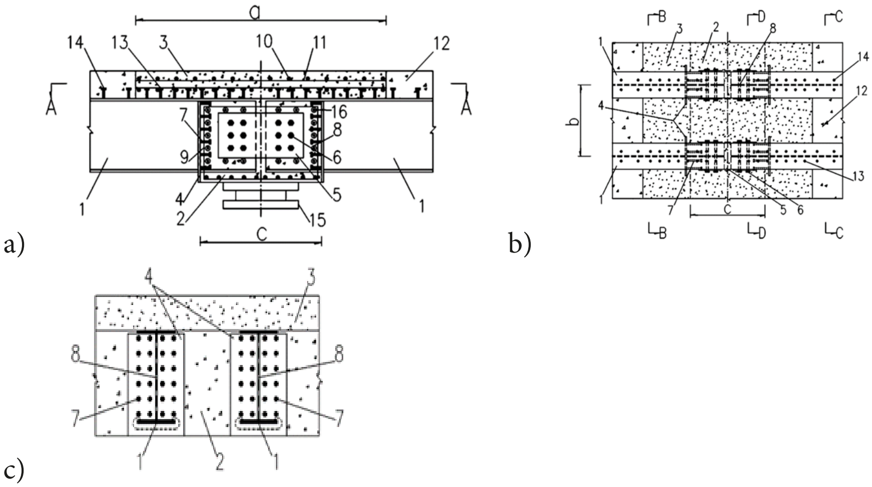

Fig. 6.12. Steel-concrete composite bridge a) longitudinal cross-section b) top view c) cross-section

CN210621439U 2020-05-26 Composite beam unit and composite beam

The utility model describes a composite beam consisting of two parts/units. The first part is a steel beam, and the other part is a composite beam encased in UHPC concrete (filler beam variant). The patented composite beam is characterised by the fact that, in the vertical plane, the steel beam is located at the bottom and the composite part is located on the top, with the top flange of the steel beam constituting the bottom flange of the composite part. A feature of the solution is that the composite beams can be made continuous by using a connecting lock made of steel flat bars, Fig. 6.13.b. The patent in question relates to a technology that has several options, including ones concerning a simple composite beam. There is also a variation of the continuity. Only the main variant is shown in Fig. 6.13.

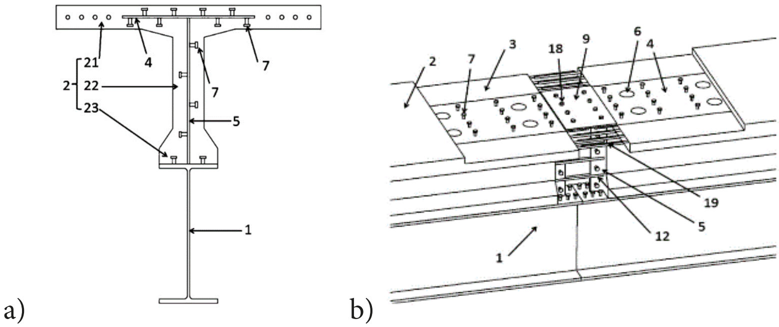

Fig. 6.13. Steel beam with a composite beam encased in UHPC concrete (filler beam) a) cross-section b) axonometric drawing of the lock

Among others, the following numerical designations appear in the drawings: 1 – steel main beam, 2 – UHPC concrete beam, 4 – slab/top shelf of the steel beam set.

The patent also appears with the designation CN106480818B, which is a simplified version.

CN112211089A 2021-01-12 Structure for hogging moment area of steel-concrete composite continuous beam bridge

The patent regards a full-continuity joint for the simply supported spans of a steel-concrete composite bridge. The patent drawings show a continuity joint which guarantees the transfer of negative bending moments occurring in the continuous composite girder. The joint is a steel-concrete structure with multiple composite connectors binding the steel beam to the applied concrete block and reinforcement released from the concrete slab. The composite beam slab of reduced height above the joint is complemented with a layer of reinforced concrete Fig. 6.14.

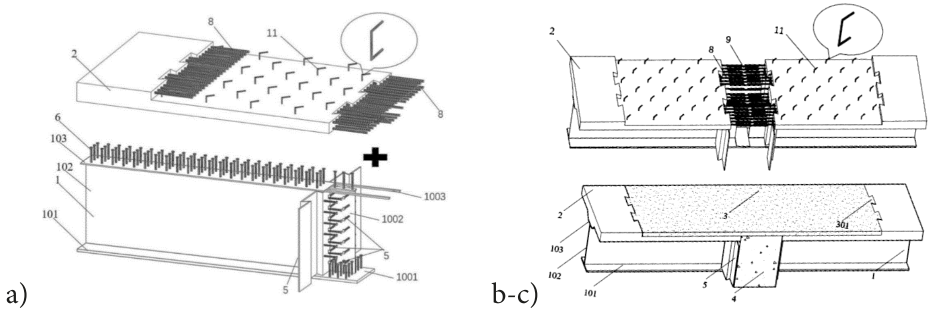

Fig. 6.14. Full composite girder continuity in the zone above the pillar a) components of the bracing b) top view of the lowered concrete slab with abutments c) image after bracing

A total of nine drawings are included in the patent description, with only three of them presented here The drawings are denoted by the following numerals: 1 – steel beam, including: 101 – bottom flange of steel beam, 102 – web, 103 – top flange, 1001 – section of an extension of the bottom flange, 1002 area of an extension of the web, 1003 extension of the top flange; 2 – concrete slab of the composite beam, 3 – concrete slab of reduced thickness and of the continuity of the composite beam slab over the pillar, where the rectangular slab (301) is made of UHPC with trapezoidal nodes; 4 – concrete block (steel-concrete composite) through connectors, 401 – expanded continuity element (block); 5 – steel beam termination element (baffle); 6 – headed pin connectors; 8 – steel bars released from the concrete slab of the composite girder; 9 – steel lap joint bars; 11 – interface connectors in the concrete slab of the deck over the pillar.

The location of the fixed bearing and possibly the temporary bearings is not indicated in the drawings or the patent description.

CN106930181A 2017-07-07 Negative moment zone structure for reinforced concrete combined bridge simply supported first and then constructed continuously

In the negative bending moment zone, reinforced concrete transverse beams and support cross-beams are used. Steel beams are connected to the concrete transverse beams via bar connectors with heads (shear connectors), Fig. 6.15.b-c. The patent applies to a bridge less than L=30 m in span. During the initial construction phase, the steel beams are freely supported on the assembly supports, and then a monolithic junction is made in the zone above the target pillar to ensure full continuity of the composite structure.

The patent description emphasises that the solution is very simple to implement, socially useful and economical. The drawings in the patent document are not of high quality. For the purposes of the article, the drawings have been specially adapted.

Selected numerical designations in Fig. 6.15: 1 – steel beam, 2 – concrete bridge deck, 3 – steel beam end plate, 4 – longitudinal steel plate (extension of steel beam web), 5 – headed pin connectors, 6 – holes for passing concrete reinforcement, 7, 8 – longitudinal and transverse reinforcement; 9 – structural reinforcement; 10 – bearing.

From the drawings it can be read that the steel beams (1) are of the HEB type with prone connectors on the upper flange and on the transverse plates (3). No intermediate cross-beams are used. A composite of a concrete slab and a steel beam without offsets or haunches, convenient during construction, is used Fig. 6.15.a. The ends of the steel beams above the pillar are free, with openings prepared in the web of the beams (4) to allow the bars of the transverse reinforced concrete beam (6) to pass through. The width of the continuity reinforced concrete beam is determined by the transverse plates (3) welded to the webs of the steel beams. The height of the welded plates is greater than the height of the steel beams by an allowance on the underside, Fig. 6.15.b and 6.15d. Once the steel beams prepared in this way are in place, a composite reinforced concrete continuity crossbar, unnumbered in the description, but marked with Chinese characters, is constructed at the ends of the steel beams with the use of stud connectors with heads. Probably the crossbar is concreted together with the deck slab.

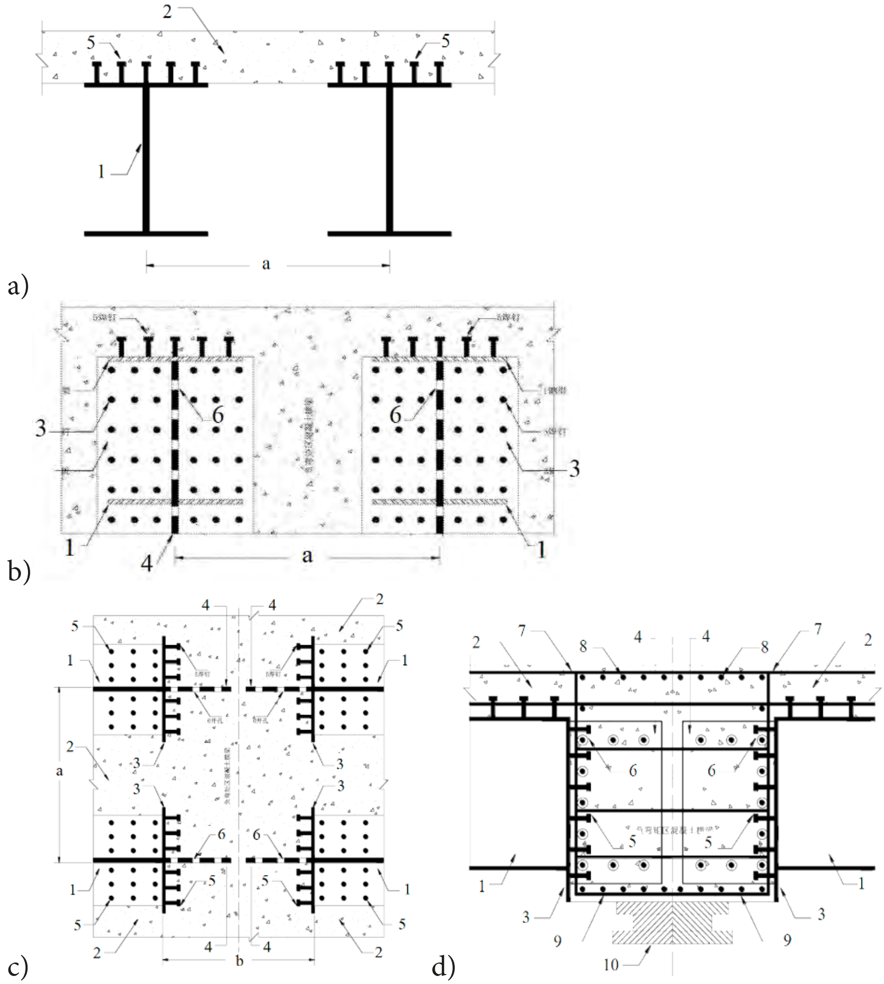

Fig. 6.15. Solid continuity of the composite girder a) cross-section in the span b) cross--section of the tensile beam c) top view of the continuity beam d) longitudinal section of the continuity beam

There are two layers of longitudinal reinforcement in the concrete deck slab, a top and a bottom one, spaced 10 cm apart. The diameter of the lower longitudinal reinforcement (compression) should not be less than 16 mm. The length of the upper longitudinal reinforcement located in the area of negative moments should be $c \geq 0.15$ Lc, where Lc is the span of the area affected by these moments.

This is an interesting technology of continuity, while in the context of the negative moments contained in the title of the patent description, it only applies to negative moments from equipment weights and service loads, which is still a significant gain in terms of the mechanics of the composite girder.

CN112252150A 2021-01-22 Combined beam bridge and construction method thereof

The patent description provides only a brief summary of the contents of the invention as the description is incomplete, while the drawings serve as a general presentation of the technology. The order of the drawings in the article follows from the sequence of the assembly of the composite bridge. The numbering in the drawings is not described, although the significance of the highlighted elements is obvious, Fig. 6.16.

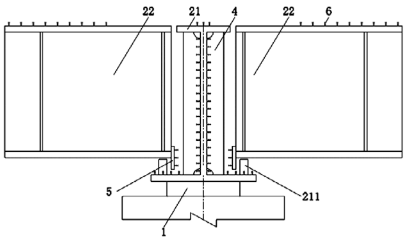

a)

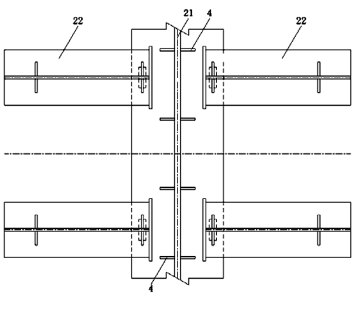

b)

c)

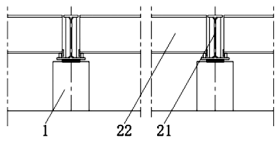

d)

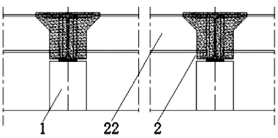

e)

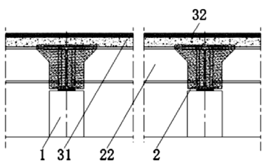

Fig. 6.16. Combined girder bridge a) detail showing the setting up of the prefabricated longitudinal and transverse steel beams with connectors b) top view c) side view before the concrete crossbar is made d) making of the concrete continuity crossbar e) making of the composite bridge

In the summary of the invention, the name combined beam bridge is used – indeed, it is a method of construction that bypasses the joining of prefabricated steel members by welding. Instead of joining the longitudinal and transverse beams by welding, a beam/filler is used which encompasses the ends of the longitudinal beams with connectors within the bottom flange together with the entire transverse beam, Fig. 6.16.a. The probable idea behind the absence of connectors in the top flange of the girder and only the local presence of connectors on the top flanges of the transverse beams is to partially exclude the upper zone from tension, Fig. 6.16.d. The final stage is the construction of the concrete slab of the entire deck, Fig. 20.e. What is not known, but certainly arouses curiosity, is the method of reinforcing the concrete slab in the zone above the pillar.

***

This concludes the survey of selected patents. Despite a large number of patent documents in the field concerning the problem under consideration, it cannot be claimed that there exists a dominant technology. On the contrary, a great diversity of proposed solutions can be observed. Simple and complex solutions are used with some of them innovative as exemplified by patent CN210621439U.

6.2. Author's proposal for the arrangement of the zone above the pillar

Again, let us recall the general principle of the composite girder concept: compression carries concrete and tension carries steel.

There are, of course, many types of composite girder and in each of them the principle operates to a different degree. However, the default is a simply supported girder. In the case of a continuous composite girder, there is a hogging moments zone where, mainly for technological reasons, an inversion takes place as a result of which the concrete slab is in tension and the lower part of the steel beam is in compression. Again, there are many ways to design a composite girder with a concrete slab in tension, as discussed above.

The concept of the formation of the steel plate in the tension zone of the concrete slab in such a way that the definition of a composite girder can also be extended to the zone of hogging moments will now be presented.

The version presented is the simplest in terms of technology, allowing only minor modifications to current technologies. A variant using headed stud connectors is considered. However, any shear transfer connectors at the steel-concrete interface can be used. Of particular interest may be the introduction of perfobond or dowel connectors.

6.2.1. The new concept

The invention concerns a structural solution for forming a steel-concrete composite girder in the zone above the pillar.

The invention takes into account an addition to the typical solution of a composite girder in the span zone – an additional steel plate above the RC slab of the deck and an additional RC plate on the bottom flanges of the steel beams – in the zone above the pillar.

The solution can be used in the design and construction of new bridges and in reconstruction with the strengthening of existing bridges. The system is applicable to road bridges, railway bridges and footbridges.

In the discussed case, with a constant steel beam height, the increase in stiffness (SLS) is determined by the cross-sectional area of the additional steel plate. The invention additionally provides for a compressed RC slab integrated in the lower flanges of the steel beams. The RC slab contributes significantly to an increase in the stiffness of the composite girder at the pillar.

In the ULS range, the additional steel slab carries tensile stresses in the dominant range, while at the same time there is a small contribution from the confined concrete of the slab. The additional lower RC slab carries compression and reduces the potential buckling/torsion of the steel beams.

The proposed solution increases the dynamic stiffness of the bridge, especially in terms of excitations transverse to the bridge axis.

The additional concrete slab reduces noise compared to the usual solution. For this reason, the invention also proposes the use of such slabs at outermost supports. The concept/innovation is shown in the diagrams in Fig. 6.17-6.21.

The shape of the additional upper steel plate, Fig. 6.19, which works in tension corresponds to the effective width to allow for shear lag.

In the drawings, the colour *magenta* indicates the new elements.

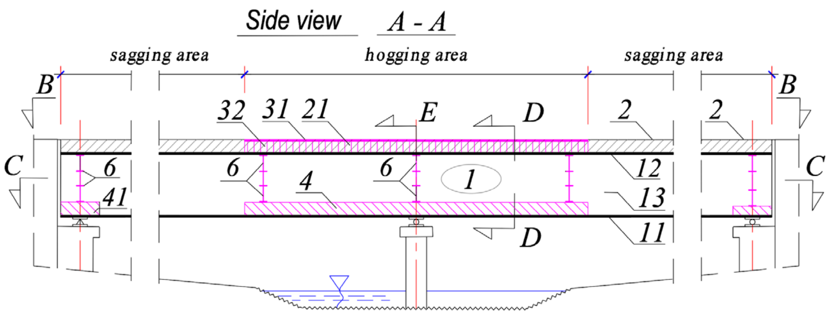

Fig. 6.17. Longitudinal section

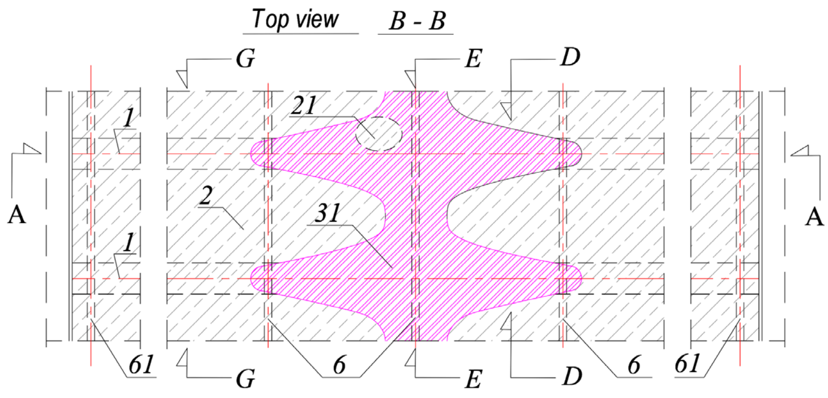

Fig. 6.18. Top view

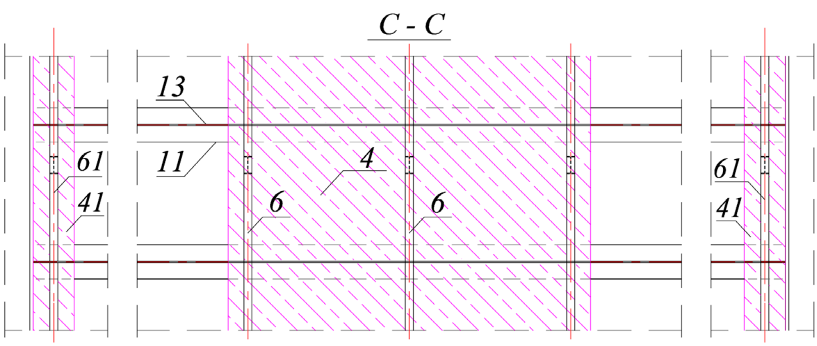

Fig. 6.19. Overhead view in C-C section

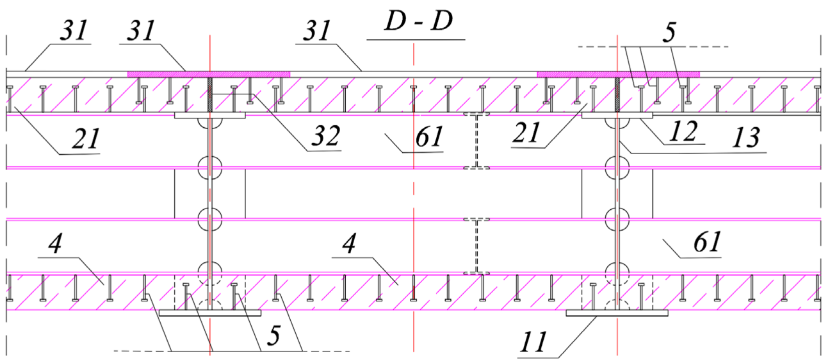

Fig. 6.20. Cross-section near the pillar

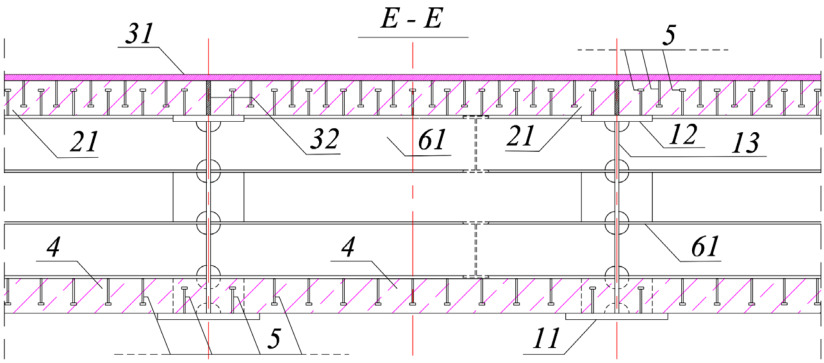

Fig. 6.21. Cross-section – E-E over the pillar

The described new concept for the layout of the zone over the pillar under the title *Continuous steel-concrete composite girder system over pillar* has been patented and carries the number P.440531.

7. Bending stiffness of a partially integrated composite concrete and steel girder

At the end of the 19th century, composite girders were not used, but it was during this period that the behaviour of wrought-iron bars formed from flat bars connected by rivets or bolts was analysed. The objective was to determine the load carrying capacity of, for example, bridge girders in the case of the loosening of plate connectors. And this is what corresponds to the issue of partial integration (partial interaction). Rzhanitsyn's[11] monograph cites dozens of works in this field, mostly in German. The archives are not analysed here – those interested are referred to the indicated sources. Instead, the following text will hint, in an abbreviated and suitably illustrative manner, at the progress in the development of the theory of composite girders, up to the point where the possibilities of cognition are determined by computer procedures.

The theory of composite beams with flexible elastic connectors could be found in Rzhanitsyn's monograph (Rzhanitsyn, 1948), although many papers were published before, starting from the end of 19th century. The second Rzhanitsyn's book (Rzhanitsyn, 1986), which gathers his earlier efforts in this field, contains a wide spectrum of basic structural problems, i.e. beams, plates, slip and up-lift in the interface, stability, vibrations, elastic foundation and numerous practical and important examples as well. However, Rzhanitsyn, in fact, did not look into a concrete-steel girder which is mainly used in bridge structures, but analysed sets of partially connected members.

Looking through the history of composite beams with imperfect connections, the work (Newmark, Siess, Viest, 1951) is crucial. At first, the authors report the results of small- and full-scale tests of T concrete-steel beams with incomplete interaction and on this basis propose the method of interface shear force, strains, and flexure calculations. The example of a simple beam with concentrated load is added as an application of the introduced theory. Conclusions look at tests results and the theory in detail. Additionally, the analysed paper mentions that this theory was developed in 1943, which is important for source search in this field.

A further extension of the Newmark et al. concept can be found in (Seracino, Oehlers, Yeo MF, 2001), where the Magnifying Factor (MF) is introduced to obtain a partial-interaction curvature (see also: Seracino, Lee, C. Lim, Y. Lim, 2004). The operated curvature is equal to the product of MF and the full-interaction curvature value. The *Partial-Interaction Focal Points* (PIFP) are also introduced. They are the points where the graphs of strain distribution in no-interaction

[11] Rus.: Алексей Руфович Ржаницын – Alexei Rufovich Rzhanitsyn (1911–1987). Soviet scientist who dealt with the mechanics of structures.

and full-interaction cases intersect, and they are used for the purpose of strain distribution calculations.

At the end of the presented paper, the approach formulated in (Karaś, 2008) is recalled. A translation of strain null lines is also undertaken there as a basis for curvature estimation and bending stiffness derivation.

The theories discussed here, in a mechanical sense, are simplified, and, in fact, concern one-dimensional problems. The most advanced studies that define the detailed initial-boundary problem of the elastic theory in the case of e.g. Stephen Timoshenko's beam model or plate theory (Sapountzakis, (2004), (Berczynski, Wroblewski, 2005) must be supported by advanced numerical programming and are too computationally intensive to be adopted in ordinary design.

Slip and up-lift characterise the partial-interaction between the bounded members, but the magnitudes of those characteristics are rather small, i.e. ~2E-4 m on a laboratory stand, (Johnson, 2004), 4.5E-4 m for a simple beam of a 10 m span. The curvature ratio of the partial-integration to full-integration of values 690/610 ≈ 1.13 is given in the same paper.

In (Shim, Lee, Chang, 2001), apart from slip and deflections, the inclinations of members' sections are measured, which is shown in Fig. 15 – it can be observed that they are not parallel.

At present, the (EN 1994) by virtue of requirement 1.5.2.1 includes the slip influence and its magnitude into elementary assessments.

7.1. Fundamentals of a composite girder with partial interaction

Let us assume that a composite beam of concrete-steel type, Fig. 7.1., is analysed and slip is taken into consideration with the exclusion of up-lift. The notation used here is sourced from (Newmark, Siess, Viest, 1951). Elastic behaviour falls within the range of the analysis. The following symbols and notation are used:

- O_c, O_s, O_i – centroids and axes crossing through the centroids of concrete, steel members and the fully integrated section, respectively,
- $E_cA_c = EA_c$, $E_sA_s = EA_s$ – tension-compression stiffness for concrete and steel elements,
- $\overline{EA}$ – doubled harmonic mean of EA_c and EA_s,
- $E_cJ_c = EJ_c$, $E_sJ_s = EJ_s$, $E_sJ_i = EJ_i$ – bending stiffness for concrete, steel components and the fully integrated cross-section, respectively,
- $\Sigma EJ = EJ_c + EJ_s$, $EJ_i = \Sigma EJ + a^2\overline{EA}$,

– ζ_c, ζ_s – positive measures of the null strain line shifts for concrete and steel elements,

– $\varepsilon_c, \varepsilon_s, \underline{\varepsilon_c}, \overline{\varepsilon^s}$ – are, generally speaking, concrete and steel strains and concrete and steel interface strains,

– $\gamma = \underline{u_c} - \overline{u_s}$ – the slip magnitude – slip, in short, is the difference between members' displacements in the interface,

– ρ_c, ρ_s – radii of concrete and steel member centroid curvatures,

The remaining symbols are commonly in use. Fig. 7.1 is a modification of Fig. 3.10. Two details are important – there is slippage at the interface, and the strain gradients in the members are not equal, as in (Seracino; Fig. 3.18). This situation differs from that discussed in (Newmark, Siess, Viest, 1951; Fig. 7), (Johnson, 1975/2004; Fig. 2.17), where the strain gradients in the members are equal, and in the case of equality of gradients, Newmark's assumption in the form (7.1) can be applied again. The mentioned approach will not be discussed here, although it is interesting.

Note that the load on the composite girder is the moment M-Na, which takes into account the effect of partial integration.

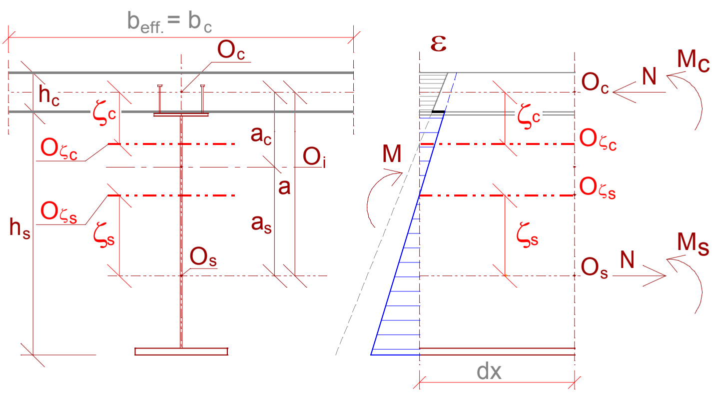

Fig. 7.1. Composite T-beam partial-integration

The (B-N) postulate is valid. It states that the plane sections in initial configuration remain plane in the deformed one, and their inclinations' angles are the same for both slab and beam members. This is expressed by the following statement

$$\left(\frac{1}{\rho_c}=\frac{M_c}{EJ_c}\right)=\left(\frac{1}{\rho_s}=\frac{M_s}{EJ_s}\right)=\frac{M-Na}{\Sigma EJ} \tag{7.1}$$

which can be read as an equality of member curvatures, or, in more detail – the curvatures of members' fibres crossing their centroids.

Here, the case of different linear gradients of the members is not considered.

From statics, the second condition is given

$$M = M_C + M_S + Na \tag{7.2}$$

However, (7.2) does not play any role because it entirely overlaps with (7.1).

The requirements for the normal force N are provided by the second order differential equation of constant coefficients, obtained as follows

- $\gamma=\dfrac{\tau}{k}$ – where $\tau=\dfrac{dN}{dx}=N^{/}$ – linear distribution of interfacial shear force,

  $k = const.$ – modulus of the connection,
- the rate of slip change is proportional to the difference between the members' strains in the interface $\dfrac{d\gamma}{dx}=\gamma^{/}=\dfrac{d}{dx}\left(\underline{u_c}-\overline{u_s}\right)=\underline{\varepsilon_c}-\overline{\varepsilon_s}$.

Combining both, one arrives at

$$N^{//}-\lambda^2 N=-\Delta M\,, \tag{7.3}$$

where $\lambda^2=k\dfrac{EJ_i}{\Sigma EJ\;\overline{EA}}=const.$, $\Delta=\dfrac{k\ a}{\Sigma EJ}=const.$, $k=const.$

Solving the equation applying the Laplace transform (7.3), one obtains

$$N(x)=\Delta\int_0^x M(x-\theta)\,f(\theta)\,d\theta+N(0)\,f^{/}(x)+N^{/}(0)\,f(x) \tag{7.4}$$

Where $f(x)=\dfrac{1}{\lambda}sh\lambda x$ (7.4.1)

$N(0)$, $N^{/}(0)$ are constants equal to the force N value and its first derivative N' at $x = 0$, respectively.

Alternatively, the expression (7.3) can be written down in the following way

$$N^{IV} - \lambda^2 N^{//} = \Delta q \;, \tag{7.5}$$

where q is the load distribution along the beam. In this option one arrives at

$$N(x) = \Delta \int_0^x q(x-\theta)\, g(\theta)\, d\theta + N(0) + N^{/}(0)x + N^{//}(0)g^{/}(x) + N^{///}(0)g(x), \tag{7.6}$$

where $$g(x) = \frac{1}{\lambda^3}(\mathrm{sh}\lambda x - \lambda x). \tag{7.6.1}$$

The forms of the solutions (7.4) and (7.6) differ slightly from those derived in (Rzhanitsyn, 1986), but are straightforward as far as the boundary conditions of all the admissible composite beam types listed there in detail are concerned. Also, in (Rzhanitsyn, 1986), apart from the above derivation, the condition (7.3) is obtained by means of the Euler-Poisson equation as a minimum of the action of internal forces in the case of multi-member beam.

When the modulus of a connection changes along the beam length, the equation (7.3) changes its classification and becomes a functionally varying coefficient class. Such cases are analysed by N. A. Jasim (Jasim, 1997), (Jasim, 1999). Several basic tasks of the varying geometry of a composite beam cross-section are discussed in (Rzhanitsyn, 1986).

The deflection y of a composite beam can be found using the following relation (Newmark, Siess, Viest, 1951, p. 86)

$$y^{//} = -\frac{M - Na}{\Sigma EJ}. \tag{7.7}$$

As can be seen from (7.7), the bending stiffness of a composite beam is, in fact, no taken into consideration. In the case of partial integration, it could be expected that bending stiffness should be present between ΣEJ and EJ_1 magnitudes. (7.7) could be understood as an examination of a substitute beam of non-integrated members instead of partially integrated ones and bent by the reduced moment (M – Na) instead of M. (7.7). Taking into consideration (7.4) as well as (7.7) and after performing some elementary operations one arrives at

$$y^{IV} - y^{//}\lambda^2 = -\frac{M^{//}}{\Sigma EJ} + \frac{M}{EJ_i}\lambda^2 \;, \tag{7.8}$$

which corresponds to the above discussion (see also: Oehlers, Bradford, 1999; p. 48). To complete the problem, let us add the solution (7.8), which can take the following form

$$y(x)=\int_0^x M(x-\theta)\left[\frac{\lambda^2}{EJ_i}g(\theta)-\frac{1}{\Sigma EJ}g^{//}(\theta)\right]d\theta+\frac{1}{\Sigma EJ}\left[M(0)\,g^{/}(x)+T(0)\,g(x)\right]+$$
$$+y(0)+y^{/}(0)\,x+y^{//}(0)\,g^{/}(x)+y^{///}(0)\,g(x)\quad . \tag{7.9}$$

Finalizing the discussion, let us recall the results included in (Newmark, Siess, Viest, 1951; Tab. 3) from which the comparison between theoretical and measured values of strains and deflections can be read. They differ from each other only by 2 to 7 percent.

Another approach to the problem could be found in the article (Seracino, Oehlers, Yeo MF, 2001). The topic discussion expanded to include beams can be found in (Seracino, Chow T. Lee, Tze C. Lim, Jwo Y. Lim, 2004). Although the partial-interaction *focal points* in concrete and steel members are visible in the figures included in (Rzhanitsyn, 1986), their first application was proposed in (Seracino, Chow T. Lee, Tze C. Lim, Jwo Y. Lim, 2004; Fig. 7.2.) (Rep.). In (Karaś, 2008), the theory of Newmark et al. is assumed and, as a result, the curvatures of the members as well as strain distribution inclinations are the same.

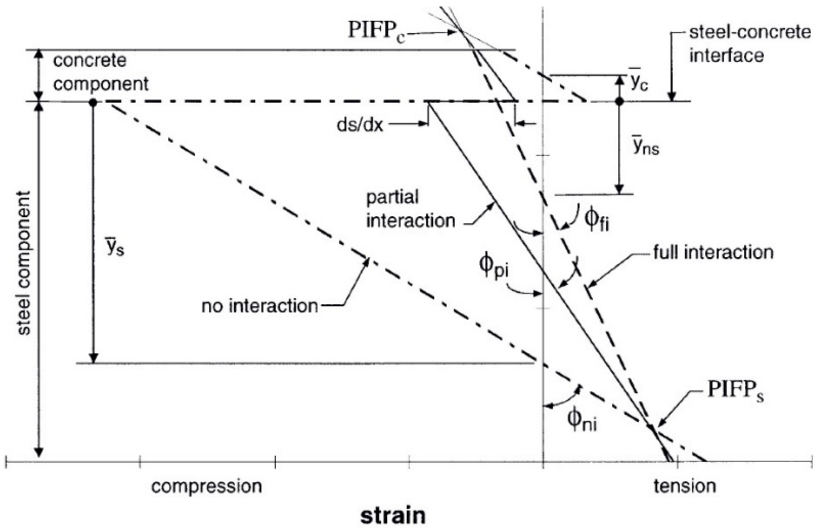

Fig. 7.2. Strain distributions, Rep. from (Seracino et al, 2004)

Seracino proved that if the bonds intersect at PIFP any strain distribution passes through the same points. The other innovation is MF (Magnifying Factor) defined as $MF=\dfrac{y^{//}_{pi.}}{y^{//}_{fi.}}$ or in conformity with the art of the article

$$y_{pi.}^{//} = y_{fi.}^{//} \, MF \qquad (7.10),$$

where $y_{fi.}^{//} = \dfrac{M}{EJ_i}$ and $y_{pi.}^{//}$ are obtained by integrating $y_{pi.}^{///} = \dfrac{-M^{/} + \gamma k a}{\Sigma EJ}$ (7.10.1)

(which is a version of (7.4) and (7.7) requirements). At first glance, MF improves nothing, but the authors provide a simplified method of MF calculation which justifies this extension. A step sequence is proposed, where, by means of MF as well as PIFP, strain and stress distributions can be obtained.

As stated before, this approach does not enable finding the bending stiffness of a composite girder but expresses it as a differential equation.

7.2. The concept of the strain zero line shifting

As mentioned at the beginning, the Newmark et al. theory belongs to simplified approaches. The strongest assumption concerns the equality of member curvatures. Actually, it means that the centroid lines of each member have the same curvature expressed by the simplified strength of materials formula $y^{//} \approx \rho^{-1} = M/(EJ)$. The relevant estimation is discussed in Fig. 7.3 showing two infinitesimal purely bent elements: non-integrated (Fig. 7.3.a) and fully integrated in Fig. (7.3.b).

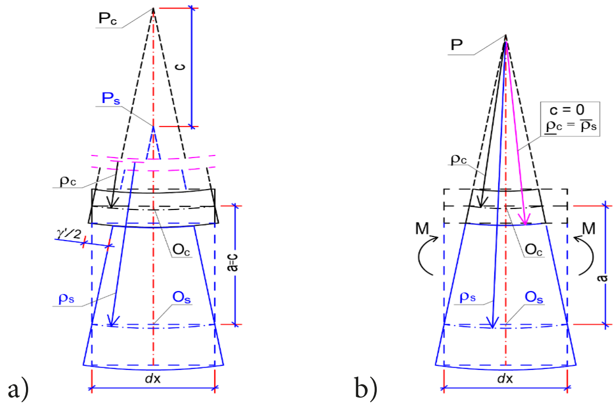

Fig. 7.3. Pure bending; a) no integration $\rho_c = \rho_s$, b) full integration $\underline{\rho_c} = \overline{\rho_s}$

In Fig. 7.3.a it can be seen that already from the beginning slip is permanently connected with this assumption $\rho_c^{-1} = \rho_s^{-1}$ (1'). Fig. 7.3.b shows the extent of the introduced approximation (1') by means of the radii of the curvature of the fibres in the axes of the elements. To compliment this, (1') should be rewritten to the form $\rho_c^{-1} = (\rho_s - a)^{-1}$ (1"), or alternatively expressed by

$$\underline{\rho_c} \approx \overline{\rho_s} \,, \tag{7.11}$$

but (11) still does not imply that the radii of centroid curvatures must be equal. The condition (1), which is used either for full- or partial integration concepts, is significantly weakened to the (11). Let us now make the next step in the analysis, and, instead of curvatures, let us account

$$\underline{\varepsilon_c} = \overline{\varepsilon_s} \,, \tag{7.12}$$

for a full-integration case. Actually, (7.12) complies with the geometry shown in Fig. 3.b and takes into consideration pure bending curvatures combined with the tension-compression of the members. Moreover, it could be understood as an incompatibility condition, too. Concluding this clarifying sequence, one obtains a basic criterion generalising the cases of integration through additional options.

Adopting the above concept, let us proceed to the partial integration case shown in Fig. 1. It is noticeable that the centroids' null strain axes of the members in the no-integration variant *shift* to the centroid axis of the transformed composite cross-section. Assuming it, for the partial integration the shifts of centroids' null strain axes of the members could achieve the positions denoted by ζ_C and ζ_S in Fig. 7.1. Furthermore, ζ_C and ζ_S could be understood as geometrical measures of near-interface zone flexibility; (Sapountzakis, 2004), (Karaś, 2008). Obviously, in this case, i.e. of partial integration, slip occurs and is in the functional relation to ζ_C and ζ_S.

In the operational sense, one has two null strain conditions and the third one for the equilibrium state

$$\varepsilon_c = -\frac{N}{EA_c} - \frac{M_c}{EJ_c}\left(y_c - \zeta_c\right) \rightarrow \varepsilon_{c0} = -\frac{N}{EA_c} - \frac{M_c}{EJ_c}\left(-\zeta_c\right) = 0 \,, \tag{7.13}$$

$$\varepsilon_s = \frac{N}{EA_s} - \frac{M_s}{EJ_s}\left(y_s + \zeta_s\right) \rightarrow \varepsilon_{s0} = \frac{N}{EA_s} - \frac{M_s}{EJ_s}\zeta_s = 0 \,, \tag{7.14}$$

and

$$M = M_C + M_S + aN, \tag{7.2}$$

where y_C, y_S are ordinates of the local Cartesian coordinate systems originating on the shifted axes ζ_C and ζ_S. By virtue of (2), (13), (14), the unknowns can be obtained as follows

$$M_c = \frac{N}{EA_c}\frac{EJ_c}{\zeta_c}, \qquad M_s = \frac{N}{EA_s}\frac{EJ_s}{\zeta_s}, \qquad N = M\left[a + \frac{\left(i_c\right)^2}{\zeta_c} + \frac{\left(i_s\right)^2}{\zeta_s}\right]^{-1}, \tag{7.15-17}$$

where $i_{(.)} = \sqrt{EJ_{(.)} / EA_{(.)}}$. (7.17.1)

Comparing the obtained solution with Newmark et al.'s and Rzhanitsyn's, a differential relation (7.3) is not needed at all. The flexibility change along the beam length is introduced by a variation of the geometrical measures ζ_c and ζ_s . In consequence, this variation implies beam stiffness changes.

The conditions (7.13), (7.14) may additionally result in different inclination angles of the sections – which are still flat – which is more general than the equality of their inclinations.

In relation to the Seracino-Oehlers approach, PIFP could be used as an approximation of the obtained section inclination angles of the transverse members.

N is in functional relation to M, ζ_c, ζ_s and other geometrical characteristics of the member cross-sections, which could be constant or vary along the beam length. For bending, their variation ranges are limited by the inequalities

$$0 \le \zeta_c \le a_c \text{ and } 0 \le \zeta_s \le a_s. \tag{7.18}$$

Additionally, for each member the bounds mean:

- $\zeta_{(.)} \le a_{(.)}$ – the case of the zero-interaction stiffness of an adequate material zone,
- $\zeta_{(.)} = 0$ – variant of infinitive stiffness,
- for both $\zeta_c = 0$ and $\zeta_s = 0$ – no-interaction in the interface,
- for both $\zeta_c = a_c$ and $\zeta_c = a_s$ – entire interaction in the interface.

Comparing the shifts ζ_c, ζ_s with the connection modulus k, used in the Newmark et al.'s theory, it is necessary to differentiate two components appropriate, respectively, for the flexibility of concrete and steel zones in the following way

$$\frac{1}{k} = \frac{1}{k_c} + \frac{1}{k_s}, \tag{7.19}$$

where $k = \infty$ denotes stiff connection and $k = 0$ concerns fulfilling the no-interaction requirements. The relation between k_c, k_s and ζ_c, ζ_s could have a linear form. Using a laboratory stand for the push-out purposes, the connection modulus values, k_c, k_s and ζ_c, ζ_s, can be obtained. The laboratory measuring position is shown in Fig. 7.4.

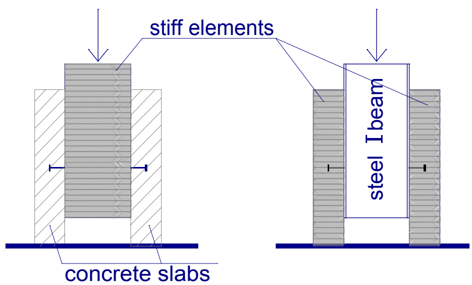

Fig. 7.4. The laboratory stand for determining the flexibility of concrete and steel zones

Now, it is possible to focus on the bending stiffness of the titular composite beam. Let us use the Steiner theorem to obtain the second moment of area (bending stiffness) of a composite girder. In this case, it is necessary to relate the problem to the full-integrated centroid axis, $O_i - O_i$ in Fig. 7.1. Two forms of bending stiffness for a partially integrated composite beam are admissible, i.e.:

$$EJ_i^{(I)} = \Sigma EJ + EA_c a_c \zeta_c + EA_s a_s \zeta_s \,, \tag{7.20}$$

and

$$EJ_i^{(II)} = \Sigma EJ + EA_c \left(\zeta_c\right)^2 + EA_s \left(\zeta_s\right)^2 . \tag{7.21}$$

Both fulfil limit approaches achieving no-integration and full-integration bending stiffness, respectively. For the beam specified in Fig. 7.5, the differences between $EJ_i^{(I)}$ and $EJ_i^{(II)}$ are searched.

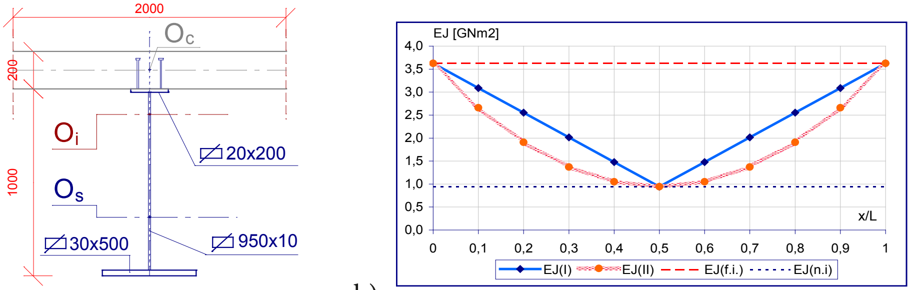

a) b)

Fig. 7.5. Cross-section [mm] b) the changes of bending stiffness with regard to (7.20) and (7.21)

With the use of dimensionless parameters

$$\mu_c = \zeta_c / a_c \text{ and } \mu_s = \zeta_s / a_s, \text{ where } 0 \le \mu_c = \mu_s \le 1, \tag{7.22-23}$$

the variation of bending stiffness expressions (7.20) and (7.21) is compared.

For the cross-section shown in Fig. 7.5., the connection changes linearly between its bounds, which implies that bending stiffness varies from the fully integrated stiffness value $EJ_i = 3{,}625$ GNm^2 at the beam ends to the non-integrated stiffness value of $\Sigma EJ = 0{,}942$ GNm^2 in span midpoint. In Fig. 7.6., the variation of bending stiffness along the simple beam length is shown. This typical connection distribution implies that the presented bending stiffness changes should be taken into account in the case of serviceability states. The visible linear and non-linear character of $EJ_i^{(I)}$ and $EJ_i^{(II)}$ come from the forms of the expressions (7.20) and (7.21), respectively.

As it seems, there is no special analytical reason to prefer any of the forms presented in (7.20) and (7.21) to the others. However, if one wants to be on the safe side, they should choose (7.21) as the best option.

***

Finally, it is possible to conclude as follows:

- A short but detailed survey of fundamentals in the field of the partial integration of a composite beam has been carried out. Following an examination, the scarcity of an adequate form of bending stiffness was noticed.
- From the beginning, the basis for the investigation was constituted by the expansion of the fully integrated composite beam stiffness by softening effect. The introduced geometrical measures allowed to find the solution without the use of Newmark's differential relation (7.7). These measures are simply related to a commonly used connection modulus. The problem of bending stiffness has not been definitively settled but, as it seems, was further advanced in comparison to the recalled approaches. The interface shearing forces have been not discussed here because their analyses overlap with the elementary strength of materials task.
- The performed analyses concern elastic behaviour. Nevertheless, the strain approach allows expansion of the analysed tasks by a plastic field, too.
- Although the problem addressed is analytically interesting, full integration is, in fact, best for the structure.

8. J. Courbon's method

Using Courbon's method (Courbon, 1940), it is possible to separate the outer girder from the deck as well as loads acting on it.

Briefly, the greatest achievement of this method is the possibility to limit a design to only one outer girder instead of an entire carrying deck. Comparing the outer girder loading to the loading of other internal girders, it can be concluded that relative overloading occurs in its case.

Comparing Courbon's method to FEM procedures commonly used nowadays, the method appears to be very crude. As such, it is a simplification, a simple approach, however, it gives reliable results, especially in the cases of carrying decks in a grid form. The method was extensively used from 1960s to 1990s. It is still in use in wooden or simple temporary bridge construction.

Moreover, it is an intelligent method allowing to understand the carrying deck response to bridge loads.

In the beginning, let us formulate the premises for further analysis:

- the main assumption is a very stiff crossbar is located in the deck cross-section (theoretically, even infinitely stiff),
- the carrying deck as well as its materials are elastic and Hooke's law can be applied,
- the *principle of stiffness* applies,
- the structure (the girder system) is symmetric,
- in calculation, superposition is allowed.

a)  b) 

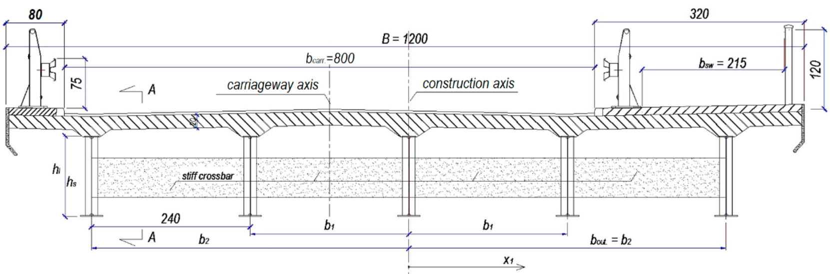

c)

Fig. 8.1. Carrying deck as a composite of steel and concrete, Lopiennik Village, Poland, Lopa River a) side view b) bottom view c) typical cross-section of a composite small bridge

Fig. 8.1.a-b show a simply supported carrying-deck produced using the composite steel-concrete technology. The average length of a Polish bridge amounts to 20-21 m. Therefore, this is the most significant group of bridges and for that reason such a small bridge is the subject of further considerations.

The arrangement of traffic on a bridge carrying deck can vary and depends mainly on the intended use of the bridge, i.e. as a highway bridge, city bridge or bridge located on local as well as country roads. Fig. 8.1.c shows a solution responding to the needs of urban and non-urban bridges. Nowadays, this solution is commonly in use.

Corresponding to the requirements of Courbon's method, a rigid crossbar is introduced.

Here, the term "antisymmetric" is used instead of "skewed".

In Fig. 8.2.a, the arbitrary concentrated force F acts within the range of the positive part of the domain and is located by the abscissa value $x_1 = x$. A comparison of the initial (marked by a dashed line) and the actual (continuous line) configurations allows to draw the vertical displacements of the girders, as well as the rotation of the cross-section. The bridge girder system conjugated with the stiff crossbars resists the action of the force producing a linear form of deformation – which results from Courbon's assumption. This is very important in general because it shows that the most important girder in the girder system is the outer one (on the side of the force action) which, compared to the others, bends maximally. In the case of small bridges, a designer can design this girder and then assume the remaining girders as the same.

Also, the following statement can be written down – the outer girder is relatively overloaded when compared to the other girders.

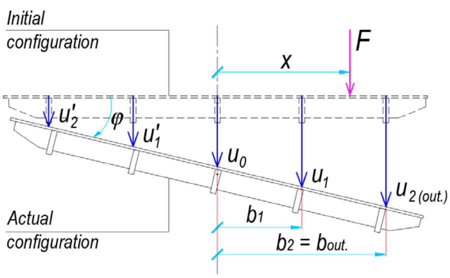

a)

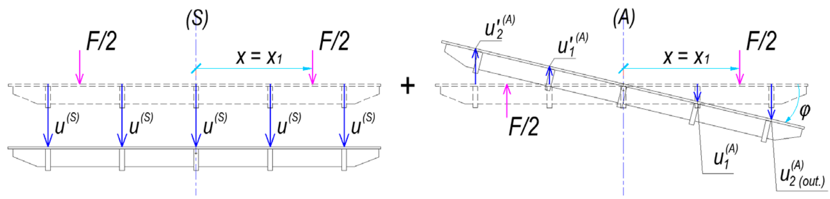

b)

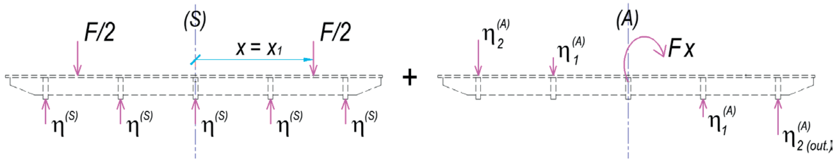

c)

Fig. 8.2. Deformation and respective forces for the bridge deck cross-section with a stiff crossbar a) general case of deformation: u – displacement, φ – rotation b) decomposition of the general deformation into symmetric (S) and antisymmetric (A) parts c) active and passive forces (reactions) in the cases of symmetric and antisymmetric deformations.

In Fig. 8.2.b, the general deformation is divided into two parts. The symmetrical deformation corresponds to the parallel shift by the displacement value u_0, which is now marked as $u^{(s)}$, and occurs for each girder. The other deformation type, antisymmetric, corresponds to the rotation of the carrying deck as a solid body in accordance with the couple Fx action. Also, the vertical shifts, $u_m{}^{(A)}$, correspond to the 'difference' between the actual and initial configurations here. Joining the symmetric and antisymmetric parts (which is symbolically marked with "+") gives the general deformation.

At this stage, it is characteristic that the displacements and actions-forces occur at the same time.

This stage must be changed to a case in which the set of equilibrium equation system can be used. Here – and probably only here – the original Hooke's law can be useful. Let us recall once again this sentence

Ut tensio, sic vis

which, in the analysed case, can be rewritten to the following form

$$u^{(s)} \sim \eta^{(s)} \quad \text{and} \quad u_m{}^{(A)} \sim \eta_m{}^{(A)}, \tag{8.1}$$

where $\eta^{(\cdot)}$ stands for the girder reactions to the actions corresponding to the F force forms.

In Fig. 8.2.c, bearing in mind the introduced decomposition, only the active and passive forces describe the problem. By virtue of the *principle of stiffness,* the forces are applied to the structure in the initial configuration.

For the plane tasks, the basic form of the equilibrium set is as follows

Symmetry

$$\begin{cases} \Sigma x_2 : F = k\eta^{(S)} \\ \Sigma x_1 : \textit{not applicable}, \\ \Sigma M_0 : 0 = 0 \end{cases}$$

Antisymmetry

$$\begin{cases} \Sigma x_2 : 0 = 0 \\ \Sigma x_1 : \textit{not applicable} \\ \Sigma M_0 : Fx = 2 \sum_{m=1}^{\mathrm{Int.}(k/2)} \eta_m^{(A)} b_m \end{cases}, \tag{8.2-3}$$

where k is the number of girders, Int.(k/2) – integer value of k/2.

In the symmetric case, the solution is as follows

$$\eta^{(S)} = \frac{F}{k}. \tag{8.4}$$

In the other part concerning antisymmetry, there is only one condition, and the number of unknowns is [k/2]. Additional conditions [k/2]-1 are necessary. Fortunately, again, the main assumption of the method can be applied, now in the form of Thales's theorem in the following form

$$\frac{\eta_i^{(A)}}{b_i} = \frac{\eta_{i-1}^{(A)}}{b_{i-1}}, \quad i-1 \geq 1 \tag{8.5}$$

or in accordance to the girder system in Fig. 8.2.b is as follows

$$\frac{\eta_{2(\mathrm{out.})}^{(A)}}{b_{\mathrm{out.}}} = \frac{\eta_1^{(A)}}{b_1} \text{ hence } \eta_1^{(A)} = \eta_{2(\mathrm{out.})}^{(A)} \frac{b_1}{b_2} \text{ is obtained.} \tag{8.6}$$

The reaction in the outer girder is given by the expression

$$\eta_{2(\mathrm{out.})}^{(A)} = \frac{F\,x\,b_{\mathrm{out.}}}{2 \sum_{m=1}^{\mathrm{Int.}(k/2)} \left(b_m\right)^2}. \tag{8.7}$$

By adding the symmetric and antisymmetric solutions, finally one arrives at

$$\eta_{(\mathrm{out.})} = \eta^{(S)} + \eta_{(\mathrm{out.})}^{(A)} = F\left(\frac{1}{k} + \frac{x\,b_{\mathrm{out.}}}{2 \sum_{m=1}^{\mathrm{Int.}(k/2)} \left(b_m\right)^2}\right). \tag{8.9}$$

Using the above formula, one can find the reaction in any girder of a bridge

$$\eta_i = \eta^{(S)} + \eta_i^{(A)} = F\left(\frac{1}{k} + \frac{x\, b_i}{2 \sum_{m=1}^{Int.(k/2)} \left(b_m\right)^2} \right), \quad i = 0,1,\ldots,[k/2] \tag{8.10}$$

Until now, the deformation of the cross-section has been analysed and the forces introduced have been used to determine the reaction of the extreme beam to the applied load.

Now, let us consider the solution obtained in a mathematical context. Let the force

$$F = 1 \tag{8.11.1}$$

and the structure characteristics be marked as constants, i.e.

$$a_0 = \frac{1}{k}, \qquad a_1 = \left[2 \sum_{m=1}^{Int.(k/2)} \left(b_m\right)^2 \right]^{-1} \tag{8.11.2}$$

Furthermore, let the position of the girder be labelled now as ξ and then it can be written

$$\eta_{(\xi)}\left(x,\xi\right) = a_0 + a_1\, x\, \xi\,. \tag{8.12}$$

This expression is linear to the x and ξ arguments, in other words, is bilinear and additionally commutative

$$\eta_{(\xi)}\left(x,\xi\right) = \eta_{(\xi)}\left(\xi,x\right). \tag{8.13}$$

Hence, the formula can be read as an influence function of the cross-section material reaction at the point ξ caused by a unite force moving along the bridge deck cross-section according to x

$$\text{Inf.Line}\left[\eta_{(\xi)}\left(x,\xi\right)\right] = a_0 + a_1\, x\, \xi\,, \tag{8.14}$$

Which can be called the *influence line* of the material reaction of the cross distribution of loads. The radical of this line can be calculated as follows

$$\eta_{(\xi)}\left(x,\xi\right) = 0 \tag{8.15.1}$$

And this obviously results in

$$x_0 = -\frac{1}{\xi}\frac{a_0}{a_1}\,. \tag{8.15.2}$$

It can be seen that for ξ = 0 the radical is a_0.

Now, let us get back to the analysis of the outer girder reaction for a fixed value $\xi = b_{out.}$. The graph of

$$\text{Inf.Line}_{\eta_{(out.)}} = a_0 + a_1 \, x \, b_{out.} \tag{8.16}$$

is shown in the Fig. 8.3.

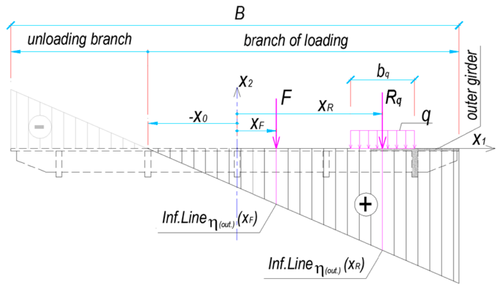

Fig. 8.3. Influence line of a reaction in the outer girder

The radical x_0 divides the cross-section width into two branches. The longer branch $\left\langle x_0 + B/2 \right\rangle$ is the branch for which with each force acting on it in the reaction of the outer girder there is a value increase. This branch is called a *branch of loading*. The remaining sector of the length $\left\langle B/2 - x_0 \right\rangle$ is called an *unloading branch*. If a force is set on this branch, this will relieve i.e. cause a reduction in the reaction value of the outer girder.

In Fig. 48, two forms of loads are shown, the concentrated force F[kN] and UDL q in [kN/m^2]. Let us determine the share of the outer girder in the carrying of the F and q actions. There are two options, although they converge. For the first one, one can use the influence line graph as follows

$$\eta^F_{(out.)} = F \left[\text{Inf.Line}_{\eta(out.)}(x_F) \right], [kN], \tag{8.17.1}$$

$$\eta^q_{(out.)} = R_q \left[\text{Inf.Line}_{\eta(out.)}(x_R) \right], [kN/m], \tag{8.17.2}$$

where R_q is a resultant force in the form of a load linear density, which can be calculated as $R_q = qb_q$, and is expressed in [kN/m].

The other option is the direct application of the expression

$$\eta^F_{(out.)} = F\left(a_0 + a_1 \, x_F \, b_{0ut.} \right), [kN], \tag{8.17.2}$$

$$\eta^{q}_{(out.)} = R_q \left(a_0 + a_1 \, x_R \, b_{0ut.} \right), [kN/m] . \tag{8.17.2}$$

Now, it is the right moment to return to the first sentence of this chapter. Having the outer girder reactions, one can change their orientation[12] and treat them as forces loading the outer girder, visualised as cut out from the carrying deck. Briefly, the simple beam is loaded by the known forces, Fig. 8.4.

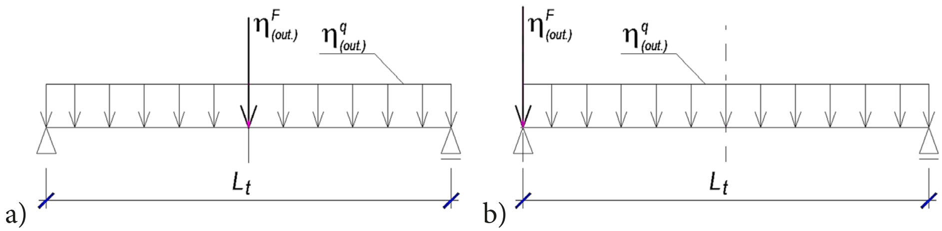

Fig. 8.4. The cut-out outer girder with its loads a) max bending moment b) extreme shearing force

This is the beauty of simplifying methods. The basic internal forces of a beam can be obtained as follows

$$M_{max} = \eta^{F}_{(out.)} \frac{L_t}{4} + \eta^{q}_{(out.)} \frac{(L_t)^2}{8} , \tag{8.18.1}$$

$$T_{extr.} = \eta^{F}_{(out.)} + \eta^{q}_{(out.)} \frac{L_t}{2} , \tag{8.18.2}$$

And the max deflection amounts to

$$u_{max} = \frac{1}{E_s J_i} \left(\frac{1}{48} \eta^{F}_{(out.)} (L_t)^3 + \frac{5}{384} \eta^{q}_{(out.)} (L_t)^4 \right) \approx \frac{5}{48} \frac{M_{max} (L_t)^2}{E_s J_i} , \tag{8.19}$$

where L_t is a theoretical bridge length, E_s – Young's modulus of steel, J_i – the moment of inertia of the integrated girder cross-section. E_sJ_i – bending stiffness of the integrated girder.

[12] A vector is characterized by its attitude, orientation, and magnitude.

8.1. Discussion of other symmetric and antisymmetric decompositions

The three functions presented in Fig. 8.5, shall be compared. All three of them are anti-symmetrical with respect to the x_2 axis:

(i) linear function – Courbon's method,

(ii) sinus hyperbolics,

(iii) $\sin(\xi)$ when $\frac{-\pi}{2} \le \xi \le \frac{\pi}{2}$.

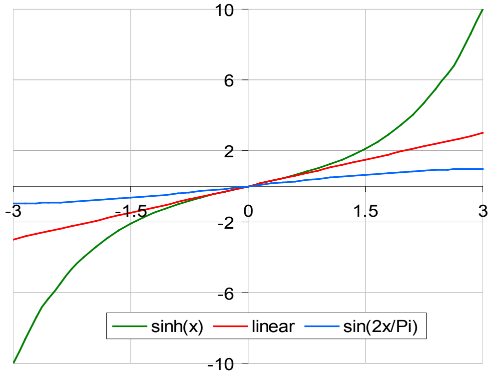

Fig. 8.5. Example of antisymmetrical functions

Let us derive a set of expressions considering the sinus hyperbolics function. The symmetric part a_0 remains unchanged, hence, the couple equivalence equation is the aim of the analysis

$$Fx = 2 \sum_{m=1}^{Int.(k/2)} \eta_m^{(A)} b_m . \tag{8.20}$$

Here, an additional condition has the form of sequential proportions

$$\frac{\eta_m^{(A)}}{\eta_{out.}^{(A)}} = \frac{\sinh(b_m)}{\sinh(b_{out.})}, \text{ hence } \eta_m^{(A)} = \eta_{out.}^{(A)} \frac{\sinh(b_m)}{\sinh(b_{out.})}, \tag{8.21}$$

then

$$Fx = 2\eta_{out.}^{(A)} \frac{1}{b_{out.}} \left[\left(b_{out.}\right)^2 + \ldots + b_{out.} \left(b_2 \frac{\sinh(b_2)}{\sinh(b_{out.})} + b_1 \frac{\sinh(b_1)}{\sinh(b_{out.})} \right) \right] = \eta_{out.}^{(A)} \frac{1}{b_{out.}} \frac{}{a}$$

(8.22)

$$\eta_{out.}^{(A)} = Fx\, b_{out.} a_1^{(sh)} . \tag{8.23}$$

Finally, the following is obtained

$$\eta^{(sh)}_{(out.)} = F\left(a_0 + x\, b_{out.} a_1^{(sh)} \right), \quad x_0^{(sh)} = -\frac{1}{b_{out.}} \frac{a_0}{a_1^{(sh)}}. \tag{8.24}$$

An analogous expression occurs when the sinus function is defined within the range of the sinus domain $\frac{-\pi}{2} \le \xi \le \frac{\pi}{2}$.

For the comparison, three variants are analysed, and the reference is Courbon's method – the linear function.

The following example demonstrates the differences. Dimensionless coordinates with the reference magnitude $b_{out} = b_2$ are introduced. The concentrated force $F = 100$ kN is placed at the abscissa's point $x_F = b_{out}$. Hence,

$$\bar{b}_n = \frac{b_n}{b_{out.}}, \ n = 1{,}2. \qquad \bar{x}_F = \frac{x_F}{b_{out.}} = 1, \quad \bar{x}_0^{(.)} = \frac{x_0}{b_{out.}}, \tag{8.25}$$

$$\eta^{(.)}_{(out.)} = F(a_0 + a_1\, x_F\, b_{0ut.}) \qquad \rightarrow \qquad \bar{\eta}^{(.)}_{(1)} = F(a_0 + \bar{a}_1^{(.)}) . \tag{8.26}$$

Thus, one has

– Ad. (i) – linear function

$$\bar{a}_1^{(lin.)} = \frac{1}{2}\left[1 + \left(\bar{b}_1\right)^2\right]^{-1} = 0.4, \tag{8.27.1}$$

$$\bar{x}_0^{(lin.)} = -\frac{a_0}{\bar{a}_1^{(lin.)}} = -0.5, \ \left(x_0^{(lin.)} = -2.4\,\mathrm{m}\right), \ \bar{\eta}^{(lin.)}_{(1)} = 60\,\mathrm{kN}. \tag{8.27.2}$$

– Ad. (ii) – sinus hyperbolic function

$$\bar{a}_1^{(sh)} = \frac{1}{2}\left[1 + \bar{b}_1 \frac{\sinh(\bar{b}_1)}{\sinh(1)}\right]^{-1} = 0.48, \tag{8.28.1}$$

$$\bar{x}_0^{(sh)} = -\frac{a_0}{\bar{a}_1^{sh}} = -0.42, \ \left(x_0^{(sh)} \approx 2.02\,\mathrm{m}\right), \ \bar{\eta}^{(sh)}_{(1)} = 67.8\,\mathrm{kN}. \tag{8.28.2}$$

– Ad. (iii) – sinus function

$$\bar{a}_1^{(sin)} = \frac{1}{2}\left[1 + \bar{b}_1 \frac{\sin(\bar{b}_1)}{\sin(1)}\right]^{-1} = 0.37, \tag{8.29.1}$$

$$\bar{x}_0^{(sin)} = -\frac{a_0}{\bar{a}_1^{(sin)}} = -0.54, \ \left(x_0^{(sin)} \approx 2.6\,\mathrm{m}\right), \ \bar{\eta}^{(sin)}_{(1)} = 57{,}1\,\mathrm{kN}. \tag{8.29.2}$$

Commenting on the obtained results, it can be stated that the differences are not negligible and amount to ~20%. The share of the outer girder in the carrying of the F force is 60%, 67.8% and 57.1%, respectively.

Despite the formal correctness using the sine and sine hyperbolic functions, the assumption regarding the existence of a rigid crossbar weakens.

To complete the above analyses, a simple computing example with the aid of the *Midas* procedure is carried out. The bridge cross-section in Fig. 45 is investigated with the following parameters – h_i = 1.5 m, h_s = 1.2 m, b_1 = 2.4 m, $b_2 = b_{out}$ = 4.8 m, x_F = 4.8 m, b_{ef} = 2.4 m, L = 22 m, L_t = 21 m, B = 12 m. The crossbar is composite, Fig. 8.1.c, with the upper element constituted by a concrete plate h_c = 0.2 m with b_{ef} = 2.4 m, and the bottom cord – by a steel HEB 600 profile.

In Fig. 8.6, two interesting issues are shown. Firstly, in the analysed special case of the assumed loading, the influence of the number of crossbars is not important. Secondly, the values of the max bending moment M_y differ very slightly, by less than 0.5%. As a consequence, also the share of F_x =100 kN force acting on the outer girder is similar. Using the formula $\eta_{out.} = 4M_y / L_t$, one arrives at the values $\eta_{out.}^{(1\,transom)} = 64.4\,\text{kNm}\ (64.4\%)$ and $\eta_{out.}^{(3\,transoms)} = 64.2\,\text{kNm}\ (64.2\%)$.

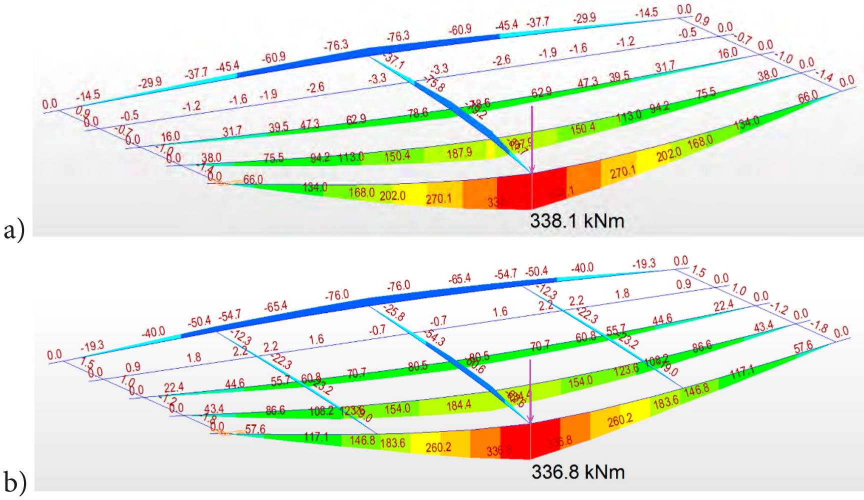

Fig. 8.6. Distribution of bending moments M_y on the grid beams a) one internal crossbar b) three internal crossbars

The computed results fall almost in the middle between the theoretical variants (i) and (ii).

The last question – how the M_y moments are distributed when the force is located between the crossbars? The answer can be obtained by analysing the computational results, see Fig. 8.7.

a)
b)

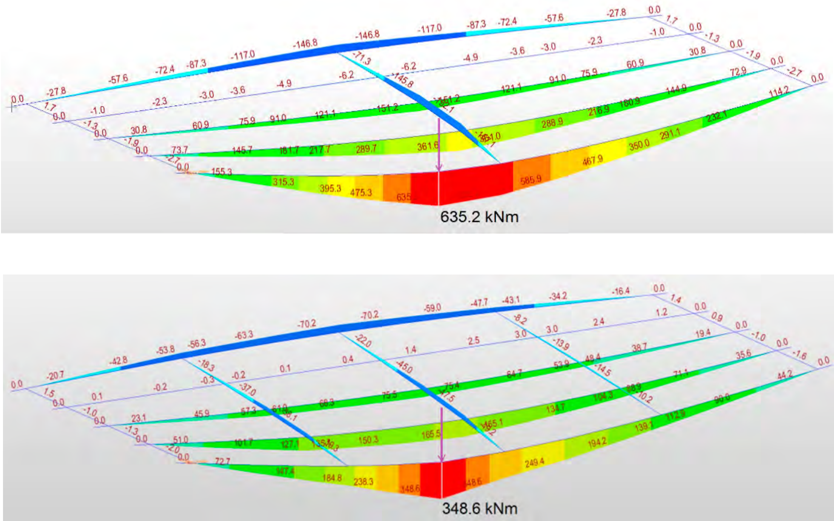

Fig. 8.7. Bending moments My distribution in the case of a force applied between crossbars a) one internal crossbar b) three internal crossbars

One can calculate the outer girder share in the carrying of the load force as $\eta_{out.}^{(1\,transom)} = 75.6\,\mathrm{kNm}$ (75.6%) and $\eta_{out.}^{(3\,transoms)} = 41.5\,\mathrm{kNm}$ (41.5%), according to Fig. 8.7.a and 8.7.b.

In the case of one crossbar, Courbon's method is useless; in the other case, significant underestimation occurs.

***

Concluding the whole chapter, it is necessary to stress that nowadays the method should be treated as a reconnaissance in the design of a carrying decks of beam bridges. It is proper for designing simple wooden and temporary bridges.

9. Dynamic amplifying factor – DAF

DAF is defined as a ratio of the dynamic effect related to the quasi-static effect. The effect can be a displacement, strain, or a rotation angle, for instance. Hence, one can write

$$\mathrm{DAF}_{(u)} = \max\left\{\frac{\left|u(v_n)_{(dyn)|x_m}\right|}{u_{(quasi-stat.)|x_m}}\right\} \tag{9.1}$$

which can be read as: DAF at a chosen group of points x_m of structure is a ratio of the max amplitude module effect (displacement) to the max quasi-static effect, both at the same point $x_{(.)}$, taking into account the different velocities v_n of the test vehicle. In many standards, monographs and papers, the denominator contains $u_{(stat.)}$, however, the name containing $u_{(stat.)}$ is more adequate.

During the dynamic bridge proof tests of road bridges, vehicles/trains should run steadily with different velocities, starting from 10 km/h to 90 km/h with a step of 10 km/h, or 20 km/h. For rail bridges, the velocity upper limit can be higher appropriately to the actual train velocity. It is frequently assumed that a run with the velocity v = 10 km/h (sometimes it is v =5 km/h) causes the quasi-static effect. The used "max" operator concerns amplitudes of n – velocities at m – measurement points.

The static effect is achieved when the vehicle/train set stays at a point for min. 30 minutes. Predominantly, the dynamic test is performed using a single truck. The effects of the static test and quasi-static test, in general, differ significantly, simply because they disclose different mechanical characteristics of a bridge structure.

A short example can illustrate the above discussion. In the autumn of 2018, a new interesting bridge was examined with the use of the proof test, both static and dynamic.

The bridge was designed by *Tadeusz Stefanowski, MSc* in accordance with the Polish bridge standard concerning the load class I included in (PN-85/S-10030), permitting the movement of vehicles with a maximum weight of 500 kN.

Two independent steel arches tied by a prestressed concrete deck form a carrying structure, Fig. 55. The span length amounts to 69.6 m. The right bevel of the bridge is α = 75 deg. The arch elevation amounts to11.625 m. In the cross-section, there is only one sidewalk of the clearance gauge of 3.0 m.

In the author's opinion, the indisputable beauty of the bridge is visible even in the photos in Fig. 9.1. During the proof test[13], the arch adjacent to the sidewalk was marked as "1" and the other as "2" (see: Tab. 9.1 and Tab. 9.2).

[13] The proof testing of the bridge was carried out by the consortium of ATEST Laboratory & Lublin University of Technology.

The static test was carried out with the use of 6 lorries of the weight of 320 kN each. During the dynamic test, only one lorry was used for sequential rides.

In the case of arch bridges, the cross section at one-quarter of the length (L/4 or 3L/4) is particularly sensitive dynamically. The testing focused on those points.

a) 

b) 

Fig 9.1. The road bridge over the Warta River, Provincial road No. 710 near the city of Warta, central Poland a) side view b) along the bridge view

The measured vertical displacement results are included in Tab. 9.1. and Tab. 9.2.

Tab. 9.1. The registered vertical displacements at one quarter of the arch support length

			Vertical displacement [mm]			
No.	v [km/h]	Direction	1. (L/4)	1. (3L/4)	2. (L/4)	2. (3L/4)
1	10	W – E	2.28	2.28	1.51	1.51
2		E – W	1.83	1.83	1.73	1.73
3	30	W – E	2,24	2,24	1.47	1.47
4		E – W	1.89	1.89	1.77	1.77
5	50	W – E	2.63	2.63	1.86	1.86
6		E – W	2.14	2.14	1.97	1.97
7	70	W – E	2.45	2.45	1.78	1.78
8		E – W	2.41	2.41	2.29	2.29
9	90	W – E	2.52	2.52	1.83	1.83
10		E – W	2.17	2.17	1.94	1.94
11	30(*)	W – E	2.83	2.83	1.88	1.88
12		E – W	2.03	2.03	2.05	2.05

(.) a run through the transverse threshold

The use of a wooden threshold, about 10 cm height, is a simulation of a heavily damaged road pavement.

Tab. 9.2. Calculated DAF values

No.	v [km/h]	Direction	DAF [1] 1. (L/4)	1. (3L/4)	2. (L/4)	2. (3L/4)
3	30	W – E	0.98	0.98	0.97	0.97
4		E – W	1.03	1.03	1.02	1.02
5	50	W – E	1.15	1.15	1.23	1.23
6		E – W	1.17	1.17	1.14	1.14
7	70	W – E	1.07	1.07	1.18	1.18
8		E – W	1.317	1.317	**1.324**	**1.324**
9	90	W – E	1.11	1.11	1.21	1.21
10		E – W	1.19	1.19	1.12	1.12
11	30(*)	W – E	1.19	1.19	1.12	1.12
12		E – W	1.19	1.19	1.12	1.12

The maximum value of DAF occurs for the girder "2" and amounts to DAF = 1.324. It is worth mentioning that according to the standard (PN-85/S-10030), the DAF coefficient should be calculated by the following linear formula

$$\varphi = 1.35 - 0.005L, \text{ (L in meters)}, \tag{9.2}$$

hence, considering the obtained DAF value, one arrives at the length $L \approx 6$ m, which approximately corresponds to the spacing of the hangers at the points where they are connected to the platform.

In conclusion, the DAF searching is only one element of the dynamic testing. Besides, they are determined by a computer modelling and by measuring the natural frequency values and the damping of the vibration of various bridge elements in situ.

The reader is referred to an interesting publication on beam dynamics (Ataman, Szczesniak, 2022), in which the damping of vibrations from moving loads is also taken into account by an analytical method. In a monograph (Szczesniak, 2000) on plate dynamics, one chapter is devoted to the problem of damping. Various forms of damping were discussed, organizing them according to the original method developed. This made it possible to unify assessments of the effects caused by various kinetic, material, dynamic and quasi-static features. The chapter includes examples for plates, including bridge plates.

***

10. The influence of a strain rate on the understanding of dynamical processes

The common understanding of statics, quaistatics and dynamics can be aided by examining the equation of equilibrium of any particle which could be elastic or viso-elastic, and has the following form

$$\nabla_m \sigma^{mn} + \rho f^n = \rho \partial^2_{(t)} u^n \,, \tag{10.1}$$

where the process arguments depend (or do not depend) on the time parameter t, ∇_m is the covariant derivation symbol in the 3-dimensional problem i, and m = 1, 2, 3, $\partial^2_{(t)}$ is the symbol of the second time derivative, σ^{mn}, f^n, u^n are contravariant, appropriately, stress tensor, load vector and displacement vector in the material particle, ρ is a particle mass density.

Statics:
is the state in the actual configuration where σ^{mn}, f^n are constant and the inertial effects are zero, $\rho \partial^2_{(t)} u^n = 0$.

Quasistatics:
is a process i.e. $\sigma^{mn} = \sigma^{mn}(t)$ and $f^n = f^n(t)$, however, the inertial effects can be neglected, i.e. $\rho \partial^2_{(t)} u^n = 0$.

Dynamics:
is characterized by the fact that all arguments depend on the time parameter t, and the inertial component is of great importance. In this case onemust consider $\sigma^{mn} = \sigma^{mn}(t)$, $f^n = f^n(t)$ and $u^n = u^n(t)$.

As early as in 1950s, significant qualitative and quantitative differences were observed in the behaviour of steel at different tensile loading rates. In Fig. 10.1., a copy of the graph sourced from (Nadai, 1950) is shown.

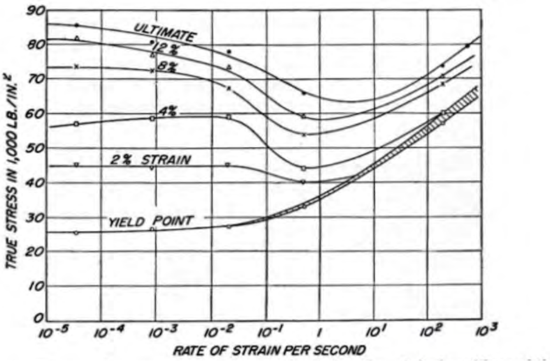

Fig. 10.1. According to the source notation, soursed from (Nadai, 1950), *Fig. 19-16,* entitled *The true flow stresses at various strains in function of the logarithms of the rates of strain (mild steel) at room temperature*

It can be seen that 2% strain, 4% strain, and the yield limit value overlap with a simultaneous value increase on the curve. At the same time, the yield limit value rises twice.

Material processes run in different ways. In the case of the creep of concrete or steel relaxation one can speak of a long process development time. In the case of road bridges, quasi-static processes – which approximately correspond to static states – occur. As regards train bridges and HSLM trains, the speed of a rolling stock induces dynamic processes.

In extreme cases involving sharp decelerations or accelerations or impacts on structural members or bridge equipment, the loading time is rapidly reduced to a few seconds or fractions of a second, corresponding to the issues of *structural dynamics or soft impact*. Modern bridges should also be designed bearing in mind impact phenomena caused by gas or explosive charges. This is a group of *high or very high impacts*.

The effect of the loading velocity on concrete compression is similarly highlighted. Based on the work (Rüsch, 1960), the following graph of $\sigma \sim \varepsilon$, Fig. 10.2 is drawn at different loading velocities up to failure.

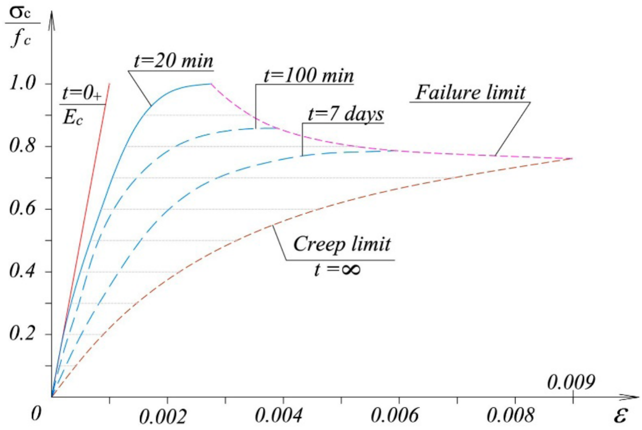

Fig. 10.2. The strain-stress compression relation envelopes for 56-day old concrete and the cylinder strenght f_c = 34.5 MPa, based on (Pająk, 2011)

In the graph, the red straight line represents Hooke's law in the elastic case, i.e. when concrete is loaded to its ultimate strength in a very short time $t \rightarrow 0_+$.

In the laboratory tests, the loading rate was chosen is such a way that the failure occurred after 20 min., 100 min. and 7 days, respectively. The concrete strengths determined in subsequent tests allowed for the extrapolation of the failure curve, which in turn allowed to estimate the creep curve as a limiting process – the lower envelope.

As in the case of tensile steel, one finds that there is a decrease in the strength of concrete when the loading process is extended, which corresponds to a decrease in strain rates.

Process measures, which are functions of the strain rate with a unit [1/s], are used to classify the effects of various actions on materials.

An example of classification as a function of the strain rate is shown in Fig. 10.3; (Lukic, 2018).

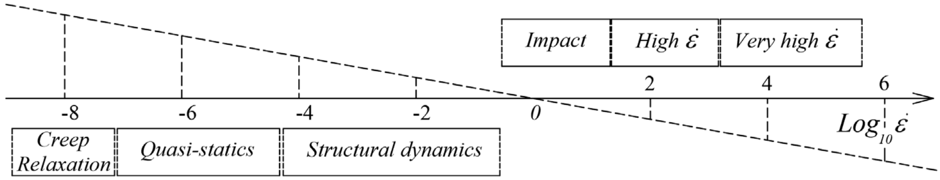

Fig. 10.3. The strain rates characteristic for different mechanical examinations of material properties

A relative measure of the effects of short-term loading is known as *Dynamic Increment Factor* (DIF), defined as the ratio of the dynamic strength to the static strength/strain, and is usually reported as a function of the strain rate. For concrete, DIF can be more than 3 times greater in compression and up to about 12 times greater in tension, see: Fig. 10.4.

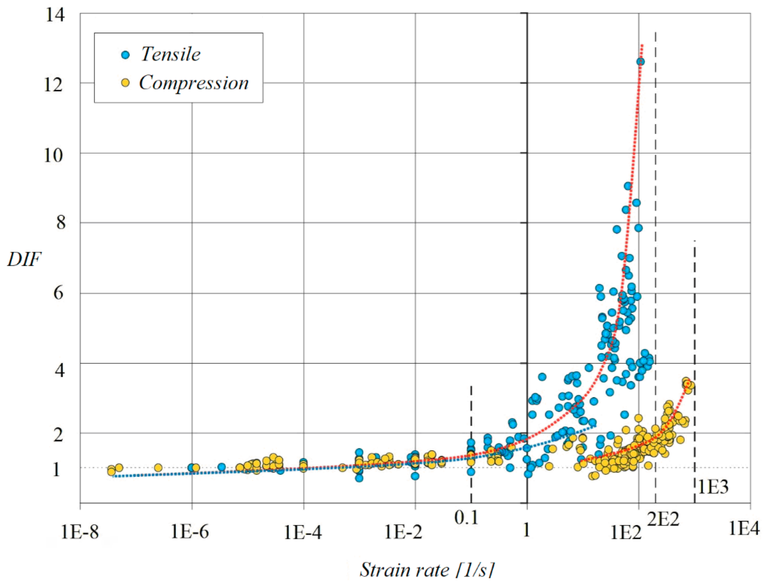

Fig. 10.4. Strain rate versus DIF for concrete in compression and tension; based on (Pająk, 2011)

A very useful definition of DIF of concrete was formulated in (*CEB-FIP Model Code 1990*). There, the following definition was made for compression strength

$$\mathrm{DIF}_{(c)} = \frac{f_c}{f_{cs}} = \begin{cases} \left(\dfrac{\dot{\varepsilon}}{\dot{\varepsilon}_s}\right)^{1.026\alpha_s} & \rightarrow \dot{\varepsilon} \le 30\ 1/s \\ \gamma_s \left(\dfrac{\dot{\varepsilon}}{\dot{\varepsilon}_s}\right)^{1/3} & \rightarrow \dot{\varepsilon} > 30\ 1/s \end{cases}, \tag{10.2}$$

where f_c = dynamic compressive strength at $\dot{\varepsilon}$,

f_{cs} = static compressive strength at $\dot{\varepsilon}_s$,

$\dot{\varepsilon}$ = strain rate in the range of 30E-6 to 3E2 1/s,

$\dot{\varepsilon}_s$ = 30 1E-6 1/s (static strain rate),

$\log \gamma = 6{,}156\alpha - 2$,

$$\alpha_s = \left(5 + 9\frac{f_{cs}}{f_{c0}}\right)^{-1}, \; f_{c0} = 10 \text{ MPa}.$$

In the case of tension, DIF is given by

$$DIF_{(t)} = \frac{f_t}{f_{ts}} = \begin{cases} \left(\dfrac{\dot{\varepsilon}}{\dot{\varepsilon}_s}\right)^{1.016\delta} & \rightarrow \dot{\varepsilon} \le 30\ 1/s \\ \beta\left(\dfrac{\dot{\varepsilon}}{\dot{\varepsilon}_s}\right)^{1/3} & \rightarrow \dot{\varepsilon} > 30\ 1/s \end{cases}, \tag{10.3}$$

where f_t – dynamic tensile strength at $\dot{\varepsilon}$,

f_{ts} – static tensile strength at $\dot{\varepsilon}_s$,

$\dot{\varepsilon}$ = strain rate in the range of 30E-6 to 3E2 1/s,

$\dot{\varepsilon}_s$ = 3E-6 1/s (static strain rate),

$\log \beta = 7.11\delta - 2.33$,

$$\delta = \left(10 + 6\frac{f_{cs}}{f_{c0}}\right)^{-1}, \quad f_{c0} = 10\,\text{MPa}.$$

10.1. Hopkinson-Kolsky bar

The above formulas were successively modified due to the development of concrete technology and improvement of measuring equipment, (Malvar, Crawford, 1998).

For the range of *high* and *very high* strain rates the Hopkinson-Kolsky bar is extensively used. The mechanical concept of the Hopkinson-Kolsky bar is an application of the theory of longitudinal elastic as well as plastic waves propagation in a bar (see: Truesdell, 1974, for instance).

The Hopkinson bar (Hopkinson, 1914), as well as its modification by Kolsky, (Kolsky, 1949), is a stand consisting of a single bar or two bars in series. The history and varieties of the Hopkinson–Kolsky bar is presented in the paper (Xia, Yao, 2015), which also extensively reviews papers on the discussed subject.

The *Spalling-Hopkinson Bar (SHB)*, Fig. 10.5, is the configuration of a research stand where one end of the tested specimen is free, while the other is attached to the measuring Hopkinson bar, the other end of which is loaded with an incident compressive wave produced by a projectile launched from an air gun, e.g. (Brara, Camborde, Klepaczko, Mariotti, 2001) (Rey-De-Pedraza, et al., 2016), (Brara, Klepaczko, 2006).

Based on (Brara, Klepaczko, 2006), Fig. 10.5.a shows the result of computer modelling of the wave superposition process in a concrete specimen subjected to SHB tensile testing. A modified scheme was used to explain the effect of superposition of transmitted and reflected waves.

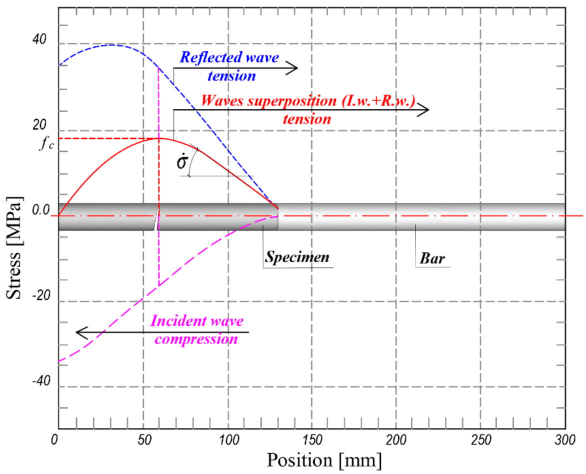

a)

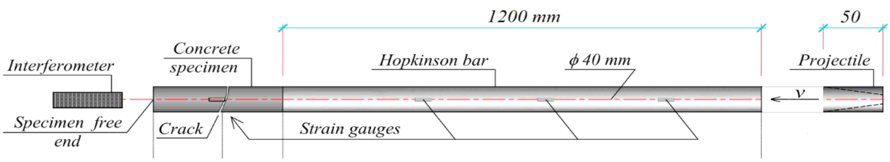

b)

Fig. 10.5. Spalling-Hopkinson Bar a) simple model of the superposition of an incident and reflected wave, reflected in the specinent b) the stand

Using a non-specialist language, the wave problem in the Hopkinson bar can be described as follows:

After a projectile impact, the compressive incident wave generated in the Hopkinson bar is transmitted onto the concrete specimen. A portion of it as a tensile wave reflected from the free end retreats into the Hopkinson bar. The superposition of the compressive incident wave and the reflected tensile wave generates a tensile stress that increases rapidly in time along the concrete specimen. The superposed tensile wave leads to tensile cracking of the specimen at some distance from the free end, where the tensile stress reaches the tensile strength of the concrete.

In general, the entire wave propagation process is recorded using three stress/strain meters on the Hopkinson bar. This arrangement allows determination of: the cracking stress due to spalling of the concrete, the stress history of the specimen, the critical loading time, and the loading rate or strain rate. An analogous explanation of spalling phenomena can be found in (Rey-De-Pedraza, et al., 2017), (Weerheijm, Van Doormaal, 2007).

An analytical description of the Hopkinson-Kolsky test can be found in the papers (Brara, Klepaczko, 1999), (Cusatis, 2011).

The Kolsky arrangement, also known as the *Split Hopkinson Pressure Bar (SHPB)*, is shown in Fig.10.6. In the case of SHPB, the speciment is located between the two bar faces.

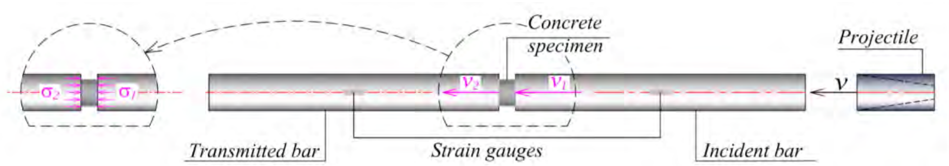

Fig. 10.6. Split Hopkinson Pressure Bar – diagram of a bar configuration and dynamic effects in the specimen

To complete the possible configurations of the Hopkinson bar, the *direct impact* case is shown in Fig. 10.7, (Rusinek, Chevrier, 2009). This arrangement is intended for compression.

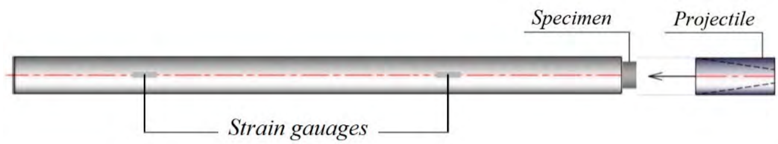

Fig. 10.7. Direct impact test

In the paper (Włodarczyk, Janiszewski, 2006), the plastic problem is analysed and a computational example is given.

In Fig. 10.8, a SHPB laboratory stand is shown in detail.

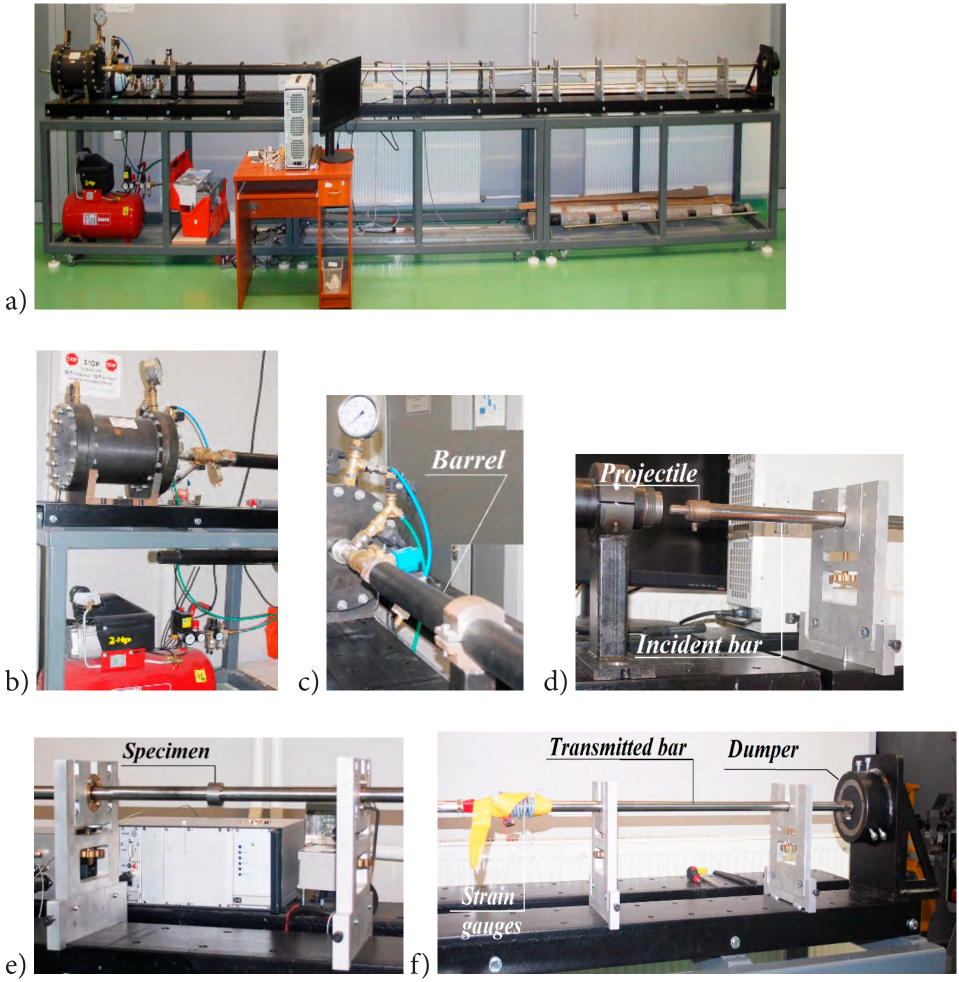

Fig. 10.8. The SHPB apparatus at the Civil Engineering Laboratory of Lublin University of Technology a) overall view b) air gun c) barrel d) projectile on the incident bar end e) specimen cylinder f) transmitted bar ended by a dumper

In this chapter, only general and basic information about the study of the dynamic behaviour of materials using the Hopkinson bar is given. It is now a dynamically developing field of mechanics. The number of citations given represents a small sample of hundreds of published research results on minerals, various types of concrete, mortars and metals, and composites.

At the end the two papers are recommended for studying. The first concerned SHPB testing of a ceramic mat applied to a CFRP substrate during the composite curing process, (Golewski, Rusinek, Sadowski, 2020). Courtesy of Przemyslaw Golewski, below are two graphs, Fig. 10.9, of waveforms measured in tests on

SHPB device. During the tests 1 V was calibrated 1000 με, Poisson modulus was assumed as 0.3. ε_I, ε_R, ε_T Denote the waveforms of incident strain, reflected strain and transmitted strain, respectively. Fig. 10.9.a shows FEM modelling of the wave process in addition to plots of the measured waveforms.

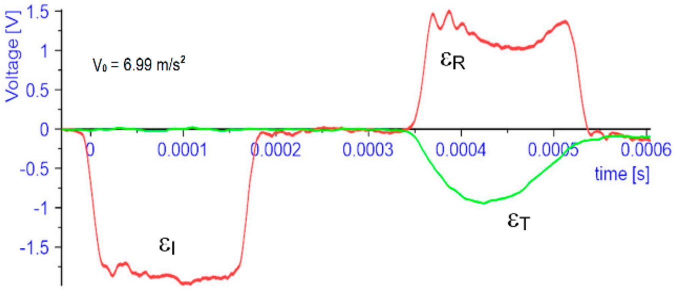

a)

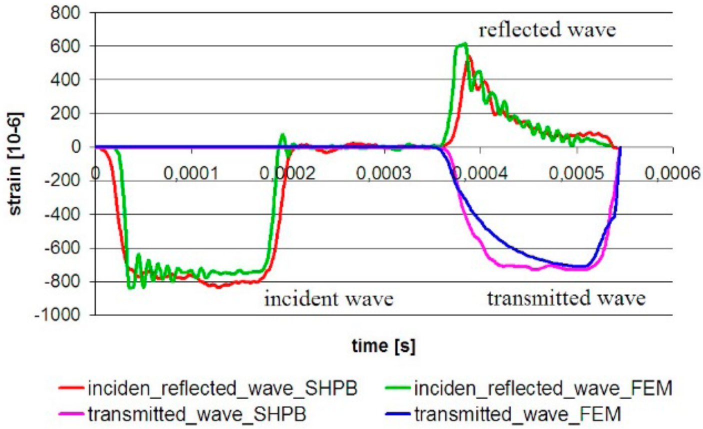

b)

Fig. 10.9. The waveform curves a) from SHPB b) FEM model of the process and its compatibility with the experimental result

Fig. 10.9.b shows two graphs of strain waveforms. The first is the SHPB results, where the incident and reflected waveforms are coloured in red, while the transmitted wave is drawn in magenta. The second group is the results of the FEM model, where the incident and reflected waveforms are coloured green, and the transmitted wave is marked in blue. The convergence of the strain waveforms measured in the SHPB device with those generated by the FEM procedure is clear.

The second recommended article to read is a paper (Lv, Chena, Chen, 2017) that deals with SHPB testing of concrete specimens. Varying impact velocities of the striker were used to demonstrate different failure patterns, i.e. light spalling, fracturing, fragmentation and comminution. The following values of 12.55 m/s, 15.33 m/s, 18.59 m/s and 21.12 m/s were assumed. The effect of striker length on deformation waveforms was discussed. It was decided that the striker length would be 800 mm. For a unidimensional problem, the definitions of stress, strain rate, strain and stress equilibrium in SHPB allow the constitutive relationship of the material sample, concrete, to be established. In addition, SHPB waveforms and degradation images of the specimen taken with a high-speed camera provide tools for detailed analysis for each strain rate tested. Therefore, the concept of load modulus is used. In the course of a strain, the elastic phase, the variety of plastic loading, the importance of compression states of micro-cracks and micro-voids, the accumulation of damage, and more are discussed. The material reinforcement phase was also distinguished, introducing the name *"double peak" phenomenon*.

No less important is the language of the paper, which is very concise and can be described as an unambiguous explanation of the problem.

10.2. Reason for significant increases in concrete strength with an increasing strain rate

The concrete strength increase at significant strain rates has been related to both micro-cracks and free water presence. H. W. Reinhardt (Reinhardt, 1982) used the SHB equipment in the cases of wet and dry concrete giving the stress-strain relation in compression as well as in tension. The paper (Reinhardt, Rossi, Mier, 1990) contains the results of the dynamic loading of micro-concrete. The conclusion states that in the case of wet specimens the strain rate effect is remarkable, although for dry specimens increase in strength at high strain rates was not observed. In 1991, M. J. Rossi (Rossi, 1991) proposed a concept based on the viscoelastic M. J. Stefan effect (Stefan, 1874) which explains the tensile strength increase (Sun, Wang, et al., 2020). Incidentally, the question arises as to what is dry concrete and wet concrete. A discussion of this issue can be found in the indicated paper.

The skeleton of microspores (pores of a diameter less than 2 nm) creates the plate network of dry concrete in which the microspores and micro cracks are filled with a Newtonian fluid. The fluid's viscosity is characterised by the η parameter.

The stress due to loading can be written as $\sigma_t = \eta \frac{dh}{dt}$. In reality, more complex rheological models are used instead of the elementary Newtonian fluid, (Pedersen, Simone, Sluys, 2008).

In Fig. 10.10, a simplified wet pore model of concrete is presented. Fig. 10.10.a shows the initial natural stage, while Fig. 10.10.b shows the actual configuration including the effect of the strain rate on the stress state at time t.

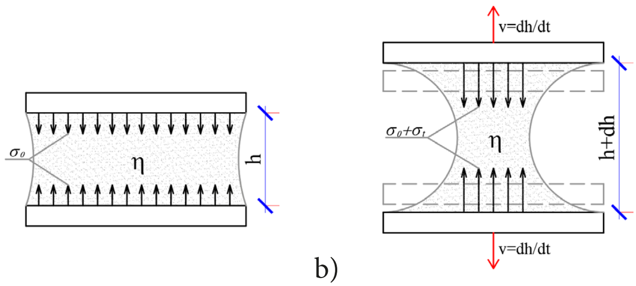

a) b)

Fig. 10.10. Illustration of the Stefan model, based on (Stefan, 1874)

Similar drawings can be made for compression and shear cases.

10.2.1. The limits of the Stefan model

Finally, note that significant saturation reduces the static and dynamic strength of concrete, see: Fig. 10.11.

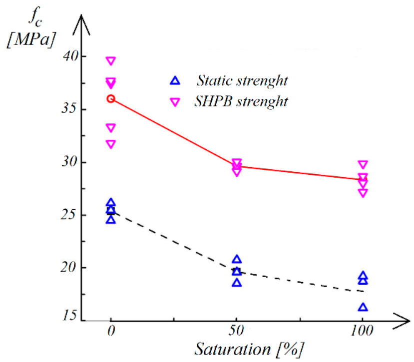

Fig. 10.11. Reduction of the static and dynamic strength f_c of concrete as a function of the pore water content, based on (Sun, Wang, et al., (2020)

It can be seen that the weakening is 30%. In the static case, the weakening is 20%. It can be read from this that $f_c^{(dynamic)}$ decreases by 30%. In the static case, the weakening of $f_c^{(static)}$ is 20%.

Similar results were published in the paper (Brara, Klepaczko, 2006).

In a sense, the results shown in Fig. 10.11 contradict the Stefan effect, i.e. Maxwell model. In this context, the saturation level of concrete needs further investigation.

***

11. Rheology and rheological models

Rheology is a relatively young discipline. Its origins can be tracked to the works and activity of E. C. Bingham (Coussot, 2017), M. Reiner (Reiner, 1958), G. W. Scott Blair (Rogosin, Meinardi, 2014), and many others. In 1929, the American Society of Rheology was founded. At that time, rheology was defined as

"The science of the deformation and flow of matter."

The term *rheology* refers to the thought of the Greek philosopher Heraclitus of Ephesus "τὰ πάντα ῥεῖ καὶ οὐδὲν μένει" which can be translated as *"everything flows and nothing stays*."

In the manuscript (Mezger, 2002), the 11th chapter is devoted to a chronological survey of rheologists and their achievements in the field.

Processes of material are processes occurring over a long period of time. Here, "a *long period*" signifies processes measured in days or years. Furthermore, let us assume that fast processes measured in e.g. seconds correspond to dynamics, where accelerations are of key significance. Somewhere between rheology and dynamics, quasi-static processes, where the duration of a process is measured in e.g. minutes, but accelerations are negligibly small, can be placed.

It can be best expressed through the dynamic balance equation, also known as the motion equation (10.1), which was examined in Chapter 10.

In the case of rheology, it may be assumed that external *loads are constant in time*. Thus, the dynamic balance equation is as follows:

$$\nabla_j \sigma^{ij}(t) + f^i = 0. \tag{11.1}$$

Rheology belongs to the area of viscoelasticity, or, conversely, rheology is a branch of science which perceives mechanical *processes as reversible or irreversible* (inelasticity).

In the case of elastic deformation, Young's *modulus of elasticity* E characterises material stiffness (resistance to being deformed).

The compliance modulus (flexibility) $J = \dfrac{1}{E}$ is inverse to stiffness and represents the material tolerance to deformation. Highly compliant materials are easily stretched or distended.

If one assumes that viscoplasticity concerns all the problems where the values of material characteristics are changeable depending on the time and velocity of deformations and stresses, then rheology relates to problems changeable over long periods of time. At the opposite extreme, there are problems of high strain rate or stress rate velocities in time, while what is discussed here are the velocities of displacements / elastic, or plastic waves of acceleration velocities of 800 m/s, or displacement velocities of 1E2 [1/s] to 1E6 [1/s]. In such cases, material studies are considered as related to Hopkinson-Kolsky bar tests.

In rheology, viscoelasticity methods are used, where the tensor description is applied in a similar manner as in the theory of elasticity. Also, the extensive use of operational calculus, mainly the Laplace transform, is typical. The Laplace transform, or its modification, the Carson transform[14], leads to so-called Alfrey's analogy (Alfrey, 1950), which gives analogous notations to the ones in the area of elastic problems.

The difference is that the Laplace transform is a complex function, while, in the case of elasticity, functions are real.

Here, the uniaxial problems dependent on t – current time are considered. Strain and stress processes are caused by loading/unloading at the time moment t_1; in general: $t > t_1$. The notation $\varepsilon\ (t, t_1)$ is understood as a strain process state at the time t, which is initiated by loading/unloading at the time moment $t = t_1$. The Laplace transform has been used.

Historically, rheological bodies/materials were constructed through defining constitutive relations $\sigma \rightarrow \varepsilon$ for uniaxial models. However, uniaxial models still play an important, even crucial, role in rheological analyses. The bases for such definitions are so-called simple Hookean, Newtonian and Saint-Venant's bodies, where Hookean body models have elastic properties, the Newtonian body represents the material flow, and Saint-Venant's body corresponds to the plastic behaviour of material. They are known as elementary models.

Below, models related to stationary problems are presented. In the case of dynamics, all the models should be modified by adding appropriate material masses (see: Bastien, Schatzman, Lamarque, 2000), for instance.

11.1. Elementary models

The *Hookean solid model* (H) is an elastic spring which is characterised by the elastic modulus E and, therefore, the stress~strain relation has the following algebraic form

$$\varepsilon = \frac{\sigma}{E}. \tag{11.2}$$

A representation and a graph of the constitutive relation are shown in Fig. 11.1.

[14] $L\left[f(t)\right] = p^{-1}\, C\left[f(t)\right]$. The transform of a real number is equal to the number $C[R] = R$.

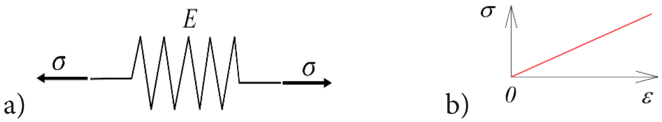

Fig. 11.1. Hookean spring model a) representation b) $\sigma \to \varepsilon$

The *Newtonian fluid model* (N) is represented by a linear viscous dashpot or piston, Fig. 11.2. The symbol of resistance against a viscous flow is η. The differential equation of the model has the following form

$$\dot{\varepsilon} = \frac{\sigma}{\eta} \tag{11.3}$$

A relevant graph is shown in Fig. 11.2.

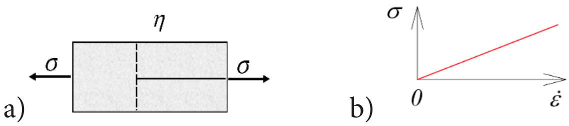

Fig 11.2. Newtonian viscous model a) dash-pot b) $\sigma \to \varepsilon$

Newton's law of viscosity defines the relationship between the shear stress and shear rate of a fluid subjected to mechanical stress.

Barré Saint-Venant's model (StV) introduces the effect related to the material limit, e.g. the yield limit σ_y. This model is dedicated to metallic materials.

It is postulated that material is rigid when stress increases monotonically from zero to a certain stress value – a yield limit, and, subsequently, the stress remains constant, while strain flows plastically with the strain rate. The model can also be identified as a switch triggering plastic flow when the stress achieves the yield limit

$$\begin{cases} \sigma < \sigma_y \rightarrow \varepsilon = 0 \\ \sigma = \sigma_y \rightarrow \varepsilon = \dot{\varepsilon}_{pl.}\, t \end{cases} . \tag{11.4}$$

The model takes the form of a slider representing static and kinetic friction, Fig. 11.3.

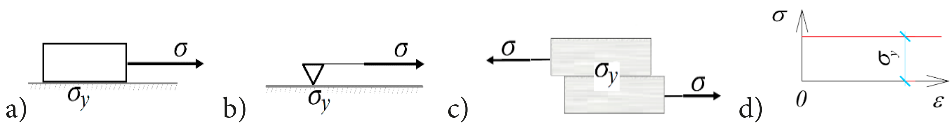

Fig. 11.3. The Saint-Venant's model (StV) of plastic flow expressed by means of a friction analogy a-c) different graphs of Saint-Venant's model d) stress-strain relation

Actually, the model is not very useful as such, however, when combined with other elementary models, it creates solid or fluid plastic bodies.

***

In Fig. 11.2 to 11.3, the stress value σ symbolises an action or a load. Simple loading and unloading in the uniaxial case of a rheological body is usually implemented. Here, the uniaxial problems depending on the current time t are considered. Strain and stress processes are caused by loading/unloading at the time moment t_1, where $t > t_1$. The record $\varepsilon\ (t, t_1)$ is understood as a strain process state at the time t, which is initiated by loading/unloading at the time moment $t = t_1$. Now, let us introduce the load case which is commonly used in rheology.

***

Step unit impulse [15]

$$\sigma(t) = 1(t - t_1)\sigma_0 \tag{11.5}$$

Here, there are three options of an analytical interpretation of the record of $1(t–t_1)$. The figures are numbered Fig. 11.4.1, Fig. 11.4.2 and Fig. 11.4.3, respectively.

(11.A) $1(t - t_1) = \begin{cases} 0 \to t < t_1 \\ 1 \to t \geq t_1 \end{cases},$

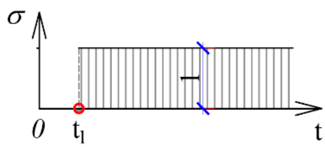

Fig. 11.4.1.

(11.B) $1(t - t_1) = \begin{cases} 0 \to t \leq t_1 \\ 1 \to t > t_1 \end{cases},$

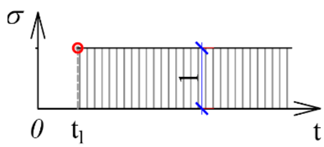

Fig. 11.4.2.

(11.C) $1(t - t_1) = \begin{cases} 0 \to t < t_1 \\ \xi \to t = t_1 \\ 1 \to t > t_1 \end{cases},$

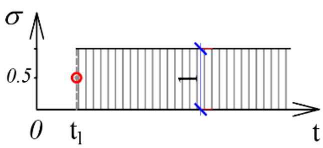

Fig. 11.4.3

[15] Previously known as the Heaviside step function *H(t)*.

where $0 < \xi < 1$ and it is mostly assumed that $\xi = \frac{1}{2}$, i.e. the variant (11.C) with the corresponding Fig. 11.4.3.

The variant choice depends on the requirements of the undertaken analyses. Let us also recall that the derivative of a step impulse is Dirac's function.

Dirac's delta function [16]

Dirac's delta can be obtained by deriving the step unit function

$$\frac{d}{dt} 1\left(t - t_1\right) = \delta\left(t - t_1\right), \tag{11.5.1}$$

The function has the following properties

$$\int_{-\infty}^{\infty} \delta\left(t - t_1\right) dt = 1 \quad \text{and} \quad \int_{t_-}^{t^-} f\left(t\right) \delta\left(t - t_1\right) dt = f\left(t_1\right), \tag{11.5.2}$$

where f(t) is a continuous function, for instance.

A description of the relaxation process requires the following function

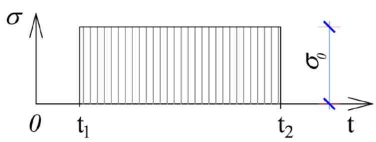

Fig. 11.5. Unit load during a time period from t_1 to t_2

The load shown in Fig. 11.5. can be written as follows

$$\sigma\left(t\right) = \left[1\left(t - t_1\right) - 1\left(t - t_2\right)\right] \sigma_0 . \tag{11.6}$$

It is useful for the purposes of finding the strain-recovery curve.

Another example relates to the case of adding two (or more) rheological processes started at different time moments, and it is as follows

[16] Maurice Dirac was an English theoretical physicist. δ(t) is the symbol of Dirac's delta which is a distribution function or a generalised function.

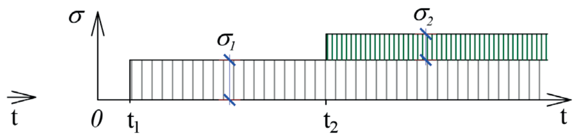

Fig. 11.6. Summation of two-unit functions obeying the history of loading

$$\sigma(t)=1(t-t_1)\,\sigma_1+1(t-t_2)\,\sigma_2 \tag{11.7}$$

Here, the load history consists of two constant actions: $\sigma_1$starting at the time moment t_1 and σ_2 starting at the time t_2.

A graphic presentation of rheological models is very useful, but proper differential equations require some skill and experience. Therefore, some classical rheological models are still shown as graphs and, at the same time, in an analytical form.

11.2. Two parameter models

The *Voigt model* [17] consists of a spring and a dashpot *connected parallelly*. The spring is characterised by E and the dashpot by η.

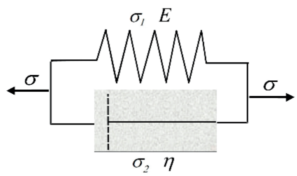

Fig. 11.7. Voigt model diagram

The strain of the model is equal to the strains of its components, while the model stress is a sum of the component stresses, which gives the following set of equations

$$\begin{cases}\varepsilon=\varepsilon^{(V)}=\varepsilon^{(H)}=\varepsilon^{(N)}\\ \sigma=\sigma^{(V)}=\sigma^{(H)}+\sigma^{(N)}\end{cases}. \tag{11.8.1}$$

[17] Also known as the Kelvin-Voigt model.

Using the definitions of the Hookean and Newtonian bodies, one can arrive at the differential equation of the Voigt body

$$\sigma = \varepsilon E + \dot{\varepsilon}\eta\,. \tag{11.8.2}$$

Applying the load in the form (11.5) allows drawing a strain-recovery curve which is characteristic for the Voigt body, see Fig. 11.8.

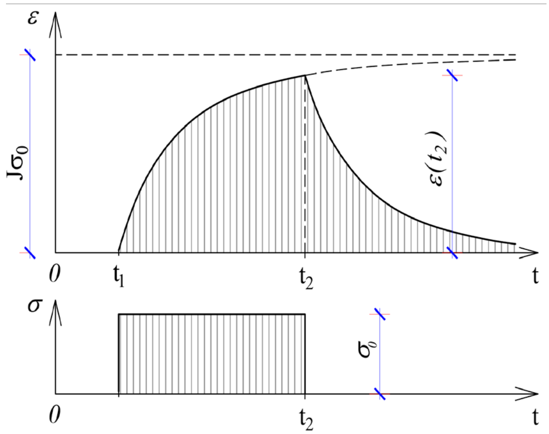

Fig. 11.8. Strain-recovery curve for the Voigt model

The curve fragment for $t \in (t_1, t_2)$ is a *creep function*, while the other curve branch is a *relaxation function*. It is worth emphasising that the *model is reversible*.

Maxwell model

The model consists of Hooke's and Newtonian models *connected in chain*, Fig. 11.9.

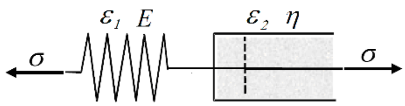

Fig. 11.9. Maxwell rheological model

For the Maxwell model one has

$$\begin{cases} \varepsilon = \varepsilon^{(M)} = \varepsilon^{(H)} + \varepsilon^{(N)} \\ \sigma = \sigma^{(M)} = \varepsilon^{(H)} = \varepsilon^{(N)} \end{cases} \tag{11.9.1}$$

It is obvious that the total strain is a sum of the strain in the spring, as well as in the dashpot, while stress has the same value in both members. Consequently, one arrives at the following differential equation

$$\dot{\varepsilon} = \dot{\varepsilon}_H + \dot{\varepsilon}_N = \frac{\dot{\sigma}}{E} + \frac{\sigma}{\eta} = \frac{1}{E}\left(\dot{\sigma} + \sigma\frac{1}{\lambda}\right), \tag{11.9.2}$$

where $\lambda = \frac{\eta}{E}$ is a model characteristic. λ is called the retardation time of the material and is a measure of time taken for the creep strain to accumulate. In this paper, the Voigt model constitutes the basic model in the sense that it is discussed most thoroughly. In the cited works, the reader will find derivations and discussions of other rheological models.

The Maxwell *model is irreversible*, which can be read from the graph in Fig. 11.10 below.

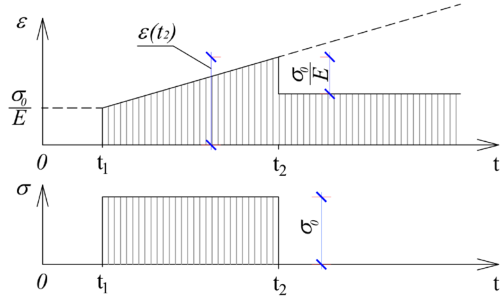

Fig. 11.10. Maxwell model – strain-recovery process

To make it reversible, an additional *"reverse' load"* is necessary.

Prandtl body

The Prandtl uniaxial body (Prandtl, 1921) is constituted by Saint-Venant's and Newtonian or Hokean bodies *connected in chain*.

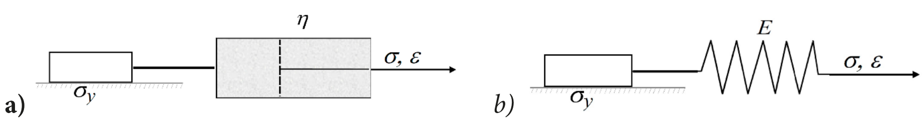

Fig. 11.11. Two versions of the Prandtl body a) StV+N b) StV+H

One can write a set of defining conditions, although, in this case, a physical description explains the model better. Both models involve friction laws. The first graph in Fig. 11.11.a presents Prandtl's model, and the other graph shows a viscoplastic model. One can understand the StV element as a model of static and kinematic friction or can just treat it as a threshold functioning as a switch.

The parallel connection, shown in Fig. 11.12, describes material strengthening.

a) 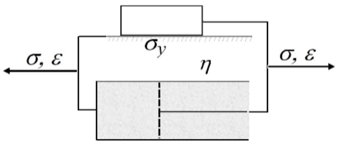

b) 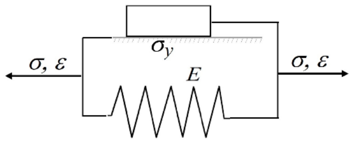

Fig. 11.12. Parallel connection a) material strengthening b) material threshold

The case shown in Fig. 11.12.a can be used for bilinear graphs of steel hardening. The model in Fig. 11.12.b behaves very similarly to Saint-Venant's model, and for this reason has no use.

Note that any model containing Saint-Venant's model is irreversible.

11.3. Three parameter models

Now, in model terminology, the term "*solid body* ", synonymous with reversible processes, is used. The liquid model is related to the concept of irreversibility, e.g. in the case of deformation processes.

Standard solid or the Zener model

a) 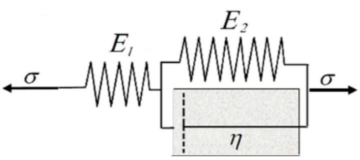

b) 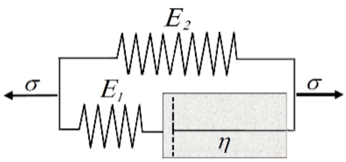

Fig. 11.13. Standard solid a) b)

Both models presented in Fig. 11.13 are *reversible*.

The Jeffrey model

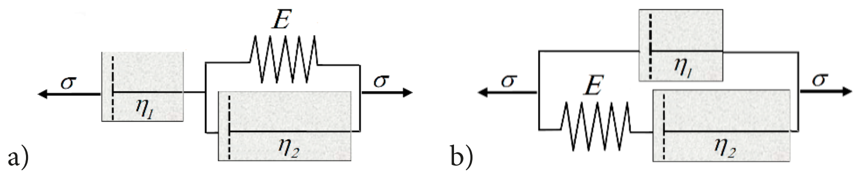

Fig. 11.14. Standard liquid

The model in Fig. 11.14.a is *irreversible*, while the other one, in Fig. 11.14.b, is *reversible*.

Differential equations of standard solids and standard liquids are to be found in (*Kelly,* 2013).

Another way to increase model sensitivity is to introduce more parameter models by extending the number of springs and dashpots even to infinity. Thus, one obtains so-called *model generalisations*.

11.4. Generalisations of the Voigt and Maxwell models

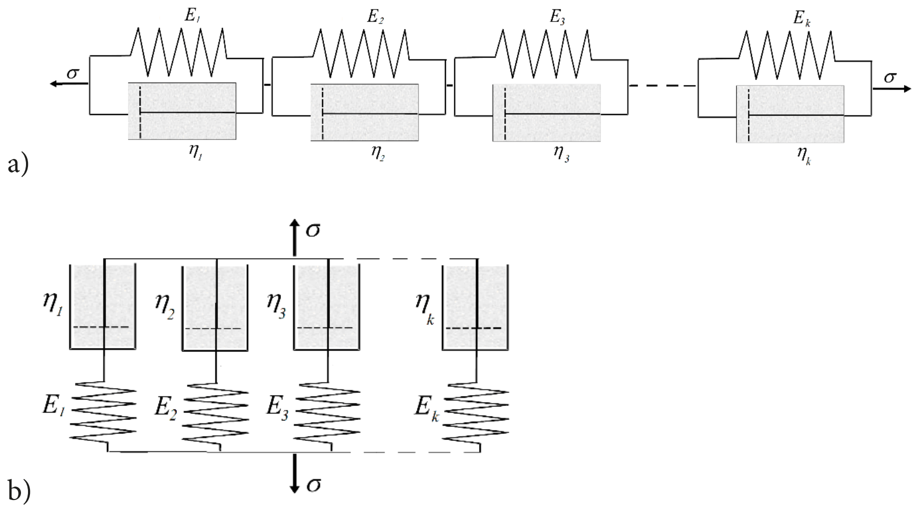

Fig. 12.15. Generalisation of two-parameter models a) generalised Voigt model b) generalised Maxwell model

There are many ways of generalising the models, although, at the same time, the graphs of models become less useful. Instead, analytical presentations should be used. Following the differential forms of Voigt's or Maxwell's models, the formula becomes obvious

$$\left(1+\sum_{n=1}^{k} a_n \frac{d^n}{d^n}\right)\sigma = \left(b_0 + \sum_{n=1}^{r} b_n \frac{d^n}{d^n}\right)\varepsilon \tag{11.10}$$

which is known as the general differential equation of rheological bodies. In particular, one can obtain

– the Zener model: $$\left(1+a_1 \frac{d}{dt}\right)\sigma = \left(b_0 + b_1 \frac{d}{dt}\right)\varepsilon \tag{11.11}$$

and

– the Burgers model: $$\left(1+a_1 \frac{d}{dt} + a_2 \frac{d^2}{dt^2}\right)\sigma = \left(b_1 \frac{d}{dt} + b_2 \frac{d^2}{dt^2}\right)\varepsilon, \tag{11.12}$$

where a_1, a_2, b_0, b_1, b_2, are rheological body characteristics, the values of which should be experimentally determined by examining the responses of real materials/structures to the action of defined loads.

The Bingham model

The Bingham model has been developed as a description of paint that flows (*liquid*) under the influence of the brush pressure, and which does not run off the painted surface (*solid*) after the pressure stops, (Bingham, Green, 1919), which qualifies it as a *plastic material.* A schematic model is shown below, Fig. 11.16.

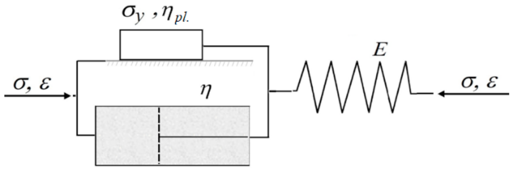

Fig. 11.16. Bingham model of plastic material

Following (Reiner, 1958), the model is defined as follows

$$\begin{cases} \sigma = 2\mu\,\varepsilon & \text{for} \quad |\sigma| < |\sigma_y| \\ \sigma - \sigma_y = 2\eta_{pl.}\dot{\varepsilon} & \text{for} \quad |\sigma| \geq |\sigma_y| \end{cases}, \tag{11.13}$$

where the yield point is given by a set of conditions

$$\begin{cases} \dot{\varepsilon} = 0 \\ \varepsilon = 0 \\ \sigma = \sigma_y = 2\mu\,\varepsilon_{pl.} \end{cases} \tag{11.14.}$$

The model – or rather its modifications – is extensively used in the drilling fluids industry to describe the flow characteristics of many types of slurries.

11.5. Boltzmann superposition

The Ludwig Boltzmann[18] superposition is a summation which takes into consideration the history of loadings. It shall be demonstrated by the use of the following loads in the case of Voigt's model:

$$\sigma(t) = \sigma_1\, 1(t - t_1) + \sigma_2\, 1(t - t_2) \tag{11.15}$$

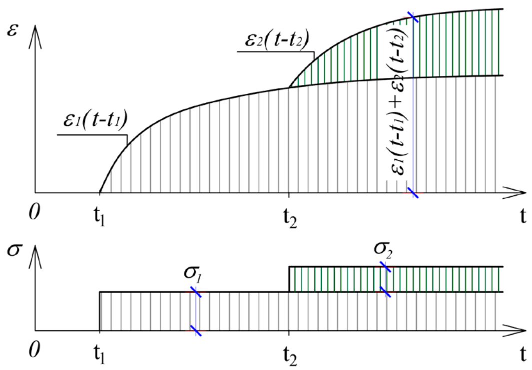

Fig 11.17. Adding two strain processes of the Voigt type. A way of including the load history. Superposition of loading effects according to their duration.

The strain development is defined in (11.16)

$$\begin{cases} t_1 < t < t_2 & \rightarrow \quad \varepsilon(t) = \varepsilon_1(t - t_1) \\ t > t_1 & \rightarrow \quad \varepsilon(t) = \varepsilon_1(t - t_1) + \varepsilon_2(t - t_2) = \sigma_1\phi(t - t_1) + \sigma_2\phi(t - t_2) \end{cases}.$$

(11.16)

[18] Ludwig Bolzmann (1844-1906), scientist from Vienna, a 19th century Austrian physicist, dealt, among other things, with the thermodynamics of liquids and gases.

11.6. Rheological models in the study of fresh concrete

Modern rheology is a very advanced and specialized branch of materials engineering. The basic rheological models discussed above are still valid and useful, but due to their linear nature, they are subject to various transformations and generalizations to mainly nonlinear models as needed.

Since the very beginning of rheology as a science, its applications have taken place in various fields. Suffice it to recall the spectacular description of the behaviour of flour dough (Schofield, Scott Blair, 1932), as well as the spreading of paint with a brush, (Bingham, 2019).

Also in the field of concrete structures, a new field of rheological research has emerged, this is the rheology of fresh concrete. Its occurrence is variously dated. A review article (Banfill, 2003) indicates that the rheology of cement-based materials has been developed since around 1980, while a review article (Nagaraj, Girish, 2021) mentions the last 20 years. Either way, both review articles are worthy of additional study.

Fresh concrete can include the phases of wet mix, batch water hydration with cement and the properties of young concrete, (Roussel, 2007).

The selection of a rheological model and its validation is a fundamental research problem, as it determines quantitative evaluations of material processes. For fresh concrete, the Bingham model is most commonly used.

Rheological parameters of a material can be obtained directly through rheometric tests or indirectly by reference to known traditional characteristics. In addition to basic parameters such as viscosity, plastic viscosity, yield stress, there may be new parameters related, for example, to shotcreting, where pumpability, cohesion and build-up thickness are important, (Liu G. et al, 2020).

One thing is certain, the rheology of fresh concrete leads to the possibility of controlling the setting and hardening processes of concrete, which in particular can result in reduced shrinkage and creep. It can also, for example, facilitate the production of concrete using a new type of recycled aggregate, i.e. coal combustion products (Alvaro, Seara-Paz, et al., 2021), which is an environmentally friendly measure.

12. Laplace transform in viscoelasticity problems

Until 1970s, the basic tool used in structural mechanics (as well as in other fields) was the solution of differential and integral equations using mathematical analysis methods. Currently, the use of numerical procedures is dominant. One of the analytical tools has been the integral Laplace transform[19].

Let us recall one of the amazing mathematical functions, the exponential function exp (t)[20]. The exponential function is an invariant of differentiation, so one has

$$\frac{d^n}{dt^n}e^t = e^t \tag{12.1}$$

where n is an integer.

This property allows solving linear differential equations with constant coefficients occurring in the problems of the linear theory of elasticity and viscoelasticity.

The Laplace transform is not the only integral transform. There are many known transforms – Laplace-Carson, Fourier, Mellin, Z-transform, Borel and other transforms used appropriately to mechanical problems.

Now, let us introduce the definition of the Laplace transform. For the sake of simplicity, let us assume that f (t) is a regular and bounded function defined on the basis of the real positive number domain (from zero to infinity). Hence, one obtains the mathematical formulae for the transform and its inverse

$$L\left[f(t)\right](p) = \int_{0_+}^{\infty} f(\tau)e^{-p\tau}d\tau = \tilde{f}(p), \tag{12.2.1}$$

$$f(t) = L^{-1}\left[\tilde{f}(p)\right] = \frac{1}{2\pi i}\int_{c-i\infty}^{c+i\infty}\tilde{f}(p)e^{pt}\,dp, \tag{12.2.2}$$

where $f(t)$ is the original or the retransformation, while $\tilde{f}(p)$ is an image or a transform of the function f, p is a complex parameter.

The fundamental handbooks on the Laplace transform were written by Louis Pipes (Pipes, 1958) and Gustav Doetsch (Doetsch, 1974).

Nowadays, both basic and more advanced and rigorous information is very easy to find with e.g. the Google Scholar search engine. A few properties of the Laplace transform that are representative in terms of its value as a mathematical tool are listed below. However, the so-called transform pairs are not included.

---

[19] Named after Pierre-Simon Laplace, a French polymath, 1799-1825. Among others, he postulated the existence of black holes.

[20] Depending on the editing requirements, the notation e^t shall be used in parallel.

12.1. Derivative transform

Let us find the transform of the first derivative $f'(t)$. Applying (12.1.1) and integrating it by parts[21], one arrives at

$$L\left[f'(t)\right]=\int_{0_+}^{\infty} f'(\tau)e^{-p\tau}\,d\tau = f(\tau)e^{-p\tau}\Big|_{0_+}^{\infty} -(-p)\int_{+0}^{\infty} f(\tau)e^{-p\tau}\,d\tau = p\,\tilde{f}(p)-f\left(0_+\right). \qquad (12.3)$$

Algebraically, the transform of the first derivative is equal to the transform of the function $f(p)$multiplied by the complex parameter p minus the value of the constant value of the initial condition $f(0_+)$.

In the case of higher range derivatives, the rule is still valid; analogously, for the transform of the third derivative, one obtains

$$L\left[f'''(t)\right]=p^3\,\tilde{f}(p)-p^2 f\left(0_+\right)-p f'\left(0_+\right)-f''\left(0_+\right). \quad (12.4)$$

The transform of the constant has the form

$$L\left[c\right]=c\int_{0_+}^{\infty} e^{-p\tau}\,d\tau=\frac{c}{p}. \qquad (12.5)$$

The transforms of derivatives have an algebraic form, although the space of transforms is complex.

12.2. Laplace transform of an integral

Keeping in mind that the Laplace transform of the derivative under homogeneous initial conditions is equal to the product of the parameter p and the transform of an original, it is expected that the transform of an integral will be the quotient of the transform of the original divided by the parameter p. This is, in fact, the integration theorem stated as

$$L\left[\int_{0_+}^{t} f(\tau)\,d\tau\right]=\frac{L\left[f(t)\right]}{p}=\frac{\tilde{f}(p)}{p}. \qquad (12.6)$$

---

21 $\int_A^B dt \rightarrow \left[(a\,b)' = a'b + a\,b'\right]_A^B$

12.3. Retransformation by virtue of the residuum theorem

Having an image, it is possible to obtain the original. Here, only one of them is presented, although without mathematical details, i.e. without the assumptions and necessary and sufficient conditions for the occurrence of retransformation, which the inquisitive reader can find in the already cited mathematical works.

Let the image has the following form

$$\tilde{Q} = \frac{1}{(p+p_1)(p+p_2)(p+p_3)} \quad , \tag{12.7}$$

where p_1, p_2, p_3 are real numbers.

Searching for the original function $Q(t)$, it is necessary to follow three steps:

- find an entire set of singularities, which can be of different kind – real, complex, single, or multiple. Let us consider three different singularities:

$$\frac{1}{p+p_1}, \ \frac{1}{p+p_2}, \ \frac{1}{p+p_3}, \tag{12.8.1}$$

- next, let us create a function

$$\theta(p,t) = \frac{e^{pt}}{\frac{d}{dp}\left[(p+p_1)(p+p_2)(p+p_3)\right]} \quad , \tag{12.8.2}$$

- by virtue of the residuum theorem, the origin Q(t) as a sum of the residues of the product $e^{et}\,\theta$ in the following form can be obtained

$$Q = \sum_{m=1}^{3} \mathrm{Res}[\theta]\Big|_{p=-p_m} = \sum_{m=1}^{3} \frac{e^{pt}}{3p^2 + 2p(p_1 + p_2 + p_3) + (p_1 p_2 + p_2 p_3 + p_3 p_1)}\Bigg|_{p=-p_m} . \tag{12.8.3}$$

The sum (12.8.3) is the sought reverse transform.

Example 1:

Let us find the inverse transform of the image $L^{-1}\left[p\frac{1}{p^2-\alpha^2}\right]$.

Bearing in mind that the multiplayer p signifies a derivative in a real space, one can rewrite the relation to the form $L^{-1}\left[\frac{p}{p^2-\alpha^2}\right]=\frac{d}{dt}\left\{L^{-1}\left[\frac{1}{p^2-\alpha^2}\right]\right\}$ and look for the inverse transform of $L^{-1}\left[\frac{1}{(p-\alpha)(p+\alpha)}\right]$ only by applying the residuum theorem, hence,

$$L^{-1}\left[\frac{1}{p^2-\alpha^2}\right]=\sum_{m=1}^{2}\frac{e^{p_m t}}{2p_m}\left|\begin{matrix}p_1=-\alpha\\ p_2=\alpha\end{matrix}\right|=\frac{1}{2\alpha}\left(e^{\alpha t}-e^{-\alpha t}\right)=\frac{sh(\alpha t)}{\alpha},$$

and, as a consequence,

$$L^{-1}\left[\frac{p}{p^2-\alpha^2}\right]=\frac{d}{dt}\left\{L^{-1}\left[\frac{1}{p^2-\alpha^2}\right]\right\}=ch(\alpha t).$$

Example 2:

Having the image $$L^{-1}\left[\frac{p}{p^2+\alpha^2}\right]=\frac{d}{dt}\left\{L^{-1}\left[\frac{1}{p^2+\alpha^2}\right]\right\},$$

one can write a set of singularities as the following set

$$p_m=\left|\begin{matrix}p_1=-i\alpha\\ p_2=i\alpha\end{matrix}\right|$$

and search for the inverse transform as before:

$$L^{-1}\left[\frac{1}{(p-i\alpha)(p+i\alpha)}\right], \text{ hence,}$$

$$L^{-1}\left[\frac{1}{p^2+\alpha^2}\right]=\sum_{m=1}^{2}\frac{e^{p_m t}}{2p_m}=\frac{1}{2i\alpha}\left(e^{i\alpha t}-e^{-i\alpha t}\right)=-i\frac{sh(i\alpha t)}{\alpha}sin(\alpha t),$$

which, following a derivation, finally results in

$$L^{-1}\left[\frac{p}{p^2+\alpha^2}\right]=\cos(\alpha t).$$

For the sake of order, let us note that $i=\sqrt{-1}$, and the relation $sh(it)=i\sin(t)$ is one of Euler's relations combining trigonometric and hyperbolic functions.

***

Commenting on the examples, one can conclude that in dynamics the occurrence of hyperbolic functions is related to the viscous damping of vibrations, while trigonometric functions indicate the domination of elastic vibrations.

Finally, it is worth mentioning that there is still only a partially functioning potential of the Laplace transform in terms of a multivariate problem.

The two basic monographs on the two-dimensional transformation (Voelker, Doetsch, 1950) and (Ditkin, Prudnikov, 1962) constitute the theoretical basis of the analysis. Nevertheless, a progress in this area is becoming more and more evident.

***

13. Viscoelasticity – applications of the Laplace transform

13.1. Solution of the Voigt model

Now, using the Laplace transform, let us solve the equation $\sigma = \varepsilon E + \dot{\varepsilon}\eta$, where E and η are material characteristics of constant value, using the Voigt model governed by (11.8). Performing the Laplace transform one obtains

$$L\left[\sigma = \varepsilon E + \dot{\varepsilon}\eta\right] \to \tilde{\sigma} = \tilde{\varepsilon}E + p\tilde{\varepsilon}\eta - \varepsilon\left(0_+\right) \to \tilde{\varepsilon} = \frac{\tilde{\sigma}}{E + p\eta} + \varepsilon\left(0_+\right)\frac{1}{E + p\eta} \tag{13.1}$$

Let the initial condition be homogenous, then

$$L^{-1}\left[\tilde{\varepsilon} = \frac{\tilde{\sigma}}{E + p\eta}\right] = \tilde{\varepsilon} = \tilde{\sigma} J \frac{1}{p\lambda + 1} \to \varepsilon = J L^{-1}\left[\tilde{\sigma}\ \frac{1}{p\lambda + 1}\right]. \tag{13.2}$$

where $\lambda = \dfrac{\eta}{E}$ is called the *retardation time* of the material and is a measure of the time taken for the creep strain to accumulate.

The shorter the retardation time, the more rapid the creep is.

$J = \dfrac{1}{E}$ is material compliance. In (13.2), in brackets, one has a product of two transforms, i.e. $\tilde{\sigma}$ and $\dfrac{1}{p\lambda + 1}$. Such a case is governed by the rule of convolution

$$L^{-1}\left[\tilde{g}\ \tilde{h}\right] = \int_{0_+}^{\infty} g\left(\tau\right) h\left(t - \tau\right) d\tau = \int_{0_+}^{\infty} g\left(t - \tau\right) h\left(\tau\right) d\tau. \tag{13.3}$$

Hence, one can write

$$\varepsilon\left(t\right) = J \int_{0_+}^{\infty} \sigma\left(t - \tau\right) L^{-1}\left[\frac{1}{p\lambda + 1}\right]\left(\tau\right) d\tau\ . \tag{13.4}$$

Now, the only challenge is to find the reverse transform $L^{-1}\left[\dfrac{1}{p\lambda+1}\right]$, or, more rigorously, $L^{-1}\left[\dfrac{1}{p+\lambda^{-1}}\right]$. Let us apply the residue theorem in the form corresponding to this uncomplicated case.

For the Voigt model, only one singularity exists, i.e. $p=-\dfrac{1}{\lambda}$, hence, one obtains

$$L^{-1}\left[\frac{1}{p+\lambda^{-1}}\right]=e^{pt}\Big|_{p=-\frac{1}{\lambda}}=e^{-\frac{t}{\lambda}}. \tag{13.5}$$

By virtue of the convolution theorem, the strain has the following form

$$\varepsilon(t)=\frac{1}{\eta}\int_0^t \sigma(\tau)\ e^{-\frac{(t-\tau)}{\lambda}}\,d\tau=\frac{1}{\eta}\int_0^t \sigma(t-\tau)\ e^{-\frac{\tau}{\lambda}}\,d\tau\,, \tag{13.6}$$

which depends on the form of the load function σ(t).

To determine the creep function and its recovery, the load is given by the relation (11.6) in the form $\sigma(t)=\left[1(t-t_1)-1(t-t_2)\right]\ \sigma_0$.

Putting the (11.6) into (13.6) gives the strain solution of the Voigt model

$$\varepsilon(t)=\frac{\sigma_0}{\eta}e^{-\frac{t}{\lambda}}\int_0^t\left[1(t-t_1)-1(t-t_2)\right]\ e^{\frac{\tau}{\lambda}}\,d\tau=$$

$$=\frac{\sigma_0}{\eta}e^{-\frac{t}{\lambda}}\left[1(t-t_1)\int_{t_1}^{t}e^{\frac{\tau}{\lambda}}\,d\tau-1(t-t_2)\int_{t_2}^{t}e^{\frac{\tau}{\lambda}}\,d\tau\right]=\frac{\sigma_0}{E}e^{-\frac{t}{\lambda}}\left[1(t-t_1)\ e^{\frac{\tau}{\lambda}}\Big|_{\tau=t_1}^{\tau=t}-1(t-t_2)\ e^{\frac{\tau}{\lambda}}\Big|_{\tau=t_2}^{\tau=t}\right]=$$

$$=\frac{\sigma_0}{E}\left[1(t-t_1)\left(1-e^{\frac{-(t-t_1)}{\lambda}}\right)-1(t-t_2)\left(1-e^{\frac{-(t-t_2)}{\lambda}}\right)\right]. \tag{13.7}$$

Examining the solution, one must pay attention to the definition of unit function. Although the analysis is not complicated, it will be carried out in detail.

First, the time interval of loading $t_1 \le t \le t_2$ (115) is considered

$$\varepsilon(t)=\frac{\sigma_0}{E}\left[1(t-t_1)\left(1-e^{\frac{-(t-t_1)}{\lambda}}\right)\right], \tag{13.8.1}$$

for the time moment t = t_2, the following is obtained

$$\varepsilon(t=t_2)=\frac{\sigma_0}{E}\left[1(t_2-t_1)\left(1-e^{\frac{-(t_2-t_1)}{\lambda}}\right)\right]=\frac{\sigma_0}{E}\left(1-e^{\frac{-(t_2-t_1)}{\lambda}}\right). \tag{13.8.2}$$

The range of unloading t≥t_2 (t_2 is assumed to be common for loading and unloading) requires the use of a full description in accordance with the formula (13.7), hence,

$$\varepsilon(t)=\frac{\sigma_0}{E}\left[1(t-t_1)\left(1-e^{\frac{-(t-t_1)}{\lambda}}\right)-1(t-t_2)\left(1-e^{\frac{-(t-t_2)}{\lambda}}\right)\right]. \tag{13.8.3}$$

Verifying (13.8.3), the strain value at t = t_2 is calculated

$$\varepsilon(t=t_2)=\frac{\sigma_0}{E}\left[1(t_2-t_1)\left(1-e^{\frac{-(t_2-t_1)}{\lambda}}\right)-1(t_2-t_2)\left(1-e^{\frac{-(t_2-t_2)}{\lambda}}\right)\right]=\frac{\sigma_0}{E}\left(1-e^{\frac{-(t_2-t_1)}{\lambda}}\right), \tag{13.8.4}$$

which is in line with (13.8.3).

Let us find the strain value after infinitely long time.

$$\begin{aligned}\varepsilon(t=\infty)&=\frac{\sigma_0}{E}\left[1(\infty-t_1)\left(1-e^{\frac{-(\infty-t_1)}{\lambda}}\right)-1(\infty-t_2)\left(1-e^{\frac{-(\infty-t_2)}{\lambda}}\right)\right]=\\&=\frac{\sigma_0}{E}\left[\left(1-e^{-\frac{\infty}{\lambda}}\right)-\left(1-e^{-\frac{\infty}{\lambda}}\right)\right]=0\end{aligned}. \tag{13.8.5}$$

This also proves that the Voigt *model is reversible*.

Some similar analyses can be found in (Karaś 2012). Also, it is worth mentioning and recommending the monograph by Witold Nowacki (Nowacki, 1963), where some basic problems of linear viscoelasticity are discussed.

13.2. Viscoelasticity – creep function

Viscoelasticity, in a mathematical sense, is a strict theory. Therefore, the problem of creep in viscoelasticity is considered more rigorously than creep in the context of engineering problems, which are dominated by experimental research applications and, sometimes, even heuristic approaches. However, it is obvious that engineering does not shy away from theoretical solutions.

Let us simplify the load function to the form

$$\sigma(t)=1(t)\ \sigma_0 . \tag{13.9}$$

Then $$\varepsilon(t)=1(t)\ \sigma_0 J\left(1-e^{-\frac{t}{\lambda}}\right). \tag{13.10}$$

The ratio $$\frac{\varepsilon(t)}{\sigma_0}=\varphi(t) \tag{13.11}$$

is known as the *creep function* of a material or the *creep coefficient* [22]. *It is a material strain process, or the structure's response to the action of a unit* 1(t) *stress load.*

In the analysed case the creep function is expressed by

$$\varphi(t)=J\left(1-e^{-\frac{t}{\lambda}}\right) \tag{13.12}$$

And the Laplace transform of the creep function has the form

$$\tilde{\varphi}=L[\varphi(t)]=J\left(\frac{1}{p}-\frac{\lambda}{p\lambda+1}\right)=\frac{J}{p(p\lambda+1)} . \tag{13.13}$$

Using (13.12) and in accordance with $\tilde{\varepsilon}=\tilde{\sigma}J\dfrac{1}{p\lambda+1}$, the relation assumes the form

$$\tilde{\varepsilon}=\tilde{\sigma}\frac{1}{\eta}\frac{1}{\lambda^{-1}+p}=p\tilde{\sigma}\tilde{\varphi} . \tag{13.14}$$

By means of the convolution theorem, the inverse transform leads to

$$\varepsilon(t)=1(t)\int_0^t \dot{\sigma}(\tau)\ \varphi(t-\tau)d\tau=1(t)\int_0^t \sigma(t-\tau)\ \dot{\varphi}(\tau)d\tau . \tag{13.15}$$

[22] The names *creep function* and *relaxation function* will continue to be used.

There is another derivation for presenting the hereditary low. If the function $\sigma(\tau)$ is given in the domain $-\infty < \tau < t$, then formula (13.15) takes the form

$$\varepsilon(t) = \int_{-\infty}^{t} \frac{\sigma(\tau)}{d\tau} \varphi(t-\tau) d\tau \, . \tag{13.16}$$

Performing integration by parts, one obtains

$$\varepsilon(t) = \sigma(t)\varphi(0) + \int_{0}^{t} \sigma(\tau) \frac{d\varphi(t-\tau)}{d\tau} d\tau \, . \tag{13.17}$$

In the case of the Voigt model $\varphi(0)$.

Usually, regarding the problem under consideration, the two-sided Laplace transform is used.

13.3. Viscoelasticity – the relaxation function and its connection with the creep function

Now, analogously to Section 13.12, let us express the transform of stress

$$\tilde{\sigma} = \frac{\tilde{\varepsilon}}{p\tilde{\varphi}} = \tilde{\varepsilon}\eta\left(p + \lambda^{-1}\right) = p\tilde{\varepsilon}\tilde{\psi} \, , \tag{13.18}$$

hence,

$$\psi(t) = L^{-1}\left[\eta\left(1 + \frac{1}{p\lambda}\right)\right] = \eta\left(\delta(t) + \frac{1}{\lambda}\right) = E\left(\lambda\delta(t) + 1\right), \tag{13.19}$$

where $\delta(t)$ stands for Dirac's generalised function (impulse), $\psi(t)$ is the *function of relaxation*, also known as the *relaxation function*.

Similarly, one can write

$$\sigma(t) = 1(t) \int_{0}^{t} \dot{\varepsilon}(\tau)\psi(t-\tau) d\tau = 1(t) \int_{0}^{t} \varepsilon(t-\tau)\dot{\psi}(\tau) d\tau \, . \tag{13.20}$$

The product of the derived functions has the form

$$\tilde{\varphi}\tilde{\psi} = \frac{1}{p^2}, \quad \varphi\psi = \left(1 - e^{-\frac{t}{\lambda}}\right)\left(\lambda\delta(t) + 1\right) . \tag{13.21}$$

The expressions are important because $\varepsilon(t)$ *and* $\sigma(t)$ *are expressed appropriately by* $\varphi(t)$ *and* $\psi(t)$.

13.4. Compliance and the relaxation moduli of creep

Introduction of the creep compliance function is another approach.

$$\varepsilon(t) = \sigma_0 \, J(t) = \sigma_0 \frac{1}{E}\left(1 - e^{t/\lambda}\right). \tag{13.22}$$

For $\sigma_0 = 1(t) \rightarrow \varphi(t) = J(t)$. (13.23)

The creep relaxation function has the form

$$\sigma(t) = \varepsilon_0 E(t) = \varepsilon_0 \, \eta\left(\delta(t) + \frac{1}{\lambda}\right) = \varepsilon_0 \, E\left(\lambda\delta(t) + 1\right). \tag{13.24}$$

For $\varepsilon_0 = 1(t) \rightarrow \psi(t) = E(t)$. (13.25)

13.5. Fractal derivative

The question of the fractional derivative was born together with the commonly known *classical* integer derivative. To begin with, let us look at historical information regarding the concept of fractional derivatives. For the readers who like investigating history, the elaborate (Lazarević, 2012), (Mehdi, 2013) is recommended.

Gottfried Wilhelm Leibniz was the inventor of the derivative notation $\frac{d^n y}{dx^n}$.

The published letters of Leibnitz, (Leibniz, 1695) and (Pertz, Gerhardt, 1971) describe a discussion carried out between the mathematicians who dealt with infinitesimal concepts including derivatives. In the letter from G. F. A. L'Hospital[23], Leibniz is asked to comment on the question

"*What if n is ½?*"

Here is a quote from Leibniz's answer:

"*Thus, it follows that d ½ x will be equal to d ½ x = x √(dx/2)***.** *This is an apparent paradox from which, one day, useful consequences will be drawn.*"

[23] Guillaume François Antoine, Marquis de l'Hôpital (L'Hospital), 1661-1704. French mathematician. He proposed limits calculation of type 0/0 and ∞/∞. The author of the monograph *Analyse des Infiniment Petits pour l'Intelligence des Lignes Courbes*. The book is a fundamental work on differential calculus.

In 1819, Sylvestre Lacroix [24] used the form of generalisation. In the case of a positive integer, the n^{th} derivative of

$$y = x^m \tag{14.1}$$

is written as

$$\frac{d^n}{dx^n}\left(x^m\right) = \frac{m!}{(m-n)!}x^{m-n} \quad , \quad m > n \,. \tag{14.2}$$

Let us now introduce another notation of the derivative operator. Instead of Leibniz's operator $\frac{d^n}{dx^\nu}$, let the derivative operator be denoted by D^n, where n is positive. The case of D^{-n} signifies the n-fold integration as an inversion to the n-fold derivative. Hence, one obtains

$$\frac{d^n}{dx^n}\left(x^m\right) = D^n\left(x^m\right) = \frac{m!}{(m-n)!}x^{m-n} \tag{14.2.1}$$

Leonhard Euler's gamma function[25] (see the graph in Fig. 14.1) is an analytical extension of the factorial over the entire complex plane, defined by the formula

$$\Gamma(z) = \int_0^\infty e^{-t}t^{z-1}dt \text{ , where } \operatorname{Re}(z) > 0 \,. \tag{14.3}$$

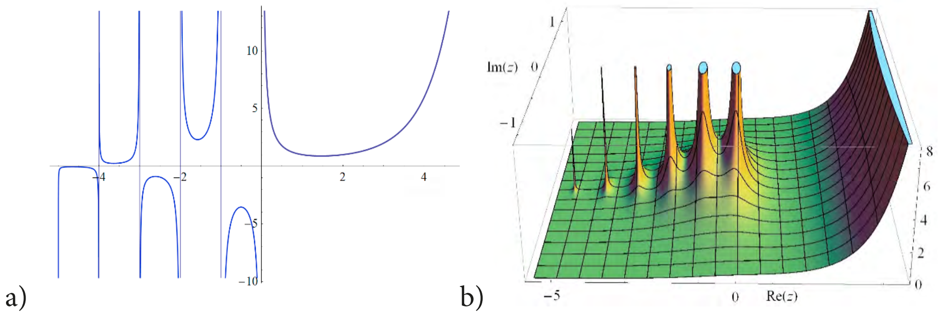

Fig. 14.1. The *Mathematica* graphs of $|\Gamma|$ function a) 2D b) 3D

Γ is holomorphic in the complex plain except for non-positive integers. In the space of the real numbers *x*, the gamma function is as follows

[24] Sylvestre François Lacroix, 1765 – 1843. French mathematician, the author of the monograph *Traité du Calcul Différentiel et du Calcul Intégral.*

[25] Derived by Daniel Bernoulli, known as Euler's gamma function.

$$\Gamma(x)=\int_{0}^{\infty} e^{-t}t^{x-1}dt \text{ for } x>0. \tag{14.4}$$

$x>0$ means that the integral converges only for positive x. For $x=n$, integrating n-times by parts, one arrives at

$$\Gamma(n+1)=\int_{0}^{\infty} e^{-t}t^{n}dt=n! \tag{14.5}$$

Other properties of the gamma function

$$\Gamma(x)=(x-1)!\,,\ \Gamma(x+1)=x\Gamma(x),\ \Gamma(x-1)=x!\ . \tag{14.6}$$

Additionally, the value sequence of Euler's function for the positive and negative fractions of the type of integer dividable by 2 can be calculated. Such values may occur when fractional derivatives are calculated. The sequences are given below

$$\Gamma\left(-\frac{11}{2}\right)=\frac{(-2)^{6}}{11!!}\sqrt{\pi}$$

$$\Gamma\left(-\frac{9}{2}\right)=\frac{(-2)^{5}}{9!!}\sqrt{\pi}$$

$$\Gamma\left(-\frac{7}{2}\right)=\frac{(-2)^{4}}{7!!}\sqrt{\pi}$$

$$\Gamma\left(-\frac{5}{2}\right)=\frac{(-2)^{3}}{5!!}\sqrt{\pi}$$

$$\Gamma\left(-\frac{3}{2}\right)=\frac{(-2)^{2}}{3!!}\sqrt{\pi}$$

$$\Gamma\left(-\frac{1}{2}\right)=\frac{(-2)^{1}}{1!!}\sqrt{\pi}$$

$$\Gamma\left(-\frac{2n-1}{2}\right)=\frac{(-2)^{n}\sqrt{\pi}}{(2n-1)!!}$$

$$\Gamma\left(\frac{13}{2}\right)=\frac{11!!}{(2)^{6}}\sqrt{\pi}$$

$$\Gamma\left(\frac{11}{2}\right)=\frac{9!!}{(2)^{5}}\sqrt{\pi}$$

$$\Gamma\left(\frac{9}{2}\right)=\frac{7!!}{(2)^{4}}\sqrt{\pi}$$

$$\Gamma\left(\frac{7}{2}\right)=\frac{5!!}{(2)^{3}}\sqrt{\pi}$$

$$\Gamma\left(\frac{5}{2}\right)=\frac{3!!}{(2)^{2}}\sqrt{\pi}$$

$$\Gamma\left(\frac{3}{2}\right)=\frac{1!!}{(2)^{1}}\sqrt{\pi}$$

$$\Gamma\left(\frac{1}{2}\right)=\frac{0!!}{(2)^{0}}\sqrt{\pi}$$

$$\Gamma\left(\frac{2n-1}{2}\right)=\frac{n!!\sqrt{\pi}}{(2)^{n-1}}$$

where n!! is an odd double factorial of n.

Now, the (14.2.1) formula can be rewritten appropriately to the needs of a fractal derivative as follows

$$\frac{d^{\nu}}{dx^{\nu}}\left(x^{m}\right)=D^{\nu}\left(x^{m}\right)=\frac{\Gamma(\nu+1)}{\Gamma(m-\nu+1)}x^{m-\nu}, \quad m>\nu . \tag{14.7}$$

For fractional derivatives, the range (0, 1) is crucial. Obviously, the first derivative has the form

$$D^{\nu}=\frac{\Gamma(\nu+1)}{\Gamma(1-\nu+1)}x^{1-\nu}=\frac{\Gamma(\nu+1)}{\Gamma(-\nu)}x^{1-\nu}, \tag{14.8}$$

and, consequently, determining the numerical sequence for the increasing ν, one obtains

$$\begin{cases} D^{0.01}x=0.998506\ x^{0.99}, \\ D^{0.25}x=0.986225\left(\sqrt[4]{x}\right)^{3}, \\ D^{0.5}x=\sqrt{x}=\left(\sqrt[4]{x}\right)^{2}, \\ D^{0.75}x=1.01397\sqrt[4]{x}, \\ D^{0.999}x=\ 1.00015x^{0.001}. \end{cases} \tag{14.9}$$

Obviously, when $\nu \to 1$, then $D^{\nu}x \to 1$. This demonstrates the quantitative and qualitative differences of the fractal derivatives of the constant 1. In consideration of the fact that “one image is worth 1000 words”, Fig. 14.2 shows graphs of the fractional derivatives of $D^{\nu}x$ functions for the selected values ν.

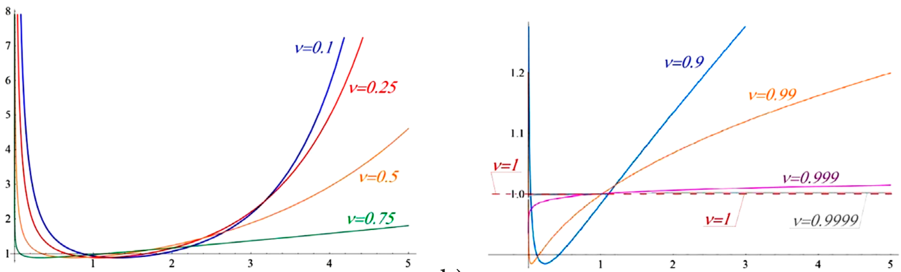

a) b)

Fig. 14.2. The *Mathematica* graphs of the fractal derivatives $D^{\nu}x$ a) $0.1 \leq \nu \leq 0.75$ b) detail in the vicinity of the beginning of the reference coordinates $0.9 \leq \nu \leq 1$

Fractional derivatives appeared with the development of the concept of the derivative about 300 years ago. The concept of the integer derivative with its ingenious geometric interpretation is an excellent tool that allows the application of infinitesimal calculus. Contemporary engineering, including bridge engineering, is firmly rooted in mathematical analysis. Although the fractional derivative is still in a state of incubation, its mathematical development does not raise any doubts. Still, there are no fields of engineering in which the fractional derivative is indispensable.

Applications of fractional derivatives are rare, but it is not that there is no work to be done in this area. An example of a beneficial application of the fractional viscoelastic Huet-Sayegh model can be found in the field of modelling asphalt road pavements, (Zbiciak, 2013).

***

14. Bridge aesthetics – an alternative approach

How long has the aesthetics of bridges been discussed? It is a rhetorical question. Probably, the oldest bridges in the world are two functioning bridges dating back to the Mycenaean period in the Bronze Age Peloponnese, (Karaś, Kowal, 2015), (Karas, Nien-Tsu Tuan, 2017). The bridges are built of cyclopean marble boulders. A strong impression they make does not stem from their beauty, but the appreciation of their constructors, who applied what is understood today as structural mechanics. It is for this reason that the bridges have survived to this day, even though there are regular daily seismic events at their location, Fig. 15.1.

The tourist information regarding the bridges state that the bridge in the vicinity of the village of Arkadiko is Mycenaean Bridge A (MBA) and the other bridge, located in a difficult to access mountainous area about 1 km away, is Mycenaean Bridge B (MBB). Fig. 15.1.a-c show images of the MBA bridge, while Fig. 15.1.d-f show photos of the MBB bridge.

a)  b) 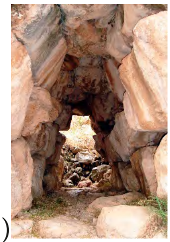 c) 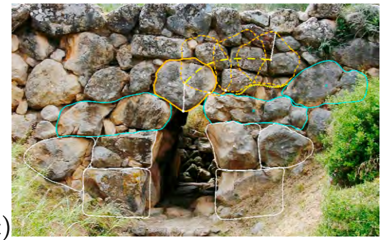

d)  e) 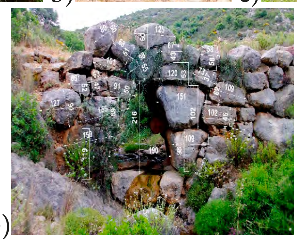 f) 

Fig. 15.1. Mycenaean bridges in Arkadiko (Kazarma), Peloponnese a) MBA – side view from the outlet b) light of the bridge c) an attempt to reproduce the technology used d) MBB sited in a natural landscape – view from the outlet e) dimensional inventory of cyclopean boulders f) the original static scheme, i.e. corbel bridge

It should be added that the two existing bridges were located in the course of a road, the trace of which is constituted by three other residual bridge remains (Jansen, 1997).

These two functioning bridges, now corresponding to the culverts, can be classified as arch bridges, although everything indicates that they were built as corbelled bridges. Another surprise, in technical terms, is that the original structure – as a result of earthquakes – has adjusted to one of the most durable static schemes, the arch. Such are the impressions experienced by a modern age person viewing these engineering works of three thousand years ago. However, this is not the sensation known today as an aesthetic impression, but rather historiosophy – which can also be exciting.

***

Aesthetic canons have been in use since antiquity – the Doric, Ionic and Corinthian orders are commonly known. Probably between 30 and 15 BC, Marcus Vitruvius Pollio collected architectural knowledge (knowledge of building the structures) from the Greek and Roman period in the work *De Architektura*, now known as *Ten Books on Architecture*.

By the way, it is worth noting that one of the world's most beautiful Roman bridge structures, the Acueducto de los Milagros in Mérida, dating from the first century AD, has a composite structure, Fig. 15.2.

Here, each visitor experiences a very strong reaction, perhaps even an aesthetic stimulation. From the author's observation, the moment a group of tourists appears at the aqueduct, the chatter stops turning to whispers. Everyone tries, within their own capacity, to become accustomed to the undoubted beauty of both the architecture and the mechanics of the structure.

It takes about 30 minutes to walk over the accessible section of the aqueduct. To enjoy the accuracy of the construction, the successive exposures of strong sun contrasts, the pleasant shade of the pillars and the damp grass takes a longer while. Only after this stage is completed does the photographing process start, and taking photographs is challenging due to the monumentality of the aqueduct (about 25 metres high). This raises historiosophical questions – how did the architect think it up, how did they plan it, how did they construct it, how is it that the aqueduct has survived to this day? Let us remember that in ancient times the constructor was called the architect.

Thus, impressions and emotions (αισθητικός – gr.) prevail both among those familiar with ancient architecture and those who find themselves there by chance. Emotions, impressions are much more than the scholastic aesthetics of bridges, which, through aesthetic canons, is framed as principles, indications, geometrical measures, etc. (Kant, *Kritik der Urteilskraft,* 1790; *Critique of judgment*, 1892). Of course, it is worthwhile to study aesthetics as a branch of philosophy but the very subject of these studies – aesthetic sensation – is an immanent human feature and is therefore fundamental. This is why aesthetic experience is as necessary as philosophical knowledge.

Let us now devote a few sentences to describing the structure of the aqueduct. Two colours dominate its image: the grey colour comes from granite stones processed in a precise manner that is apparent even today, while the red colour is Roman brick, which builds two important structural elements. These are the brick interlayers in the pillars, which occur every five layers of the granite stones. Another element is constituted by two arch braces between the pillars, and the proper arches at the top of the aqueduct, where the water channel runs.

The Roman brick-making technology was adopted from the Greeks. After a brick was formed from clay, a drying process in the kiln followed, which prevented the brick from cracking. The thickness of the brick is about 4 cm, other dimensions are not available. In the Roman times, stone was often interlaced with thin layers of brickwork at specific intervals -in this case, there are five bricks in each interlace layer. In addition to the interesting ornamental polychrome, the resulting layers served to create a levelling layer between the successive segments of granite blocks. It is also possible that the brick interlayers stabilised the relatively high pillars during earthquakes, so they may have acted as a kind of mass vibration damper. The compressive strength of the Roman brick is much lower than that of cut granite blocks, but its load-bearing capacity is sufficient for the construction of small arches.

Unfortunately, judging by the photos, the arches that stabilise the entire aqueduct longitudinally are the least durable. The lateral stability of the pillars depends on the visible buttresses. Unfortunately, they are missing in many places. Some of the buttresses have deteriorated, making it possible to look inside the pillar. Note that the buttresses are only made of cut granite blocks, without layers of brick, and are about 10 cm higher than those found in the pillars. At the same time, it is clear (Fig. 15.2.c) that the buttresses were very shallowly embedded in the pillars. With their considerable heights and poor anchorage, spalling and destruction of the buttresses occurred. There are no remains of the buttresses in the vicinity of the aqueduct.

The purpose of the last paragraphs is to discuss the content of Fig. 15.2.d, i.e. the composite filling of the interior of the pillar with a Roman concrete-based material called *pozzolana* (hydraulic cement, i.e. ash mixed with lime in a ratio of ~ 2:1; once water was added, the setting took place). Fig. 15.2.d shows an aggregate of volcanic stones with a conventional diameter fraction of 10 cm. There also appear three times larger grains/stones. The vertical section is a segment five granite blocks high. Therefore, it can be concluded that the pillar was built together with the buttresses.

An extensive search of internet resources has been carried out, but, unfortunately, it was not possible to find any contemporary inventory of the aqueduct. The detailed dimensions are not known. Nothing is known of the foundations.

Fig. 15.2. Acueducto de los Milagros, Mérida, Spain a) general view with a water intake b-c) close-up showing the absence of pillar buttress c) composite structure

***

The Greek architectural canons and the book *De Architecture* do not refer to bridges. The arch bridge appeared as early as the times of Alexander the Great, but the development of this technology took place in Roman times. By Roman times one understands the period of the Western and Eastern Empires. Suffice it to say that Roman military roads were initially winding to avoid water obstacles. It was only with time that bridges began to be built, of which about a thousand were constructed. About half of these have survived in various forms to the present day. Arch structures are mechanically very efficient and therefore durable.

Aesthetic canons for bridges appeared in the 20th century. The most famous set of criteria is developed by Fritz Leonhardt. His book starts on a high note with the author quoting *de gustibus non disputandum est*. If this is the case, then the only way is a subjective discussion of the aesthetics of bridges through numerous examples of their images taking into account significant interactions with the environment, current technological possibilities, the usability of an object, current aesthetic trends, etc. Such an approach is always burdened with some form of decision-making and remains valid over a period of time corresponding to one to three generations. For this reason, one can discuss the aesthetics of Gustave Eiffel's, Robert Maillard's, Fritz Leonhardt's, Riccardo Morandi's or, nowadays, Santiago Calatrava's bridges. The paper (Leonhardt, 1968) is an excerpt from a bible of bridge aesthetics, an example of which is the book by Fritz Leonhardt (Leonhardt, 1984). The content of the book is cited on every occasion, so it is probably fair to say that it is now a classic in the field of bridge structure assessment. In particular, a set of criteria for a proper bridge is listed, including the aesthetic criteria defining an aesthetic canon:

> fulfilment of purpose/function – proportion – order – refinement of form – integration into the environment – surface texture – colour – character – complexity – incorporating nature.

Numerous applications of Leonhardt's canon can be cited but let us refer here to a professional blog entitled *The Happy Pontist* that has been kept for over a decade. The author of the blog is skilful in applying all the ten criteria of Leonhardt's canon to the description of bridges. However, applying the classical Leonhardt's criteria sometimes does not lead to sufficient results. These are open judgements, ending with unanswered questions. An example is the article (http://happypontist, 2009) which considers the new style and aesthetics of Santiago Calatrava.

The magnificent Viaduc de Millau designed by Michel Virlogeux and Norman Foster meets Leonhardt's criteria by 100 percent. However, the last twenty years have seen a new bridge concept formulated and implemented by Santiago Calatrava, laid down in *On the Foldability of Space Frames* (Calatrava, 1984). Some of Calatrava's bridges differ so significantly from Leonhardt's classic that the new concept is on the verge of validity of Thomas Kuhn's paradigm.

The author takes the opportunity to present the work of the Warsaw Polytechnic professor Zbigniew Wasiutyński entitled *On the Architecture of Bridges* (Wasiutyński, 1971), written in the 1970s, which corresponds to the classical description of bridges. Unfortunately, the book is not popular enough. It is written in Polish and therefore not generally available. The book is a multi-level study with chapters devoted to psychophysical processes, feelings and moods, the importance of feelings in architecture and construction, visual perception, the formation of perception, perception of shapes, traces and associations of perceptive processes, the principles of architecture, and an overview of bridge architecture.

The seriousness of the content, the narrative used, and the resulting statements are difficult to question. Even if a thought of discussing the architecture of bridges arises, it is not to question the formulated concept.

Let us consider the bridge aesthetics proposed by Z. Wasiutyński as a list of the following principles:

> wholeness – making an aesthetic impression is conditioned by the perceptibility of all the elements of the form and their interrelations – simplicity of the form – the number of elements in the form should be small enough for the interdependence of the elements in the form to be perceptible – legibility of the form – for the form to evoke aesthetic impressions, the element associations should be easily perceptible – avoiding emptiness – for

> the form to make an aesthetic impression, it must satisfy the cognitive aspirations of the observer – regularity of the form – regular (equal) forms are conducive to arousing aesthetic sensations.

Classifying a single structure is relatively straightforward. However, the variety of bridges makes an aesthetic comparison of several bridges complicated or even impossible. An example here is a set of photographs of various well-known contemporary bridges considered to be pretty and interesting, while each of them is different, Fig. 15.3.

It is stipulated at the outset that the author shall not undertake an aesthetic evaluation of the bridges, ranking them from position 1 to 14. The author is in a privileged position anyway, since he has examined each of the bridges in situ, studied their technical documentation, and, finally, met their designers or builders. He also had some time to contemplate them independently in situ. So, he has formed his own impressions of the bridges, although he has no mandate to pronounce judgements. Even if the author proposed a classification of the structures, it would still be a very subjective verdict. If nobody can offer a scoring system to characterise an aesthetic impression, what can he give, then? He can introduce his own individual scoring method, which can potentially be contrasted with other ones.

Alternatively, the aesthetics of a bridge can be assessed by verifying its aesthetic features against a selected canon of bridge aesthetics. However, it should be borne in mind that such behaviour is personality-laden which is the case of any decision-making process.

***

Now let us add brief information/commentary on each of the bridges in Fig. 15.3.

Fig. 15.3.a: A cable-stayed bridge over an artificial lake on the Euphrates River in the rugged mountains of Taurus. The bridge is at an advanced stage of construction, literally moments before the main span is welded together. The approaches and pylons are made of concrete, while the main span is steel.

Fig. 15.3.b: A night photo of Istanbul's steel cable-stayed metro bridge over the Golden Horn. *Old Istanbul* is an ultra-historical place, a heritage of humanity. The histories of the Greeks, Romans, Byzantines, and Ottomans intertwine here. The construction of the bridge has caused worldwide discussion about its monumental form in such a culturally important place.

Fig. 15.3.c: The River Douro flows through a deep gorge through Porto. The arched reinforced concrete motorway bridge is located at the mouth of the river. When the bridge was completed, the span of the arch (270 m) was the longest in the world. The white bridge is a gateway to the Atlantic.

Fig. 15.3.d: An amazing footbridge in London (owned by Her Majesty the Queen). It has been opened twice. In 2000, there was a blockage phenomenon (lock-in) of such dramatic proportions that the footbridge was closed for 2 years. Transverse vibration damping was introduced, and it works brilliantly now. The footbridge is a landmark of London. The static scheme is difficult to define – one could say it is a suspended, or ribbon structure, or one could use a more fashionable term – hybrid. Its position on the New Tate Gallery – St. Paul's Cathedral axis is visible in the photograph.

Fig. 15.3.e: Rome is a city of arch bridges built from Roman times to the present day. The view of an arch bridge is always enhanced by the mirror image of its structure in the watercourse. Overall, the image is doubled by the symmetry. The bridge in the picture is a crude non-elevated reinforced concrete arch. One can best describe this bridge, if compared to other bridges over the Tiber River, saying that it is modest, cubist and poor.

Fig. 15.3.f: The photo shows a temporary, cable-stayed support structure for the formwork of the main arch bridge. The cinematic character is emphasised by the fact that the photograph was taken from the window of a moving train. The harsh and impoverished landscape of Estremadura forms a natural decoration. This "*film*" cannot be watched a second time.

Fig. 15.3.g: It is Calatrava's first monumental bridge – primarily, a reinforced concrete and prestressed structure. A delicate, silvery steel truss departs from the massive arch heads. Here, the architect developed the bridge deck scheme which he later reapplied to the *El Alamillo* steel bridge.

Fig. 15.3.h: This is a cantilevered footbridge. The left-hand girder, visible in the picture, is supported by cables running almost parallel to each other from the high pylon. The footbridge is stable under full (whatever that means) load. As it has turned out, the bridge shakes noticeably when several people walk on it, but there is no danger of resonance. As Calatrava said, the architecture of the footbridge is a nod to ancient Greek architecture. Many people perceive the footbridge as a transformation of a Greek boat going out to sea. The tight fit of the footbridge into the densely urbanised uninteresting space of the city makes it impossible to take a

good postcard photo. The same pedestrian bridge suspension scheme was used for the much longer Sundial Bridge in Turtle Bay, California.

Fig. 15.3.i: Bilbao's famous urban nodal point has a bridge element. An ordinary cable-stayed bridge, the first in Spain, has been adapted to the architectural and cultural level established by Frank Gehry. The colouring of the bridge pylon has been remade using structurally advanced materials, giving the pylon its name – L'Arc Rouge. The French artist Daniel Buren is the author of this arrangement.

Fig. 15.3.j: Rather than being cut up for scrap, Pratt's[26] steel truss from a rusting railway bridge has been given a new aesthetic role. The cut truss pieces, arranged in an architectural manner, are now a distinctive reference point on the outskirts of Victoria, indicating the presence of the bus station.

Fig. 15.3.k: Anyone in Badajoz walking from the train station towards the old town must walk over the renovated 16th-century multi-arc stone bridge over the Guadiana River. This 600-metre walk offers interesting views. Looking to the right, one can "*watch a video*" of the moving cable-stayed bridge incorporated into the reinforced concrete arch bridge. The captured stop-frame is an unintentional visual sore spot that can be found in many places, e.g. in Seville or Warsaw.

Fig. 15.3.l: Bilbao has become a place enlivened by culture in various dimensions. The attention to interesting architecture attracts creators. Here, in 1997, Calatrava designed a white-coloured steel arch bridge with a tempered glass deck. The structure is interesting through its individuality and is known as "*Zubizuri zubia*", which means 'white bridge' in Basque. The side view shows an average simple arch bridge. It is different. Yes, there is an arch, which in the plan is supported at the diagonal points of the bridge deck. The bridge deck is in a small vertical and horizontal arch at the same time. The bottom chord (tie) of the arch also has a small vertical and horizontal curvature. The hangers running from the arch towards the edge of the bridge deck form two ruled surfaces. The hangers are full circular steel bars. Calatrava uses a platform that is illuminated from below. The tempered glass used is only glass. In rainy weather, the pavement becomes slippery and accidents involving pedestrians occur. As can be seen in the attached photo, this problem has been addressed through reducing the illuminated area and using rough carpeting.

[26] The *Pratt truss* bridge mode was patented in 1844 by Thomas Willis Pratt and his father Caleb Pratt, both of whom were American engineers.

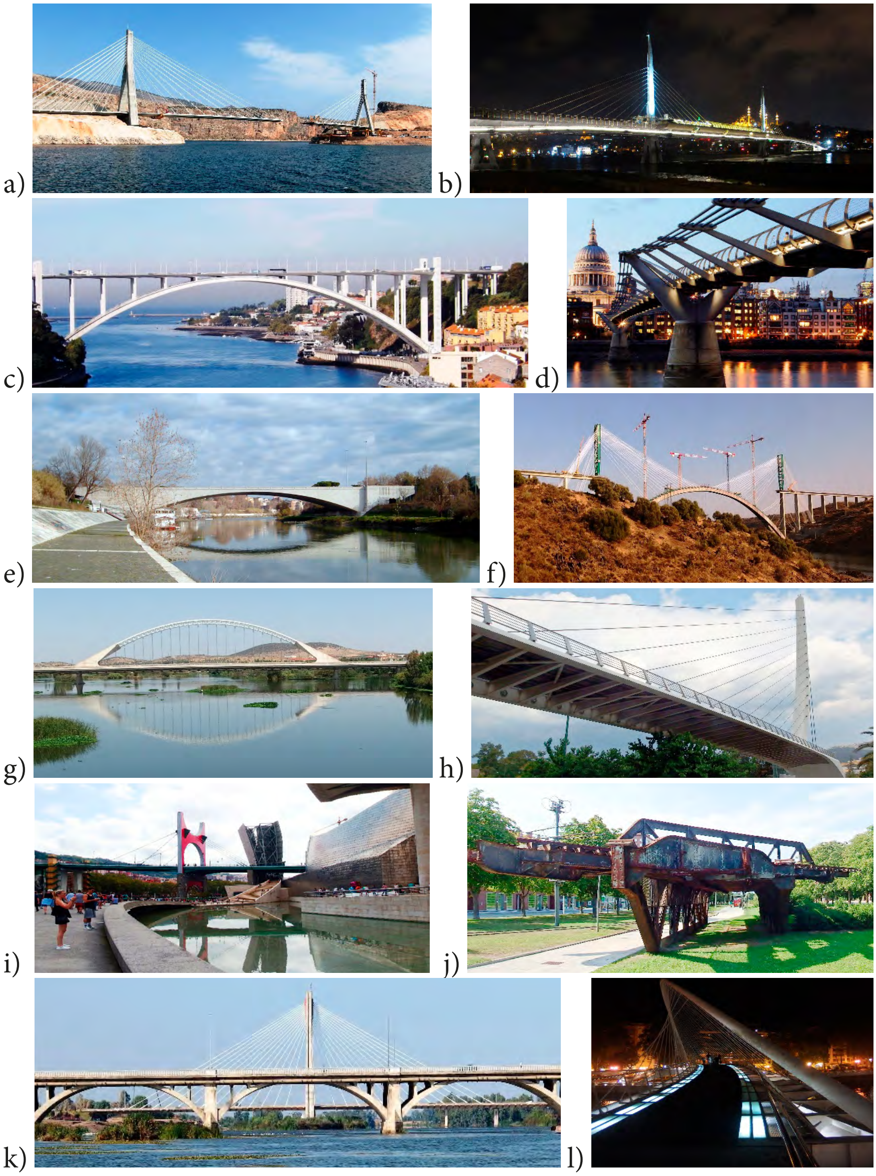

Fig. 15.3. Examples of modern, aesthetically interesting bridges or bridge events a) *Nissibi Euphrates Bridge* (2015) b) *Haliç Metro Bridge*, Istanbul (2014) c) *Ponte da Arrábida*, Porto (1963) d) *London Millennium Footbridge* (2000) e) *Ponte Duca d'Aosta*, Rome (1942) f) temporary scaffolding, Extremadura (2015) g) *Puente Lusitania*, Mérida (1991) h) *Katehaki Pedestrian Bridge*, Athens (2004) i) *La Salve zubia*, *L'Arc Rouge*, Bilbao (2019) j) sculpture made from railroad bridge in front of bus station, Vitoria-Gasteiz, Vizcaya k) view from *Puente de Palmas*, Badajoz l) *Zubizuri zubia*, Bilbao (1997)

The classical criteria can certainly be applied to a large extent, but at the same time contemporary bridge aesthetics is rapidly diverging towards the forms of Calatrava's bridges. The two footbridges in Bilbao and Athens can only be seen through the prism of *Foldability of Space Frames*.

In conclusion of the considerations on the aesthetics of bridges, the proven rule *de gustibus non disputandum EST* is recalled again. As it seems, it is possible to escape recognized situations in aesthetic evaluation. If tastes are not the subject of discussion, then statistical estimation can be used, e.g. the demanding zero-one evaluation, (*0* – negative; *1*- positive), (Karas, 2017).

The use of statistics can significantly moderate the importance of authority figures and at the same time increase the potential of individual sensitivity.

Fig. 15.4. Erasmus students assessing the footbridge aesthetics

In the case of the footbridge in the People's Park in Lublin (Karas, Gnyp, 2022), a group of international Erasmus students of architecture/civil engineering, using the zero-one evaluation of the footbridge, have obtained to the following result:

(*0*: 1; *1*: 14).

In the case of the footbridge in the People's Park in Lublin, the aesthetic evaluation demonstrated a clear acceptance of its aesthetics. Only after the zero-one evaluation is carried out does the discussion take place, which is a defence of an individual assessment of the aesthetics of an object. Usually, a heated debate is an added value to the perceived impression.

***

Bibliography

ACI (2005), *Report on Factors Affecting Shrinkage and Creep of Hardened Concrete*. ACI 209.1R-05, p. 12; http://dl.mycivil.ir/dozanani/ACI/ACI%20209.1R-05%20Report%20on%20Factors%20Affecting%20Shrinkage%20and%20Creep_MyCivil.ir.pdf.

Alfrey. T., (1950), *Non-homogeneous stresses in viscoelastic media*. Quart. Appl. Mech. 8.

Alvaro R., Seara-Paz S., González-Fonteboa B., Martínez-Abella F., *Use of granular coal combustion products as aggregates in structural concrete: Effects on properties and recommendations regarding mix design*, Construction and Building Materials, 273, 121690, p. 1–17; https://doi.org/10.1016/j.conbuildmat.2020.121690.

Andrä H-P. (1987), *Neues vorteilhaftes Verbundmittel für Stahlverbund-Tragwerke mit hoher Dauerfestigkeit*. Beton Stahlbetonbau, 82, S. 325–331; https://doi.org/10.1002/best.198700500.

Andrä H-P., (1990), *Economical shear connectors with high fatigue strength*, PDF erstellt am: 08.06.2022; http://doi.org/10.5169/seals-46457.

Ataman M., Szcześniak W., (2022), *Infuence of inertial Vlasov foundation parameters on the dynamic response of the Bernoulli-Euler beam subjected to a group of moving forces – analytical approach*, Materials, 15, 3249, p. 16; https://doi.org/10.3390/ma15093249.

Banfill P.F.G., (2003), *The rheology of fresh cement and concrete – a review*, p. 14; https://www.researchgate.net/publication/255652324.

Bastien J, Schatzman M., Lamarque C-H., (1921), *Study of some rheological models with a finite number of degrees of freedom*, European Journal of Mechanics – A/Solids, 19, 2, p. 277–307; doi.org/10.1016/S0997-7538(00)00163-7 .

Bažant Z., (1975), *Theory of Creep and Shrinkage in Concrete Structures*, Mechanics Today, Vol. 2, ed. Nemat-Nasser, Pergamon Press, pp. 1–93.; http://www.civil.northwestern.edu/people/bazant/PDFs/Papers/S2.pdf.

Bažant Z., (1982), Wittmann F. ed.: *Creep and Shrinkage in Concrete Structures*, John Willey and Sons; http://cee.northwestern.edu/people/bazant/PDFs/Papers/S09.pdf.

Bazant Z., (2001): *Prediction of concrete creep and shrinkage: past, present and future*, Nuclear Engineering and Design, 203, p. 27–38; http://cee.northwestern.edu/people/bazant/PDFs/Papers/396a.pdf.

Bazant Z.P, Wittmann H.F., (1982), *Creep and Shrinkage in Concrete Structures*, John Wiley & Sons, New York, p. 363.

Berczyński S. Wróblewski T., (2005), *Vibration of steel–concrete composite beams using the Timoshenko beam model*, Journal of Vibration and Control, 11: p. 829–848.

Bingham E., *Fluidity and Plasticity*, p. 270, McGraw Hill, 1922.

Bingham, E. C., Green, H., (1919), *Paint, A Plastic Material and Not a Viscous Liquid, The Measurement of Its Mobility and Yield Value*, Proc. Am. Soc. Test. Mater., Vol. 19, p. 640–664.

Birkeland H. W., (1960), *Differential shrinkage in composite Beams*, ACI Journal Proceedings, V. 56, No. 11, p. 1123_1146.

Blaszkowiak S., (1958), *Einfluß des Kriechens beim Stahl-Vollwand-Verbunddträger, erfaßt durch n(φ) = E/Ec(φ)n*, Die Bautechnik, Vol. 35, S. 66–100.

Brara A., Klepaczko J. R., (1999), *Erude experimentale de la traction dynamique du béton par écaillage*, in: Recueil de communications GEO-réseau de laboratoires, groupe (comportement des ouwages en dynamique rapides), Aussois, France.

Braraa A., Camborde F., Klepaczko J. R., Mariotti C., (2001), *Experimental and numerical study of concrete at high strain rates in tension*, Mechanics of Materials 33, p. 33–45.

Braraa A., Klepaczko J. R., (2006), *Experimental characterization of concrete in dynamic tension*, Mechanics of Materials, Volume 38, Issue 3, March 2006, p. 253–267; https://doi.org/10.1016/j.mechmat.06.004.

Calatrava. S., (1984), *Zur Faltbarkeit von Fachwerken* (*On the Foldability of Space Frames* [27]*)*, Ph.D. thesis, Diss. ETH Nr. 6870, p. 276; https://doi.org/10.3929/ethz-a-000240711.

CEB-FIP Model Code 1990, Comité Euro-International du Béton, 1993; https://www.icevirtuallibrary.com/doi/book/10.1680/ceb-fipmc1990.35430.

Collings D., (2005), *Steel-concrete composite bridges*, Thomas Thelford Publissing.

Courbon J., (1940) *Calcul des ponts à pouters multiples solidarisées par des entretoises*, Annales des Ponts et Chaussées, mémoires et documents relatyfis à l'art des constructions au service de l'ingénieur, No. 17, p. 293–322.

Coussot P., (2017), *Bingham's heritage*. Rheologica Acta, Springer Verlag, 56 (3), p. 163–176. 10.1007/s00397-016-0983-y. HAL Id: hal-01784850.

Cusatis G., (2011), *Strain-rate effects on concrete behaviour*, International Journal of Impact Engineering, 38, p. 162–170.

Davison L., (2008), *Fundamentals of Shock Wave Propagation in Solids*, Springer, S. 433.

Ditkin V. A., Prudnikov A. P., (1962), *Operational Calculus in Two Variables and its Applications*, (International Series of Monographs on Pure and Aplied Mathematics, General Ed.: Snedon I.N., Ulam S., Stark M.), Pergamon Press, Oxford-London-New York-Paris, 1962, p. 167. (Translation of the original volume: *Opieracionnoye ischislenie po dvum peremiennym i ego prilozhenya*, Fizmatgiz, Moscow, 1958).

Doetsch G., *Introduction to the Theory and Application of the Laplace Transformation*, Springer-Verlag, 1974, S. 326.

[27] The literal dictionary translation is: *About the foldability of trusses.*

EN 12390-13 *Testing hardened concrete* – Part 13: *Determination of secant modulus of elasticity in compression.*
EN 1992 Eurocode 2: *Design of concrete structures – Part 1-1* : General rules and rules for buildings.
EN 1994-2 *Design of composite steel and concrete structures* – Part 2: General rules and rules for bridges.
EN 1994-2 Design of composite steel and concrete structures – Part 2: General rules and rules for bridges.
EN 1994-2 Eurocode 4 – *Design of composite steel and concrete structures* Part 2: General rules and rules for bridges.
EN 206-1 Concrete – Part 1: *Specification, performance, production and conformity*
Feldmann M., Kopp M., Pak D., (2016), *Composite dowels as shear connectors for composite beams – background to the German technical approval*, Steel Construction, Vol. 9, 2, p. 80–88; https://doi.org/10.1002/stco.201610020.
Flaga K., Furtak K., (2014), *Application of composite structures in bridge engineering,* Problems of construction process and strength analysis, Civil and Environmental Engineering Reports 2014; 14 (3), p. 57–85; DOI: 10.1515/ceer-2014-0035.
Furtak K., (1999), Composite bridges,(in Polish – Mosty zespolone), PWN.
Grzesikiewicz W., Zbiciak A., (2012), *Study of generalized Prandtl rheological model for constitutive description of elastoplastic properties of materials*, JAMME, Vil. 55I, p. 504–510.
Hai N. M., Nakajima A., Fujikura S., Murayama T., Mori M., (2020), *Shear behavior of a perfobond strip with steel fiber- reinforced mortar in a condition without surrounding reinforcements*; https://doi.org/10.1617/s11527-020-01474-z.
Heath A., Roesler J., (1999), *Shrinkage and thermal cracking of fast setting hydraulic cement concrete pavements in Palmdale*, Preliminary Report Prepared for California Department of Transportation; http://www.ucprc.ucdavis.edu/PDF/Shrinkage%20and%20Therm%20Crack.pdf.
Holt E., (2001): *Early age autogenous shrinkage of concrete*, Technical Research Centre of Finland; http://www.vtt.fi/inf/pdf/publications/2001/P446.pdf.
Hooke R., (1678), *De Potentia Restitutiva, or of Spring. Explaining the Power of Springing Bodies*, p. 56, London.
Hopkinson B., (1914), *A method of measuring the pressure produced in the detonation of high, explosives or by the impact of bullets*, Phil. Trans. R. Soc. of London. Vol. 213, p. 437–456; https://doi.org/10.1098/rsta.1914.0010. http://*happypontist.* blogspot.com/2009/02/bridge-criticis m-8-good-bad-and-ugly.html.
Huber M. T., (1929), *Probleme der Statik technisch wichtiger orthotroper Platten*, insbesondere S. 42, Warschau.
Jansen A., (1997, *Bronze Age Highways at Mycenae*, Echos du Monde Classique. Classical Views. Classical Association of Canada, University of Calgary Press, 41, 16, p. 1–16.

Jasim N. A., (1997), *Computation of deflections for continuous composite beams with partial interaction*, Proc Instn Civ Engrs Structs and Brdgs, 122, 3, p. 347–354; https://doi.org/10.1680/istbu.1997.29806.

Jasim N. A., (1999), *Deflections of partially composite beams with linear connector density*, Journal of Constructional Steel Research, 49, p. 241–254; https://doi.org/10.1016/S0143-974X(98)00206-5.

Johnson R. P., (1975/2004), *Composite structures of steel and concrete*, Blackwell Pub., Third Ed.

Johnson R. P., Buckby R. J., (1979), *Composite structures of Steel and Concrete*, Granada Publishing.

Kant I., (1790), *Kritik der Urteilskraft*; (1892), *Critique of Judgment,* Translated by J.H. Bernard, New York: Hafner Publishing, 1951. (Original publication date 1892).

Karaś S. , Kowal M., (2015). *The Mycenaean bridges – technical evaluation trial*, bilingual journal: Roads and Bridges – Drogi i Mosty, Vol. 14, no. 4, p. 285–302; DOI 10.7409/rabdim.015.019.

Karaś S., (2008), *The new concept of composite girder elasticity analysis*, VIIth Scientific Conference on Composite Structures, Zielona Góra.

Karaś S., (2012), *Solution of Extended Kelvin-Voigt Model*, Construction and Architecture, 10, p. 119-130; http://wbia.pollub.pl/files/83/attachment/10_10.pdf,

Karas S., Gnyp K., (2022), *One-of-a-Kind Footbridge, Lublin, Poland*, Journal of Civil Engineering and Architecture 16, p. 24–37; DOI:10.17265/1934-7359/2022.01.003.

Karas S., Nien-Tsu Tuan, (2017), *The World's Oldest Bridges – Mycenaean Bridges*, American Journal of Civil Engineering and Architecture, 5(6), p. 237–244; DOI:10.12691/ajcea-5-6-3

Karas S.: (2010), *Bending Stiffness of Partially-Integrated Composite*, International Journal of Earth Sciences and Engineering, Vol. 03, No. 02, p. 264–271.

Karas, S. (2017), *Bridge Graffiti, Aesthetical Assessment,* American Journal of Civil Engineering and Architecture 5 (3), p. 108–12; doi: 10.12691/ajcea-5-3-5.

Kelly P., (2013) *Solid Mechanics Part I – Engineering, Publisher, Chapter 10. Viscoelasticity*, The University of Auckland, p. 283–342.

Kołakowski, T., Lorenc, W., (2015). *Bridges by VFT method in Poland: state-of-the-art*. In: Petzek, E., Băncilă, R. (eds) *Economical Bridge Solutions based on innovative composite dowels and integrated abutments*. Springer Vieweg, Wiesbaden; https://doi.org/10.1007/978-3-658-06417-4_7.

Kolsky, H. (1949) *An Investigation of the Mechanical Properties of Materials at Very High Rates of Loading*. Proceedings of the Physical Society. Section B, 62, p. 676–700.

Lazarević M., Rapaić M., Šekara T., (2012), *Introduction to Fractional Calculus with Brief Historical Background*, Part I. Introduction to Fractional Calculus, Ed: Mladenov V., Mastorakis N.: Advanced Topics on Applications of Fractional Calculus on Control Problems, System Stability and Modeling, WSEAS Press, p. 4–15.

Leibniz G. W.; (1695), *Letter from Hanover; Germany; to G.F.A. L'Hopital*, September 30; 1695; in Mathematische Schriften 1849, reprinted 1962, Hildesheim, Germany, Olms Verlag, S. 301–302.

Leonhardt F., (1968), *Aesthetics of Bridge Design,* PCI Journal 13: p.14–31.

Leonhardt F., (1984), *Brücken Bridges Ästhetik und Gestaltung, Aesthetics and Design*, Wissenschaftliche Buchgesellschaft-Darmstadt" In Structural Mechanics, MIT Press, S. 308; http://worldcat.org/isbn/0262121050.

Liu G., Cheng W., Chen L., Pan G., Liu Z., (2020), *Rheological properties of fresh concrete and its application on shotcrete*, Construction and Building Materials, 243, 118180, p. 16; https://doi.org/10.1016/j.conbuildmat.2020.118180.

Lorenc W., (2020), *Concrete failure of composite dowels under cyclic loading during full-scale tests of beams for the "Wierna Rzeka" bridge*, Engineering Structures, Vol. 209; https://doi.org/10.1016/j.engstruct.2020.110199.

Lukic B. (2018), *Mise au point d'une technique de mesure de champs pour la caracterisation du comportement dynamique du beton en traction*: PhD Thesis. Grenoble: University Grenoble Alpes, p. 256.

Machelski Cz., (2022), *Main girder deformation functions from service life of composite bridges*, Roads and Bridges 21, p. 217–237; DOI: 10.7409/rabdim.022.013.

Malvar L. J., Crawford J.E., (1998), *Dynamic increase factors for concrete*, Twenty-Eighth DDESB Seminar Orlando, FL, August 98; https://apps.dtic.mil/sti/pdfs/ADA500715.pdf.

Mehdi D., (2013), *Introduction of Derivatives and Integrals of Fractional Order and Its Applications*, Applied Mathematics and Physics 1.4 p. 103-119.

Mezger T. G., (2002), *The Rheology Handbook*, 3rd revised edition, Hanover Vincentz V., p. 252.

Mladenov V., Mastorakis N., (2012), In: *Advanced Topics on Applications of Fractional Calculus on Control Problems, System Stability and Modelling*, Published by WSEAS Press, p. 4-15

Nadai A., (1950), *Theory of flow and fracture of solids*, McGraw-Hill, New York, Toronto and London, p. 572

Nagaraj, A. S. G., Girish S., (2021). *Rheology of fresh concrete – a review*, Journal of Rehabilitation in Civil Engineering, 9(3), p. 118-131; https://doi.org/10.22075/jrce.2021.20557.1425.

Newmark N. M., Siess C. P, and Viest I. M., (1951), *Tests and analysis of composite beams with incomplete interaction*, Proc. Soc. Exp. Stress Anal, vol.8, issue.1, p. 75–92.

Newmark N. M., Siess C. P., Penman R. R., (1946), *Studies of slab and beam highway bridges: Part I. Tests simple-span right I-beam bridges*, University of Illinois Bulletin, vol. 43, No. 42, p. 132.

Nowacki W., (1963): *Creep theory Teoria pełzania (in Polish; Teoria pełzania)*, p. 170, Arkady.

Nowacki W., (1965),*Théorie du fluage*, Eyrolles, p. 219.

Oehlers D. J., Bradford M. A., (1999), *Elementary behavior of composite steel & concrete structural members*, Butterworth-Heinemann, Oxford GB.

Oehlers D. J., Saracino R., (2004), *Design of FRP and steel plated RC Structures: retrofitting beams and slabs for strength, stiffness and ductility*, Elsevier Internet Homepage, p. 228; http://www.elsevier.com

Pająk M., (2011), *The influence of the strain rate on the strength of concrete takin into account the experimental technics*, Architecture of Civil Environment, Silesian University of Technology, 3/2011, p. 77–86.

Partov D., Kantchev V., (2007), *Contribution to the methods of analysis of composite steel-concrete beams, regarding rheology*, Engineering Mechanics, Vol. 14 No. 5, p. 327–343.

Partov, Kantchev V., *Contribution to the methods of analysis of composite steel-concrete beams, regarding rheology*, Engineering Mechanics, Vol. 14, 2007, No. 5, p. 327–343.

Pedersen R. R, Simone A., Sluys L. J., (2008), *An analysis of dynamic fracture in concrete with a continuum visco-elastic visco-plastic damage model*, Engineering Fracture Mechanics, 75, 13, p. 3782–3805; doi.org/10.1016/j.engfracmech.2008.02.004

Pelke E., Kurrer K-E., (2015), *On the evolution of steel-concrete composite construction*, 5th International Congress on Construction History; https://bautechnikgeschichte.files.wordpress.com/2015/07/pelke.pdf

Pertz G. H. and C. J. Gerhardt, ed., (1971). *Leibnizens gesammelte Werke, Lebinizens mathematische Schriften, Erste Abtheilung*, Band II, pages 301.302. Dritte Folge Mathematik (Erster Band). A. Asher & Comp., Briefwechsel zwischen Leibniz, Hugens van Zulichem und dem Marquis de l'Hospital, 1849.

Pipes L. A., (1958), *Applied mathematics for engineers and physicist* 2nd Edition, McGraw-Hill, p. 723.

PN-85/S-10030 *Bridge structures. Loads. (In Polish)*

Prandtl L., (1921), *Über die Eindringungsfestigkeit (Härte) plastischer Baustoffe und die Festigkeit von Schneiden*, Z. Angew. Math. Mech.1, S. 15–20; https://doi.org/10.1002/zamm.19210010102.

Prandtl L., (1928), *Ein Gedankenmodell zur kinetischen Theorie der festen Körpe*r. Z. Angew. Math. Mech. 8, S. 85–106; https://link.springer.com/content/pdf/10.1007/978-3-662-11836-8_12.pdf.

Preco-Beam – European Commission, Directorate-General for Research and Innovation, (2013), Seidl G., Viefhues E., Berthellemy J., Mangerig I., Wagner R., Lorenc W., Kozuch M., Franssen J.-M., Janssen D., Ikäheimonen J., Lundmark R., Hechler O., Popa N., *Prefabricated enduring composite beams based on innovative shear transmission (Preco-Beam)*, Publications Office; https://data.europa.eu/doi/10.2777/9363.

Regulation of the Minister of Infrastructure of 1 August (2019), statute book 2019 item 1642.

Reiner M., *Rheology*, (1958), Ed. Flügge S., Handbuch der Physik, *Elasticity and Plasticity / Elastizität und Plastizität*, Springer, p. 434–549.

Reinhardt H.W., (1982), *Concrete under Impact Loading, Tensile Strength and Bond*, HERON, 27 (3), p. 5–48.

Reinhardt H.W., Rossi, P. & van Mier J.G.M., (1990), *Joint investigation of concrete at high rates of loading*. Materials and Structures 23, 213–216; https://doi.org/10.1007/BF02473020

Rey-De-Pedraza V., D. A. Cendón, V. Sánchez-Gálvez, F. Gálvez: (2016,), *Measurement of fracture properties of concrete at high strain rates*, Phil. Trans. R. Soc. A375: 20160174, p. 1–13; https://doi.org/10.1098/rsta.

Rogosin S., Meinardi F., (2014), *George William Scott Blair – the pioneer of fractional calculus in rheology*, Communications in Applied and Industrial Mathematics, DOI: 10.1685/journal.caim.481,

Rossi P., (1991), A *physical phenomenon which can explain the mechanical behaviour of concrete under high strain rates*, Materials and Structures 24**,** p. 422–424; https://doi.org/10.1007/BF02472015

Roussel N., (2012): *Understanding the Rheology of Concrete*, Woodhead Publishing Limited; http://www.sciencedirect.com/science/book/9780857090287.

Rüsch H., (1960), *Researches toward a general flexural theory for structural concrete*, Journal of the American Concrete Institute, p. 1–28.

Rusinek A., Chevrier P. (Eds.), (2009), *Workshop in memory of prof. J.R. Klepaczko: Dynamic Behaviour of Materials*, LPMM, Metz, p. 295.

Rzhanitsyn A. P., (1948), *Теориа составных стержней строителных конструкций*, Стройиздат.

Rzhanitsyn A. P., (1986), *Составные стержни и пластинкн*, Стройиздат

Saint-Venant B., (1855), *Mém. savants étrangers*, vol. 14.

Sapountzakis E. J., (2004), *Dynamic analysis of composite steel–concrete structures with deformable connection*, Computers and Structures 82, p. 717–729; https://doi.org/10.1016/j.compstruc.2004.02.012.

Sattler K., (1953), *Theorie der Verbundkonstruktionen*. Berlin: Ernst & Sohn.

Schofield R. K. and Scott Blair G. W., (1932), *The relationship between viscosity, elasticity and plastic strength of soft materials as illustrated by some mechanical properties of flour doughs*, I. Proceedings of the Royal Society of London, Series A, Vol. 138 , pp. 707–719.

Seidl G., Petzek E., Băncilă R., (2013), *Composite Dowels in Bridges – Efficient Solution*, Advanced Materials Research (Volume 814); https://doi.org/10.4028/www.scientific.net/AMR.814.193, p. 193–206.

Seracino R., (1999), *Partial-integration behaviour of composite steel-concrete bridge beams subjected to fatigue loading*, Department of Civil and Environmental Engineering at the University of Adelaide; https://digital.library.adelaide.edu.au/dspace/bitstream/2440/19519/2/02whole.pdf.

Seracino R., Chow T. Lee, Tze C. Lim, Jwo Y. Lim, (2004), *Partial interaction stresses in continuous composite beams under serviceability loads*, Journal of Constructional Steel Research 60, p. 1525–1543; 10.1016/j.jcsr.2004.01.002

Seracino R., Oehlers D. J., Yeo MF., (2001), *Partial-interaction flexural stresses in composite steel and concrete bridge beams*, Engineering Structures; 23, p. 1186-1193; https://doi.org/10.1016/S0141-0296(00)00121-8.

Shim Ch., Lee P., Chang S., (2001), *Designing of shear connection in composite steel and concrete bridges with precast decks*, Journal of Constructional Steel Research, 57(3); p. 203-219; DOI:10.1016/S0143-974X(00)00018-3.

Siess C. P., Viest I. M., Newmark N. M., (1952), *Studies of slab and beam highway bridges: part III: Small-scale tests of shear connectors and composite t-beams*, ideals.illinois.edu; https://www.ideals.illinois.edu/items/4898.

Stefan M. J., (1874), *Versuch über die scheinbare Adhäsion, (Attempt on apparent adhesion),* Aus. D. Anzeiger d. Kais. Akad. zu Wien, No. 12, S. 713–735.

Su Q., Yang G., Bradford M.A., (2016), *Bearing Capacity of Perfobond Rib Shear Connectors in Composite Girder Bridges*, Journal of Bridge Engineering, Vol. 21/4; https://doi.org/10.1061/(ASCE)BE.1943-5592.0000865.

Sun X., Wang H., Cheng X., Sheng Y., (2020), *Effect of pore liquid viscosity on the dynamic compressive properties of concrete*, Construction and Building Materials 231(181):117143; doi.org/10.1016/j.conbuildmat.2019.117143.

Szcześniak W., (2000), *Selected issues in plate dynamics (In Polish)*, Publishing House of the Warsaw University of Technology, p. 295.

Timoshenko S. P., (1953), *History of strength of materials: with a brief account of the history of elasticity theory and theory of structures*, McGrave-Hill Book Company, New York, p. 449.

Troitsky M. S., (1976), *Stiffened plates: bending, stability, and vibrations*, Elsevier Scientific Pub. Co., p. 410.

Trost H., (1968), *Zur Berechnung von Stahlverbundträgern im Gebrauchszustand auf Grund neuerer Erkenntnisse des viskoelastischen Verhaltens des Betons*, Der Stahlbau, Vol. 37, S. 321–331.

Truesdell C., (1974), *Mechanics of Solids*: Volume IV: *Waves in Elastic and Viscoelastic Solids (Theory and Experiment)*, Springer Verlag, Berlin-Heidelberg, S. 334.

Wasiutyński Z., (1971), *On the Architecture of Bridges, (in Polish)*, PAN, PWN, Warsaw, p. 651.

Weerheijm J., Van Doormaal J., (2007), *Tensile failure of concrete at high loading rates: New test data on strength and fracture energy from instrumented spalling tests*, International Journal of Impact Engineering 34 p. 609–626, doi:10.1016/j.ijimpeng.2006.01.005.

Włodarczyk E., Janiszewski J., (2006), *Construction of a dynamic diagram (s – e) on the basis of permanent deformations of a bar loaded by shock, (In Polish)*, Biuletyn WAT, LV, 4, p. 191-208.

Xia K., Yao W., (2015), *Dynamic rock tests using split Hopkinson (Kolsky) bar system – A review*, Journal of Rock Mechanics and Geotechnical Engineering, 7, 1, p. 27–59; https://doi.org/10.1016/j.jrmge.2014.07.008.
Zbiciak A., (2013), *Mathematical description of rheological properties of asphalt-aggregate mixes*, Bulletin of the Polish Academy of Sciences: Technical Sciences 61 (1), p. 65-72; DOI: 10.2478/bpasts-2013-0005.
Zerna, W. und Trost, H. (1967). *Rheologische Beschreibungen des Werkstoffes Beton,* in Beton- und Stahlbetonbau 62, S. 165–170. Ernst & Sohn, Berlin.

Summaries in Polish and English

Streszczenie

Monografia jest wynikiem prowadzenia przez ponad dekadę zajęć z przedmiotu *Fundamentals of Bridges* dla studentów programu Erasmus.

Stalowo-betonowy dźwigar kompozytowy jednocześnie obejmuje zagadnienia mostów stalowych i betonowych. Mosty zespolone budowane są od ponad 100 lat. Do podstawowego projektowania wystarczy znajomość mechaniki klasycznej, jednakże z uwzględnieniem reologii stosowanych materiałów, znajomości dynamiki konstrukcji mostowych, inżynierii materiałów budowlanych, a także zrównoważonego budownictwa i estetyki obiektów mostowych. Oczywistym elementem projektowania i badania mostów jest umiejętność stosowania odpowiednich procedur numerycznych i zdolność do tworzenia efektywnych modeli MES. W monografii zastosowano taką właśnie perspektywę problemów inżynierskich. Krótko, ale wystarczająco, wspomniano o rachunku operatorowym, dynamice w ujęciu dużych prędkości odkształceń, rachunku różniczkowym z pochodnymi ułamkowymi oraz o nowym sposobie oceny estetyki. Wszystkie tematy są opisane na tle historycznym mechaniki i matematyki. Bibliografia zawiera odniesienia do prac historycznych i współczesnych, a nawet najnowszych.

Książka jest adresowana do inżynierów mostowych oraz studentów inżynierii lądowej, w tym w szczególności studentów programu Erasmus.

Słowa kluczowe: stalowo-betonowy dźwigar zespolony, metoda Courbona, rachunek operatorowy, modele reologiczne, dynamika – duże prędkości odkształcenia, estetyka mostów

Summary

The monograph is the result of teaching the *Fundamentals of Bridges* course to Erasmus students for over a decade.

The steel-concrete composite girder covers steel and concrete bridge issues simultaneously. Composite bridges have been built for more than 100 years. For basic design, a knowledge of classical mechanics is sufficient, however, taking into account the rheology of the materials used, knowledge of the dynamics of bridge structures, construction materials engineering, as well as sustainable construction and bridge aesthetics. An obvious part of designing and testing bridges is the ability to apply appropriate numerical procedures and the ability to create effective FE models. The monograph applies this perspective to engineering problems. Brief but sufficient mention is made of operator calculus, dynamics in terms of high strain rates, differential calculus with fractional derivatives and a new way of evaluating aesthetics. All topics are described against the historical background of mechanics and mathematics. The bibliography includes references to historical and contemporary and even recent works.

The book is aimed at bridge engineers and civil engineering students, including in particular Erasmus students.

Keywords: steel-concrete composite girder, Courbon method, operator calculus, rheological models, dynamics – high strain rates, aesthetics of bridges

POLITECHNIKA
LUBELSKA

Review quote:
The monograph is intended for civil engineering students at Polish technical universities, and in particular for Erasmus students from abroad. It can also be used by bridge designers as well as engineers designing composite structures in the general sense. … Writing a monograph on steel-concrete composite bridges for students from various countries and many universities with different specializations and different levels of mathematical, physical and technical background required the author's many years of teaching experience … . All this, however, did not prevent the author from writing a monograph at a high mathematical level with an excellent background in theoretical mechanics, strength of materials, mechanics of structures and theory of elasticity and rheology.

Full Professor Wacław Szcześniak, Warsaw University of Technology

Review quote:
The book is well structured with interesting contents that are really clear and well-explained using a good number of references. It is easy to follow and understand for the reader and provide useful information for students of bridge construction field, young graduates or researchers and even as basic guidelines for bridge design.

Assoc. Professor, Sindy Seara-Paz, University of A Coruña

ISBN: 978-83-7947-539-1

9 788379 475391